JOURNAL OF PETROLOGY | VOLUME 46 | NUMBER 6 | PAGES 1243–1282 | 2005 | doi:10.1093/petrology/egi015

Geochemical Evidence for Mantle Origin and Crustal Processes in Volcanic Rocks from Popocatépetl and Surrounding Monogenetic Volcanoes, Central Mexico

PETER SCHAAF[1]*, JIM STIMAC[2], CLAUS SIEBE[3] AND JOSÉ LUIS MACÍAS[3]

[1]LABORATORIO UNIVERSITARIO DE GEOQUÍMICA ISOTÓPICA (LUGIS), INSTITUTO DE GEOFÍSICA AND INSTITUTO DE GEOLOGÍA, UNIVERSIDAD NACIONAL AUTÓNOMA DE MÉXICO (UNAM), 04510 MÉXICO, D.F., MEXICO

[2]PHILIPPINE GEOTHERMAL INC., 12TH FLOOR, CITIBANK TOWER, 8741 PASEO DE ROXAS BLVD., MAKATI CITY, PHILIPPINES

[3]DEPARTAMENTO DE VULCANOLOGÍA, INSTITUTO DE GEOFÍSICA, UNAM, 04510 MÉXICO, D.F., MEXICO

RECEIVED JUNE, 2004; ACCEPTED JANUARY 17, 2005
ADVANCE ACCESS PUBLICATION FEBRUARY 25, 2005

Elemental, isotopic, and mineral compositions as well as rock textures were examined in samples from Popocatépetl volcano and immediately surrounding monogenetic scoria cones of the Sierra Chichinautzin Volcanic Field, central Mexico. Magma generation is strongly linked to the active subduction regime to the south. Rocks range in composition from basalt to dacite, but Popocatépetl samples are generally more evolved and have mineral compositions and textures consistent with more complicated, multi-stage evolutionary processes. High-Mg calc-alkaline and more alkaline primitive magmas are present in the monogenetic cones. Systematic variations in major and trace element compositions within the monogenetic suite can mostly be explained by polybaric fractional crystallization processes in small and short-lived magmatic systems. In contrast, Popocatépetl stratovolcano has produced homogeneous magma compositions from a shallow, long-lived magma chamber that is periodically replenished by primitive basaltic magmas. The current eruption (1994–present) has produced silicic dome lavas and pumice clasts that display mingling of an evolved dacitic component with an olivine-bearing mafic component. The longevity of the magma chamber hosted in Cretaceous limestones has fostered interaction with these rocks as evidenced by the chemical and isotopic compositions of the different eruptive products, contact-metamorphosed xenoliths, and fumarolic gases. Popocatépetl volcanic products display a considerable range of $^{87}Sr/^{86}Sr$ (0·70397–0·70463) and ε_{Nd} (+6·2 to +3·0) whereas Pb isotope ratios are relatively homogeneous ($^{206}Pb/^{204}Pb$ 18·61–18·70; $^{207}Pb/^{204}Pb$ 15·56–15·60).

KEY WORDS: *Popocatépetl; Sierra Chichinautzin Volcanic Field; arc petrogenesis; radiogenic isotopes*

INTRODUCTION

Popocatépetl [5452 m above sea level (a.s.l.)], located in a densely populated region 70 km SE of Mexico City and 40 km west of the city of Puebla, is perhaps the most well-known stratovolcano of the Trans-Mexican Volcanic Belt (TMVB; Fig. 1). The volcano forms the southern end of an 80 km long, north–south-trending highland (Sierra Nevada) that includes Iztaccíhuatl volcano (5272 m a.s.l.) and divides the Mexico City basin to the west from the Valley of Puebla to the east (Fig. 2). Despite the prominent location and recent activity of Popocatépetl, knowledge of its geological history is still fragmentary, and a detailed geological map of the volcano is not yet available. The age of the oldest rocks from Popocatépetl has not been determined, but they appear to be stratigraphically younger than rocks from Iztaccíhuatl volcano to the north (Fig. 2), whose oldest dated lavas yielded a K–Ar age of 0·9 ± 0·07 Ma (andesitic whole-rock sample; Nixon, 1989).

The modern cone of Popocatépetl consists of numerous interlayered lava flows and pyroclastic deposits of

*Corresponding author: Telephone: +52 55 56224221. Fax: +52 55 55509395. E-mail: pschaaf@geofisica.unam.mx

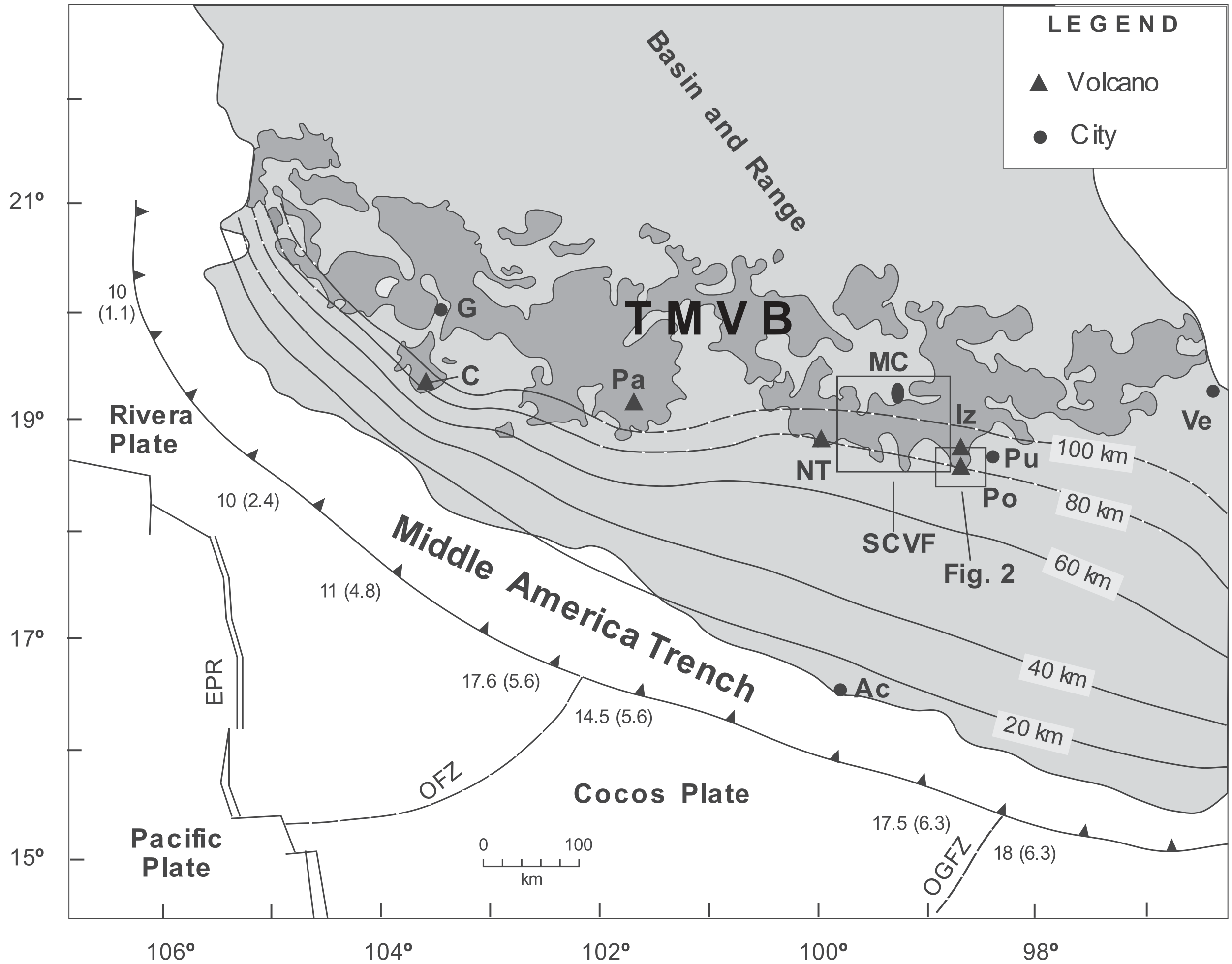

Fig. 1. The Trans-Mexican Volcanic Belt (TMVB) and its spatial relationship to the Middle America Trench. Dark grey indicates volcanism from 0 to 6 Ma [modified from Blatter *et al.* (2001)]. The tectonic features are from Pardo & Suárez (1995). EPR, East Pacific Rise; OFZ, Orozco Fracture Zone; OGFZ, O'Gorman Fracture Zone. The numbers along the Middle America Trench indicate the age of the subducting oceanic crust in million years (first number) and the convergence rate at the location in cm/year (number in parentheses); the black contours represent the depth of the subducted slab (Pardo & Suárez, 1995). Volcanoes (triangles): SCVF, Sierra Chichinautzin Volcanic Field; NT, Nevado de Toluca; Po, Popocatépetl; Iz, Iztaccíhuatl; Pa, Parícutin; C, Colima. Cities (circles/oval): Ac, Acapulco; Ve, Veracruz; G, Guadalajara; MC, Mexico City; Pu, Puebla.

andesitic to dacitic composition (Robin, 1984) deposited in the current eruptive cycle that began *c.* 23 ka BP (Siebe & Macías, 2004). Siebe & Macías also identified debris-avalanche deposits that were emplaced to the south of the volcano, bearing witness to the existence of large ancestral cones that were subsequently destroyed by repeated flank failure and cone collapse (Fig. 2).

During the past 23 kyr Popocatépetl's activity was characterized by at least seven Plinian eruptions as deduced from extensive pumice-fall and ash-flow deposits (Fig. 3). The most recent Plinian eruption occurred between AD 675 and 1095 within the period of human settlement, as evidenced by archaeological remains buried by ash beds and pottery shards incorporated in ash-flows and lahars (Siebe *et al.*, 1996; Siebe & Macías, 2004). Historical eruptions have largely been restricted to smaller pumice-fall, ash-flow, and dome-building cycles (e.g. 1919–1927 eruptions; Friedländer, 1921; Waitz, 1921). After a period of quiescence that lasted more than six decades, Popocatépetl renewed its activity on December 21, 1994, with continuous to pulsating emissions of phreatic ash. Juvenile tephra first appeared in March 1996 and a new lava dome was observed growing in the summit crater on March 29, 1996. This activity peaked with a strong explosion and the formation of an eruptive column of ash and pumice on June 30, 1997. The column was dispersed towards Mexico City during the evening and a thin veil of silty ash accompanied by rain blanketed the city. Another episode of dome growth reached a peak on January 22, 2001, when a strong explosion produced small pyroclastic flows (Fig. 2) that reached the timberline and ignited forest fires on Popocatépetl's northern slopes not far from Tlamacaz.

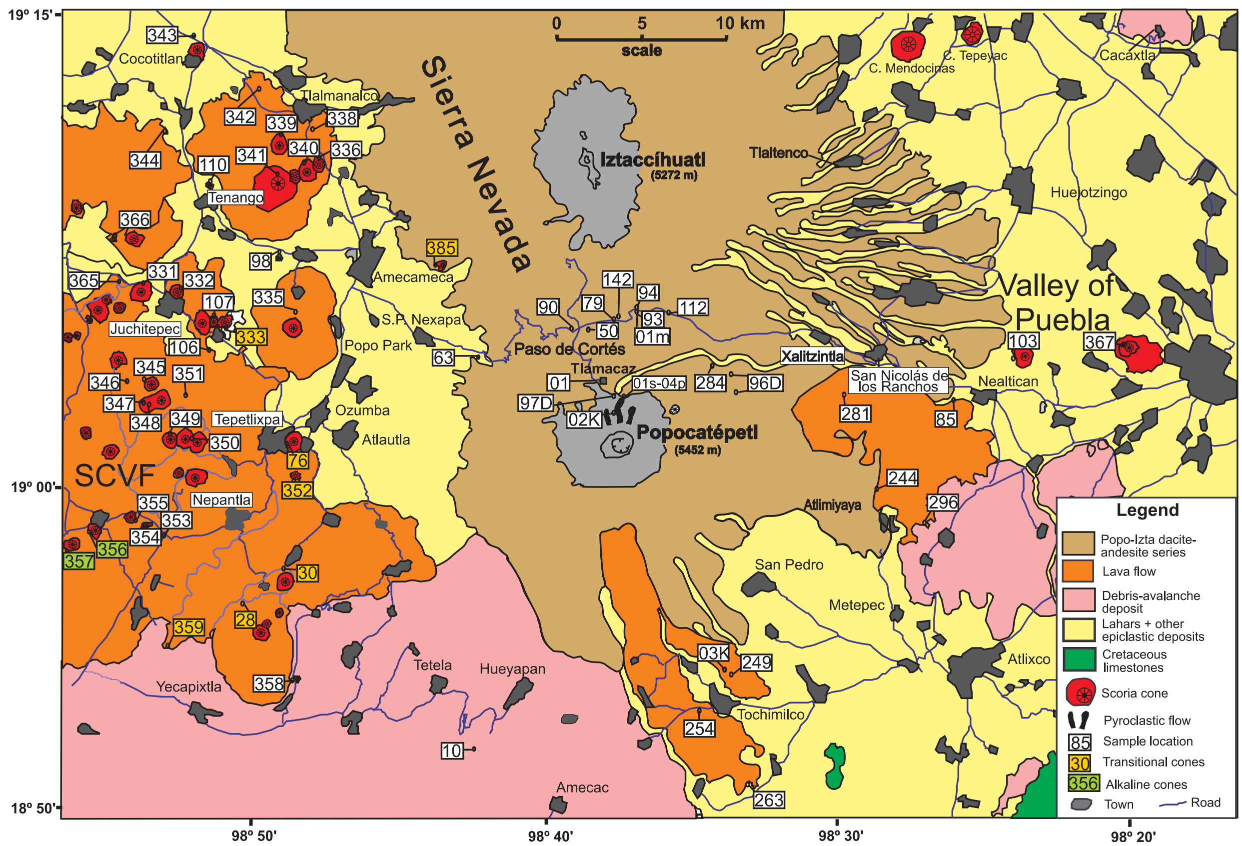

Fig. 2. Geological sketch map of Popocatépetl volcano and surrounding scoria cones of the SCVF (west) and Valley of Puebla (east). Sampling locations are also indicated (see also Table 1) and sample numbers are given with the last two or three digits. Popocatépetl and Iztaccíhuatl stratocones are shown in grey.

The last important dome explosion occurred on July 19, 2003, when the wind was blowing to the WNW and fine ash again reached the southern suburbs of Mexico City. Since March 1996, more than 25 domes have grown within Popocatépetl's crater (Macías & Siebe, 2005). Each of these viscous lava domes was emplaced rapidly over a period of a few days. On each occasion, after cessation of dome growth, days to weeks of quiescence would elapse before renewed strong explosions would destroy the dome, producing several kilometre-high eruptive columns and ash fallout. In this context it is worth mentioning that the once more than 250 m deep crater is now filled almost to the rim with 35×10^6 m^3 of dome material (Global Volcanism Network, 1998; Fig. 4a). As the crater was progressively filled, the frequency of pyroclastic flows gradually increased. We expect that this tendency will be accentuated in the future because growing domes and subsequent explosions will no longer be contained by steep crater walls. If dome growth continues, lava will spill over the crater rim and increase the risk of associated pyroclastic flows and lahars.

Popocatépetl volcano is surrounded by monogenetic volcanoes of the Sierra Chichinautzin Volcanic Field (SCVF) to the west and a few additional scoria cones in the Valley of Puebla to the east (Fig. 2). The SCVF comprises more than 200 scoria cones and lava flows (e.g. Siebe *et al.*, 2004*a*) whose estimated total volume (>200 km^3) is similar to that of Popocatépetl (*c.* 300 km^3). Monogenetic volcanism of the SCVF may have begun as early as 0·7–0·8 Ma, but, based on morphological observations, it has been suggested that many individual cones and lavas are less than 40 kyr old (Bloomfield, 1975).

The subduction zone south of Cordilleran Mexico constitutes a dominant tectonic feature (Fig. 1) to which magma generation beneath the TMVB is generally believed to be related (e.g. Negendank, 1972; Carmichael *et al.*, 1996; Siebe *et al.*, 2004*b*). The complex plate geometry (e.g. variable slab dip) and the oblique angle of the subducting Cocos and Rivera plates, compared with the east–west trend of the TMVB, however, complicate our understanding of the geodynamic setting.

Since the influential work of Bowen (1928), the most commonly proposed process for the origin of calc-alkaline rocks in general, and orogenic andesites in particular, has been fractional crystallization from basaltic magmas. Most work has been dedicated to

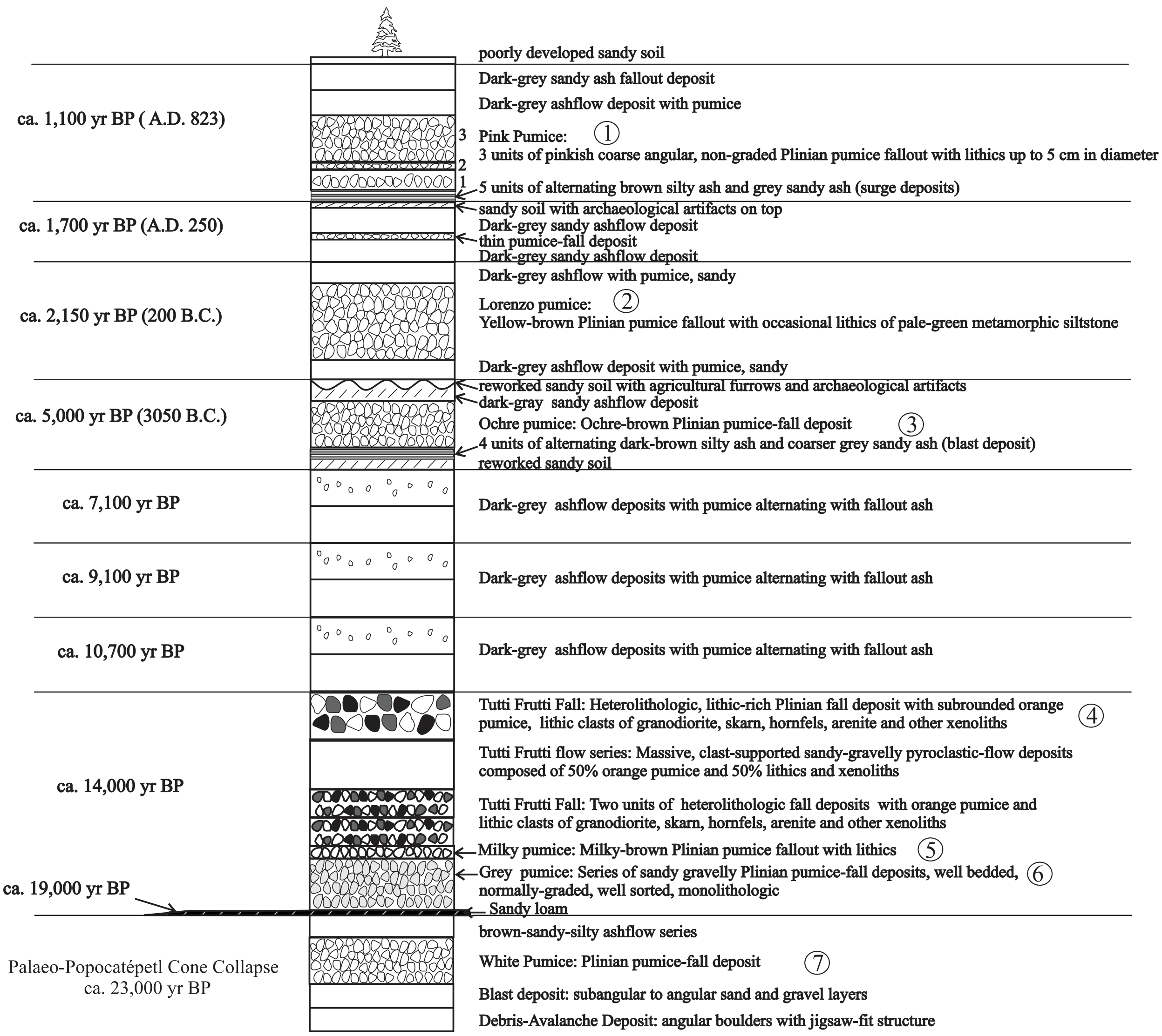

Fig. 3. Composite stratigraphic section of Popocatépetl volcano for the past 23 kyr BP [modified from Siebe & Macías (2004)]. Circled numbers refer to Plinian eruptions.

determining compositional ranges and origins of parental magmas, and the sequence of fractionation leading to observable mineral assemblages (e.g. Gill, 1981). However, it has also become widely accepted that processes such as magma mixing, crustal assimilation, and degassing play important roles in determining the range of compositions and textures of more evolved calc-alkaline rocks (e.g. Eichelberger, 1980; Gill, 1981; Grove & Donnelly-Nolan, 1986), and that a wide range of parental magmas such as high-Mg tholeiite, high-Al basalt, boninite, and sanukitoid (high-Mg andesite) may give rise to the more evolved members of the calc-alkaline suite (Gill, 1981; Tatsumi & Ishizaka, 1982; Luhr *et al.*, 1989).

In this paper we document the mineralogical, chemical, and isotopic compositions of selected products from modern Popocatépetl (<23 ka BP) and coeval surrounding scoria cones. We then examine their genetic relationships, discuss the mantle- and crustal-level processes that contribute to the erupted magmas, and establish a common petrogenetic model for magma generation in this part of the TMVB.

PREVIOUS WORK

Basic aspects of the geology and stratigraphy of Popocatépetl were addressed by Robin (1984), Robin & Boudal (1987) and Boudal & Robin (1988), who divided the history of the volcano into two main periods, separated by a large Plinian eruption that also produced an extensive debris-avalanche deposit. In a more detailed

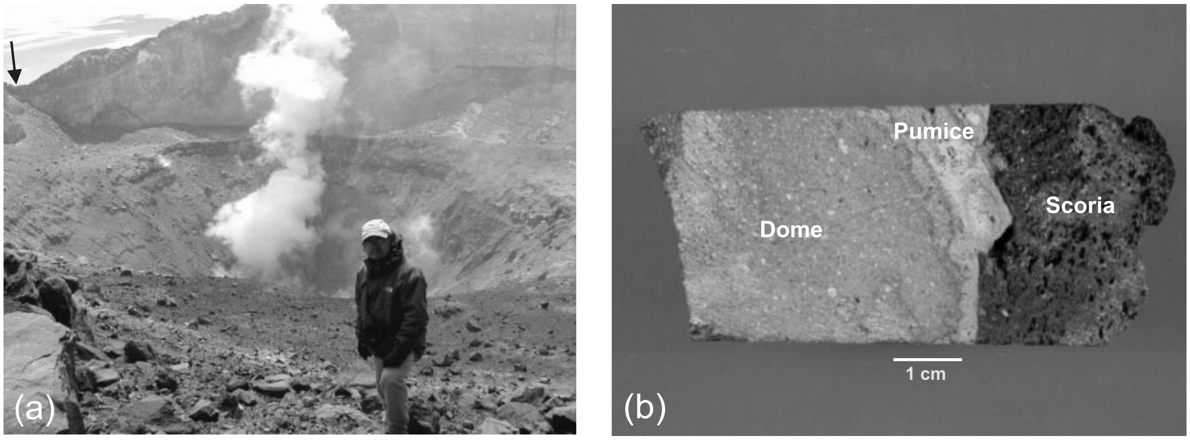

Fig. 4. (a) View from the northeastern rim of Popocatépetl's main crater. The internal smaller crater has a diameter of *c.* 350 m. The lowest point of the crater rim (small arrow) is less than 50 m above the present level of the crater fill. Photograph by J. L. Arce on February 14, 2004. (b) Scoria clast from the January 22, 2001, pyroclastic-flow deposit (Fig. 2) enclosing earlier dome fragments as well as pumice from the dome carapace.

study, Siebe *et al.* (1995) recognized the existence of not only one, but at least three debris-avalanche deposits, the youngest of which occurred *c.* 23 ka BP. Furthermore, Siebe *et al.* (1996) dated the youngest Plinian pumice deposits and documented their disastrous impact on Prehispanic settlements. More recently, Siebe *et al.* (1999) reported mammoth bones embedded in late Pleistocene pumice-bearing lahar deposits and presented the first Sr and Nd isotope data on Popocatépetl pumices.

On the other hand, broad and systematic geological mapping (Nixon, 1989) and petrological studies that document chemical and isotopic trends are available for the neighbouring Iztaccíhuatl volcano (Nixon, 1988*a*, 1988*b*). Iztaccíhuatl consists mainly of coalesced dacitic to andesitic lavas and domes, ranging in age from >900 ka to *c.* 12 ka BP (Nixon, 1989). Detailed mineralogical and textural studies highlighted the importance of primitive basaltic magma recharge to the Iztaccíhuatl magma system and documented the resulting textures and zoning patterns in hybrid andesite and dacite lavas (Nixon & Pearce, 1987). Similar detailed studies of mineral-zoning patterns and their origins were carried out for Popocatépetl by Kolisnik (1990), but no comprehensive study of either the older or younger volcanic products of the volcano comparable with Nixon's work has been published. Kolisnik (1990) found abundant evidence for mafic contributions to andesitic and dacitic eruptions. She observed that the presence of olivine was associated with other textural and compositional evidence of magma mixing including plagioclase with fritted (corroded) cores and calcic overgrowths, reverse-zoned pyroxene, and large ranges in mineral compositions. She emphasized that homogeneous hybrid magma dominates at andesitic compositions.

Several aspects of Popocatépetl's current activity have been studied in detail, including seismology (e.g. Shapiro *et al.*, 2000), gravimetry and deformation patterns (Espíndola *et al.*, 2004), gas chemistry (e.g. Goff *et al.*, 1998, 2001; Love *et al.*, 1998), and spring chemistry (e.g. Werner *et al.*, 1997). Stratigraphic studies include those by Siebe *et al.* (1996, 1999), Panfil *et al.* (1999), and Siebe & Macías (2004). Straub & Martin-Del Pozzo (2001) published petrological data on tephras from the 1996–1998 ash emissions, and Obenholzner *et al.* (2003) performed micro-analysis of ash particles by scanning electron microscopy (SEM).

SAMPLE DESCRIPTIONS

A total of 82 samples were collected for this project during the period 1993–2004 from the modern Popocatépetl cone and surrounding monogenetic volcanoes. Samples can be divided into rapidly cooled tephra and more slowly cooled lava. Tephra samples include pumice clasts erupted from Popocatépetl over the past 23 kyr, as well as ash and dome fragments ejected by explosions during the current eruptions (1994–present). In detail, from Popocatépetl we sampled eight lava flows (and additionally one from Iztaccíhuatl volcano), seven pumice fallout layers, eight xenolith clasts from the 14 ka BP Plinian pumice deposit (Siebe *et al.*, 1997), four ash fallout layers, nine ballistic ejecta fragments from crater domes (April 30, 1996, and June 30, 1997, events) and four scoria samples from the January 22, 2001, pyroclastic-flow deposit. Additionally, 42 scoria and lava flow samples were obtained from monogenetic cones at the western and eastern lower slopes of Popocatépetl and Iztaccíhuatl volcanoes. Sampling of scoria cones in the SCVF and Valley of Puebla was restricted to the morphologically youngest constructs nearest to Popocatépetl and Iztaccíhuatl. Sample locations are shown in Fig. 2 and sample coordinates are given in Table 1.

Table 1: Whole-rock major (wt %) and trace element (ppm) concentrations of Popocatépetl and SCFV and Valley of Puebla scoria cones

Suite:		Popocatépetl												
Sample:		95244	9485	95296	95281	95249	95263	95254	95284	9594	9479o	9310w	9490g	9463tf
Location:		N Atlimiyaya	SW Nealtican	Nealtican N Tianguismanalco	Nealtican S San Nicolas	N Tochimilco	SW Tejupa	W Tochimilco	Cañada Xallipilcayatl	Buenavista (Iztaccíhuatl)	E Paso de Cortés	S Tetela	Paso de Cortés	E San Pedro Nexapa
Rock type:		Lava	Lava	Lava	Lava	Lava	Lava	Lava	Lava	Lava	Ochre pumice	White pumice	Grey pumice	Tutti-Frutti pumice
Mineralogy:		pl>ol>px>2ox	pl>2px>ol	pl>2px	pl>2px	pl>2px	pl>2px	pl>2px>ol	pl>2px	pl-qz-ol ± hb ± bi	pl>2px>2ox>po	pl=2px>hb>2ox>po	hb>2px>pl>ol>ox	hb>2px>pl>ol>ox
Latitude N:		19°00′21″	19°02′48″	18°58′52″	19°02′55″	18°54′14″	18°50′37″	18°53′11″	19°03′45″	19°05′21″	19°05′12″	18°51′34″	19°05′13″	19°04′31″
Longitude W:		98°28′48″	98°26′12″	98°27′18″	98°29′28″	98°33′25″	98°33′06″	98°34′45″	98°34′12″	98°36′35″	98°37′32″	98°42′17″	98°38′37″	98°42′21″
Altitude (m):		2405	2200	2100	2540	2155	1850	2115	3080	3420	3570	2110	3680	2970
Distance from Popocatépetl crater:		15·5 km E	20 km E	18·5 km E	13·5 km E	15 km SE	21·2 km SSE	16 km S	5·7 km NE	8·1 km N	7·5 km N	20 km SSW	7 km N	9·7 km NW
wt %	Detection limits													
SiO_2	0·01%	59·34	61·20	61·94	62·10	62·13	63·29	63·58	63·92	61·90	57·36	58·90	58·99	59·32
TiO_2	0·01%	0·67	0·87	0·89	0·84	0·84	0·71	0·65	0·78	0·81	0·81	0·78	0·81	0·83
Al_2O_3	0·01%	15·67	16·27	16·45	16·27	15·61	16·44	15·77	16·57	16·74	18·04	16·63	16·51	16·52
Fe_2O_3(tot)	0·01%	6·19	5·64	5·72	5·70	5·50	4·78	4·20	5·38	5·48	4·65	4·71	5·78	5·45
MnO	0·01%	0·10	0·09	0·09	0·09	0·08	0·08	0·07	0·09	0·09	0·07	0·06	0·09	0·10
MgO	0·01%	6·20	3·72	3·74	3·79	4·29	3·02	2·28	2·83	3·45	2·52	2·21	4·41	4·57
CaO	0·01%	6·21	4·88	5·03	5·06	4·99	5·00	4·41	4·85	4·90	4·55	4·00	5·78	6·14
Na_2O	0·01%	3·76	4·41	4·43	4·27	4·18	4·23	4·27	4·31	4·47	4·06	3·21	4·11	3·70
K_2O	0·01%	1·51	2·07	2·07	1·85	2·17	2·10	2·01	1·90	1·78	1·49	1·91	1·57	1·49
P_2O_5	0·01%	0·15	0·22	0·22	0·21	0·23	0·19	0·19	0·18	0·18	0·21	0·15	0·22	0·18
LOI		0·84	0·12	0·08	0·12	0·25	1·05	0·74	0·06	0·19	4·14	5·27	1·20	1·16
Total		100·64	99·49	100·67	100·29	100·26	100·89	98·15	100·87	99·99	97·90	97·83	99·47	99·45
ppm														
Sc	2	18	13	13	13	13	11	9	13	13	11	11	14	16
Be	1	1	2	2	2	2	1	1	2	1	1	1	2	1
V	5	125	100	104	109	112	90	72	105	105	82	88	115	129
Cr	10	499	70	100	78	147	417	<10	23	74	11	35	96	90
Co	0·1	23·9	14·8	16·2	15·6	17·7	12·9	8·7	13·1	14·8	8·4	9·9	16·7	14·4
Ni*	1	167	56	58	54	110	49	30	28	56	40	37	89	69
Cu*	1	32	14	15	16	15	11	10	9	14	18	13	22	17
Zn*	1	68	72	74	73	67	65	62	74	72	58	57	73	72
Ga	1	21	24	21	23	24	20	20	22	23	19	23	24	20
Rb	0·01	37·6	52·8	48·8	49·6	61·5	49·2	52·4	50·2	40·7	31·1	55·2	35·3	33·7
Sr	0·01	364·3	470·2	469·0	437·8	465·6	526·0	457·0	417·5	433·7	404·7	377·3	653·4	562·8
Y	0·1	15·1	20·1	20·2	20·2	21·1	16·9	14·4	21·0	17·0	15·3	18·7	18·0	17·4

Suite:		Popocatépetl												
Sample:		95244	9485	95296	95281	95249	95263	95254	95284	9594	9479o	9310w	9490g	9463tf
Location:		N Atlimi-yaya	SW Nealtican	Nealtican N Tianguis-manalco	Nealtican S San Nicolas	N Tochimilco	SW Tejupa	W Tochimilco	Cañada Xallipilca-yatl	Buenavista (Iztaccíhuatl)	E Paso de Cortés	S Tetela	Paso de Cortés	E San Pedro Nexapa
Rock type:		Lava	Lava	Lava	Lava	Lava	Lava	Lava	Lava	Lava	Ochre pumice	White pumice	Grey pumice	Tutti-Frutti pumice
Mineralogy:		pl>ol> px>2ox	pl> 2px>ol	pl>2px	pl>2px	pl>2px	pl>2px	pl> 2px>ol	pl>2px	pl-qz-ol ± hb ± bi	pl>2px> 2ox>po	pl=2px> hb>2ox>po	hb>2px> pl>ol>ox	hb>2px> pl>ol>ox
Latitude N:		19°00′21″	19°02′48″	18°58′52″	19°02′55″	18°54′14″	18°50′37″	18°53′11″	19°03′45″	19°05′21″	19°05′12″	18°51′34″	19°05′13″	19°04′31″
Longitude W:		98°28′48″	98°26′12″	98°27′18″	98°29′28″	98°33′25″	98°33′06″	98°34′45″	98°34′12″	98°36′35″	98°37′32″	98°42′17″	98°38′37″	98°42′21″
Altitude (m):		2405	2200	2100	2540	2155	1850	2115	3080	3420	3570	2110	3680	2970
Distance from Popocatépetl crater:		15·5 km E	20 km E	18·5 km E	13·5 km E	15 km SE	21·2 km SSE	16 km S	5·7 km NE	8·1 km N	7·5 km N	20 km SSW	7 km N	9·7 km NW
Zr	0·01	120·0	165·5	166·3	160·0	190·1	164·1	149·5	149·3	128·7	152·4	219·6	159·5	139·2
Nb	0·01	3·48	7·24	7·65	7·03	7·45	9·70	5·07	5·29	4·93	5·67	7·75	5·10	4·82
Mo	0·01	1·57	2·12	1·93	1·82	2·25	2·15	1·87	1·90	1·90	0·45	1·55	0·53	0·51
Cs	0·01	2·14	2·98	2·90	2·93	3·57	3·09	3·19	2·90	2·80	1·98	3·76	2·11	1·94
Ba	0·01	319·5	1301·7	431·6	457·3	499·2	456·3	437·7	451·0	385·4	356·7	610·4	1184·1	551·5
La	0·01	12·72	20·18	18·69	19·53	23·28	16·93	17·84	17·24	15·62	15·89	19·45	20·57	17·24
Ce	0·01	27·19	42·45	39·60	41·02	50·40	35·44	36·61	36·47	31·64	32·54	46·94	43·87	39·15
Pr	0·005	2·79	4·37	4·15	3·99	5·02	3·30	3·87	3·54	3·25	3·59	4·35	4·78	4·09
Nd	0·01	13·73	20·05	19·31	19·77	24·24	14·82	18·06	17·15	15·29	17·01	20·26	22·49	19·31
Sm	0·01	3·14	4·94	4·82	5·11	5·75	6·19	3·77	4·20	4·15	3·68	4·71	5·25	4·75
Eu	0·005	1·07	1·24	1·32	1·49	1·45	1·61	1·12	1·27	1·21	1·10	1·13	1·57	1·28
Gd	0·01	3·47	4·31	4·14	4·32	5·08	3·00	3·54	3·76	3·32	3·71	4·00	4·34	3·88
Tb	0·01	0·44	0·75	0·61	0·67	0·69	0·51	0·54	0·70	0·52	0·65	0·77	0·77	0·67
Dy	0·01	2·47	3·46	3·39	3·95	4·01	2·75	2·64	3·87	2·85	2·92	3·50	3·25	3·38
Ho	0·01	0·46	0·71	0·66	0·74	0·70	0·50	0·47	0·73	0·63	0·63	0·73	0·70	0·68
Er	0·01	1·59	2·13	2·02	1·89	2·00	1·12	1·45	2·03	1·92	1·59	2·12	1·88	2·01
Tm	0·005	0·23	0·30	0·33	0·26	0·28	0·36	0·18	0·32	0·20	0·23	0·24	0·24	0·22
Yb	0·01	1·29	2·01	1·82	1·59	1·76	1·95	1·18	1·95	1·58	1·16	1·70	1·59	1·73
Lu	0·002	0·216	0·305	0·287	0·283	0·355	0·295	0·230	0·295	0·264	0·262	0·284	0·254	0·270
Hf	0·05	3·51	4·37	4·37	4·15	5·16	4·54	4·26	4·24	3·63	4·41	6·22	4·31	3·88
Ta	0·005	0·26	0·52	0·51	0·44	0·53	0·40	0·35	0·37	0·34	0·41	0·62	0·36	0·31
Pb	5	6	18	7	13	14	32	9	7	7	<5	14	7	<5
Th	0·05	3·60	5·36	5·10	5·24	6·36	4·49	5·29	5·15	4·93	4·43	6·63	4·38	3·89
U	0·005	1·49	1·90	1·80	1·81	2·43	2·19	1·93	1·61	1·69	1·60	2·02	1·62	1·41
Ba/Nb		91·81	179·79	56·42	66·05	67·01	47·04	88·33	85·26	78·17	62·90	78·76	232·17	114·42
Ce/Yb		21·08	21·12	21·76	25·80	28·64	18·17	31·03	18·70	20·02	28·05	27·61	27·59	22·63

Table 1: continued

Suite:		Popocatépetl													
Sample:		9490m	95112lp	9450p	0101s	0102s	0103d	0104p	97D1	96D3-1	96D4-A1	96D4-Com	96D3-3	96D3-2	97D2
Location:		Paso de Cortés	E Paso de Cortés	E Paso de Cortés	E Tlamacaz	E Tlamacaz	E Tlamacaz	E Tlamacaz	E Tlamacaz	Near Bon-sai seism. stat.	NE Popo-catéptl flank	Near Bon-sai seism. stat.	Near Bon-sai seism. stat.	Near Bon-sai seism. stat.	E Tlamacaz
Rock type:		Milky pumice	Lorenzo pumice	Pink pumice	Scoria, pyrocl. fl. 22.1.2001	Scoria, pyrocl. fl. 22.1.2001	Dome fragm., pyrocl. fl. 22.1.2001	Pumice in pyrocl. fl. 22.1.2001	Dome fragm., 30.6.1997	Dome fragm., 30.4.1996	Dome fragm., 30.4.1996	Dome fragm., 30.4.1996	Dome fragm., 30.4.1996	Dome fragm., 30.4.1996	Dome fragm., 30.6.1997
Mineralogy:		hb>2px>pl>ol>ox	pl>2px>2ox>po	pl>2px>ol>2ox>po	pl>2px=ol>ox	pl>2px=ol>ox	pl>ol>2px>ox	pl>ol>2px>ox	pl>2px>ol	pl>2px>ol	pl>2px>ol	pl>2px>ol	pl>2px>ol	pl>2px>ol	pl>2px>ol
Latitude N:		19°05′13″	19°04′57″	19°05′09″	19°03′00″	19°03′00″	19°03′00″	19°03′00″	19°02′48″	19°02′59″	19°03′43″	19°02′59″	19°02′59″	19°02′59″	19°02′48″
Longitude W:		98°38′37″	98°35′48″	98°38′41″	98°37′15″	98°37′15″	98°37′15″	98°37′15″	98°38′01″	98°33′36″	98°34′10″	98°33′36″	98°33′36″	98°33′36″	98°38′01″
Altitude (m):		3680	3690	3690	3825	3825	3825	3825	3800	3500	3100	3500	3500	3500	3800
Distance from crater:		7 km N	8·7 km NE	6·7 km N	2·5 km N	2·5 km N	2·5 km N	2·5 km N	2·7 km N	8 km NE	7·4 km NE	8 km NE	8 km NE	8 km NE	2·7 km N
wt %	Detection limits														
SiO_2		60·52	61·04	61·74	53·75	59·33	61·42	62·67	58·20	60·81	62·12	63·23	62·63	62·82	62·92
TiO_2		0·77	0·80	0·75	0·77	0·87	0·79	0·72	0·92	0·67	0·71	0·71	0·71	0·69	0·73
Al_2O_3		16·77	16·63	15·87	14·37	16·02	16·11	15·57	16·06	15·84	16·10	16·28	16·31	16·09	16·58
Fe_2O_3(tot)		5·64	5·57	5·15	5·66	6·25	5·51	5·08	6·58	5·8	5·39	5·11	5·65	5·36	5·05
MnO		0·09	0·09	0·08	0·09	0·10	0·09	0·09	0·10	0·09	0·09	0·08	0·09	0·09	0·10
MgO		3·75	4·13	3·44	5·26	5·53	4·29	3·67	6·97	3·48	3·81	3·39	3·78	3·03	3·55
CaO		5·72	4·96	4·80	5·79	6·47	5·69	5·00	6·24	5·04	5·08	4·96	5·18	4·79	5·05
Na_2O		4·10	4·23	4·25	3·84	4·20	4·37	4·61	4·21	4·21	4·33	4·36	4·40	4·40	4·56
K_2O		1·57	1·67	1·97	1·22	1·30	1·55	1·74	1·34	1·67	1·72	1·75	1·65	1·78	1·81
P_2O_5		0·21	0·21	0·21	0·16	0·20	0·18	0·17	0·22	0·17	0·17	0·17	0·17	0·17	0·17
LOI		0·49	1·03	0·40	8·87	−0·12	−0·01	0·96	−0·18	−0·01	−0·04	0·08	0·29	0·77	0·06
Total		99·63	100·35	98·66	99·78	100·16	99·98	100·27	100·661	97·78	99·50	100·12	100·86	99·98	100·58
ppm															
Sc		13	13	11	15	17	14	12	14	11	12	12	13	11	11
Be		1	2	1	1	1	2	2	n.d.	1	1	<1	<1	1	n.d.
V		118	97	100	109	126	108	93	150	98	101	95	101	96	99
Cr		42	115	114	170	313	263	109	485	130	139	111	138	101	126
Co		14·2	15·7	13·8	26	28	18	15	25	17·9	18·7	15·6	18·1	16·0	14·8
Ni*		48	87	75	74	85	63	55	150	82	88	56	81	55	58
Cu*		15	22	20	48	53	33	32	29	24	19	19	22	20	18
Zn*		69	67	74	36	87	70	85	70	72	73	74	72	76	68
Ga		23	23	22	15	19	19	19	n.d.	19	17	20	20	21	n.d
Rb	(†2)	39·1	40·7	52·7	31†	36†	42†	55†	27†	47·8	51·4	53·3	48·3	52·6	44†
Sr	(†2)	591·4	426·2	480·0	408†	485†	460†	438†	486†	444·2	458·5	453·6	446·5	450·4	479†

Suite:		Popocatépetl													
Sample:		9490m	95112lp	9450p	0101s	0102s	0103d	0104p	97D1	96D3-1	96D4-A1	96D4-Com	96D3-3	96D3-2	97D2
Location:		Paso de Cortés	E Paso de Cortés	E Paso de Cortés	E Tlamacaz	E Tlamacaz	E Tlamacaz	E Tlamacaz	E Tlamacaz	Near Bon-sai seism. stat.	NE Popo-catéptl flank	Near Bon-sai seism. stat.	Near Bon-sai seism. stat.	Near Bon-sai seism. stat.	E Tlamacaz
Rock type:		Milky pumice	Lorenzo pumice	Pink pumice	Scoria, pyrocl. fl. 22.1.2001	Scoria, pyrocl. fl. 22.1.2001	Dome fragm., pyrocl. fl. 22.1.2001	Pumice in pyrocl. fl. 22.1.2001	Dome fragm., 30.6.1997	Dome fragm., 30.4.1996	Dome fragm., 30.4.1996	Dome fragm., 30.4.1996	Dome fragm., 30.4.1996	Dome fragm., 30.4.1996	Dome fragm., 30.6.1997
Mineralogy:		hb>2px> pl>ol>ox	pl>2px> 2ox>po	pl>2px> ol>2ox>po	pl>2px= ol>ox	pl>2px= ol>ox	pl>ol> 2px>ox	pl>ol> 2px>ox	pl>2px> ol	pl>2px> ol	pl>2px> ol	pl>2px> ol	pl>2px> ol	pl>2px> ol	pl>2px> ol
Latitude N:		19°05′13″	19°04′57″	19°05′09″	19°03′00″	19°03′00″	19°03′00″	19°03′00″	19°02′48″	19°02′59″	19°03′43″	19°02′59″	19°02′59″	19°02′59″	19°02′48″
Longitude W:		98°38′37″	98°35′48″	98°38′41″	98°37′15″	98°37′15″	98°37′15″	98°37′15″	98°38′01″	98°33′36″	98°34′10″	98°33′36″	98°33′36″	98°33′36″	98°38′01″
Altitude (m):		3680	3690	3690	3825	3825	3825	3825	3800	3500	3100	3500	3500	3500	3800
Distance from crater:		7 km N	8·7 km NE	6·7 km N	2·5 km N	2·5 km N	2·5 km N	2·5 km N	2·7 km N	8 km NE	7·4 km NE	8 km NE	8 km NE	8 km NE	2·7 km N
Y	(†1)	17·8	17·7	19·1	16†	20†	18†	18†	19†	16·4	18·1	16·9	17·5	17·2	17†
Zr	(†5)	150·8	156·8	180·7	108†	137†	139†	141†	144†	131·1	137·7	135·3	275·5	135·7	130†
Nb	(†1)	4·83	6·58	6·64	4†	5†	4†	5†	n.d.	5·00	4·74	4·60	4·64	5·07	n.d.
Mo	(†2)	0·85	0·85	1·73	<2†	<2†	2†	<2†	<2†	2·97	2·11	2·03	2·32	2·37	<2†
Cs	(†0·5)	2·17	2·46	3·38	1·6†	2·0†	2·2†	2·5†	1·3†	2·7	2·86	2·88	2·82	3·07	2·1†
Ba	(†3)	468·8	552·0	512·6	298†	354†	377†	433†	318†	339·4	364·1	368·2	347·1	365·6	384†
La	(†0·1)	17·67	16·00	21·82	12·3†	14·3†	14·2†	15·7†	12·8†	13·80	14·93	14·88	14·27	14·40	13·1†
Ce	(†0·1)	37·46	34·54	48·86	27·7†	32·1†	31·3†	33·5†	27·0†	29·43	31·69	31·43	30·24	30·40	30·2†
Pr	(†0·05)	4·04	3·56	4·82	3·37†	3·96†	3·82†	3·93†	n.d.	3·30	3·54	3·50	3·42	3·43	n.d.
Nd	(†0·1)	19·41	16·70	22·74	15·3†	17·8†	17·4†	17·3†	16·0†	15·17	16·25	15·91	15·48	15·58	14†
Sm	(†0·1)	4·39	3·74	5·23	3·6†	4·1†	3·9†	3·9†	3·18	3·60	3·72	3·77	3·73	3·84	3·12
Eu	(†0·05)	1·19	1·11	1·27	1·12†	1·31†	1·22†	1·16†	1·14†	1·09	1·05	1·09	1·04	1·04	1·04†
Gd	(†0·1)	3·73	4·03	4·35	3·6†	4·2†	4·1†	3·8†	n.d.	3·40	3·64	3·42	3·43	3·36	n.d.
Tb	(†0·1)	0·71	0·67	0·77	0·5†	0·6†	0·6†	0·6†	0·5†	0·49	0·50	0·50	0·49	0·50	0·6†
Dy	(†0·1)	3·29	3·13	3·64	3·1†	3·6†	3·4†	3·3†	n.d	2·95	3·10	2·89	3·09	3·00	n.d.
Ho	(†0·1)	0·63	0·66	0·76	0·6†	0·7†	0·6†	0·6†	n.d.	0·55	0·60	0·58	0·6	0·59	n.d.
Er	(†0·1)	1·85	1·67	2·18	1·7†	2·0†	1·9†	1·8†	n.d.	1·73	1·83	1·80	1·83	1·74	n.d.
Tm	(†0·05)	0·25	0·23	0·31	0·24†	0·30†	0·28†	0·25†	n.d.	0·24	0·24	0·24	0·25	0·24	n.d.
Yb	(†0·1)	1·86	1·45	1·69	1·6†	1·9†	1·7†	1·7†	1·56	1·56	1·63	1·54	1·62	1·63	1·46
Lu	(†0·04)	0·276	0·277	0·326	0·23†	0·27†	0·26†	0·25†	0·23†	0·248	0·272	0·244	0·270	0·263	0·22†
Hf	(†0·2)	4·13	4·05	5·18	2·5†	3·1†	3·3†	3·5†	3·2†	3·92	4·09	3·78	7·28	3·97	3·4†
Ta	(†0·1)	0·34	0·46	0·52	0·2†	0·3†	0·3†	0·4†	0·3†	0·37	0·33	0·35	0·36	0·35	0·5†
Pb		8	8	13	<5	17	13	13	n.d.	9	9	10	11	11	n.d.
Th	(†0·1)	4·01	4·00	5·86	3·1†	3·6†	4·2†	4·9†	2·6†	4·06	4·18	4·29	4·08	4·32	3·8†
U	(†0·1)	1·39	1·47	2·17	1·1†	1·2†	1·4†	1·7†	0·8†	1·48	1·59	1·57	1·53	1·61	1·2†
Ba/Nb		97·06	83·90	77·20	74·5	70·8	94·25	86·6		67·88	76·81	80·05	74·81	72·11	
Ce/Yb		20·14	23·82	27·73	17·31	16·89	18·41	19·71	17·31	18·87	19·44	20·41	18·67	18·65	20·55
Fo av.		80·4	76·1							88·96					

Table 1: continued

Suite:		Popocatépetl													
Sample:		96D3 B	96D3-Com	9501	9601K	9602K	9603K	9463A	9593B	96341B	9490B	95142A	95142C	9490C	0401m
Location:		Near Bonsai seism. stat.	Near Bonsai seism. stat.	Tlamacaz	Tlamacaz	Refugio El Canario	Tochimilco	E San Pedro Nexapa	W Buenavista	Cerro Chinconquiat	Paso de Cortés	E Paso de Cortés	E Paso de Cortés	Paso de Cortés	W Buenavista
Rock type:		Dome fragm., 30.4.1996	Dome fragm., 30.4.1996	Ash January 1995	Ash 5.3.1996	Ash 10.3.1996	Ash 11./12.3.1996	Xenolith Skarn in Tutti Frutti pumice	Xenolith Skarn in TF pum.	Xenolith foliated granodior. in TF pum.	Xenolith Granodior. in TF pum.	Xenolith Metasdst. in TF pum.	Xenolith Px-granodiorite in TF pum.	Xenolith Metasdst. in TF pum.	Xenolith Marble in TF pum.
Mineralogy:		pl>2px>ol	pl>2px>ol	n.d.	n.d.	n.d.	n.d.	pl-2px-bi-qz	n.d.	pl-qz-hb>bi-ox	n.d.	n.d.	pl>2px>ol-ox-qz	qz>pl=2px	n.d.
Latitude N:		19°02′59″	19°02′59″	19°03′20″	19°03′20″	19°02′28″	18°54′22″	19°04′31″	19°05′21″	19°10′33″	19°05′13″	19°05′34″	19°05′34″	19°05′13″	19°05′13″
Longitude W:		98°33′36″	98°33′36″	98°37′57″	98°37′57″	98°37′41″	98°33′50″	98°42′21″	98°36′38″	98°48′46″	98°38′37″	98°37′26″	98°37′26″	98°38′37″	98°36′38″
Altitude (m):		3080	3080	3960	3960	4170	n.d.	2970	3680	2550	3680	3520	3520	3680	3700
Distance from crater:		8 km NE	8 km NE	3·6 km N	3·6 km N	2 km NNW	14·2 km S	9·7 km NE	7·5 km N	24·6 km NW	7 km N	7·2 km N	7·2 km N	7 km N	7·8 km NNE
wt %	Detection limits														
SiO_2		63·06	63·23	61·36	61·36	62·89	63·01	37·59	41·21	56·12	60·29	61·83	63·26	81·74	n.d.
TiO_2		0·63	0·71	0·75	0·73	0·77	0·77	0·18	0·93	0·86	0·83	0·92	0·74	0·30	n.d.
Al_2O_3		15·84	16·28	16·22	15·50	15·41	16·25	20·37	10·21	18·24	16·12	11·81	16·35	7·65	n.d.
Fe_2O_3(tot)		4·90	5·11	5·13	4·61	4·99	4·96	3·19	3·15	7·52	5·90	6·11	5·10	2·14	n.d.
MnO		0·08	0·08	0·06	0·04	0·05	0·06	0·05	0·07	0·12	0·09	0·06	0·08	0·02	n.d.
MgO		2·06	3·39	2·72	1·58	2·40	2·62	22·27	31·89	4·04	5·15	3·39	3·79	1·15	n.d.
CaO		4·27	4·96	4·82	4·80	4·27	4·59	17·13	13·03	7·09	5·79	12·69	5·07	5·87	n.d.
Na_2O		4·40	4·36	4·10	3·39	3·63	4·20	0·02	<0·01	3·95	4·16	2·51	4·39	0·97	n.d.
K_2O		1·91	1·75	1·68	1·46	1·65	1·66	<0·01	<0·01	1·47	1·54	1·49	1·79	0·63	n.d.
P_2O_5		0·16	0·17	0·16	0·17	0·17	0·17	<0·01	<0·01	0·17	0·19	0·14	0·18	0·06	n.d.
LOI		0·22	0·08	2·22	5·69	3·08	1·63	0·12	0·17	0·64	<0·01	<0·01	<0·01	<0·01	n.d.
Total		97·54	100·12	99·24	99·34	99·31	99·91	100·90	100·67	100·20	99·92	100·79	100·58	100·51	n.d.
ppm															
Sc		9	12	12	12	12	12	1	3	18	25	16	12	8	n.d.
Be		1	1	2	2	1	1	<1	<1	1	1	1	1	<1	n.d.
V		82	100	88	86	95	97	14	<5	190	109	152	91	48	n.d.
Cr		62	118	35	52	65	43	<10	<10	<10	194	115	98	<10	n.d.
Co		11·9	17	15·8	12·3	12·7	13·6	9·6	6·4	19·3	18·7	15·5	14·1	6·6	n.d.
Ni*	(†5)	28	69	66†	51†	59†	43†	14	16	26	124	38	86	13	n.d.
Cu*	(†5)	17	18	19†	30†	23†	21†	9	9	56	6	12	3	4	n.d.
Zn*	(†2)	75	73	183†	80†	59†	74†	17	17	95	63	81	65	26	n.d.
Ga		21	21	22	19	21	22	26	13	22	20	22	20	9	n.d.
Rb		59·8	54·1	43·0	40·7	38·0	41·5	1·0	1·3	34·7	45·2	37·4	49·1	21·0	n.d.
Sr	(‡1·8%)	448·2	465·6	452·9	447·9	435·7	463·5	27·4	20·5	526·6	451·9	500·0	430·8	222·5	274·9‡

Suite:	Popocatépetl													
Sample:	96D3 B	96D3-Com	9501	9601K	9602K	9603K	9463A	9593B	96341B	9490B	95142A	95142C	9490C	0401m
Location:	Near Bon-sai seism. stat.	Near Bon-sai seism. stat.	Tlamacaz	Tlamacaz	Refugio El Canario	Tochimilco	E San Pedro Nexapa	W Buenavista	Cerro Chincon-quiat	Paso de Cortés	E Paso de Cortés	E Paso de Cortés	Paso de Cortés	W Buenavista
Rock type:	Dome fragm., 30.4.1996	Dome fragm., 30.4.1996	Ash January 1995	Ash 5.3.1996	Ash 10.3.1996	Ash 11./12.3.1996	Xenolith Skarn in Tutti Frutti pumice	Xenolith Skarn in TF pum.	Xenolith foliated granodior. in TF pum.	Xenolith Granodior. in TF pum.	Xenolith Metasdst. in TF pum.	Xenolith Px-grano-diorite in TF pum.	Xenolith Metasdst. in TF pum.	Xenolith Marble in TF pum.
Mineralogy:	pl>2px>ol	pl>2px>ol	n.d.	n.d.	n.d.	n.d.	pl-2px-bi-qz	n.d.	pl-qz-hb>bi-ox	n.d.	n.d.	pl>2px>ol-ox-qz	qz>pl=2px	n.d.
Latitude N:	19°02′59″	19°02′59″	19°03′20″	19°03′20″	19°02′28″	18°54′22″	19°04′31″	19°05′21″	19°10′33″	19°05′13″	19°05′34″	19°05′34″	19°05′13″	19°05′13″
Longitude W:	98°33′36″	98°33′36″	98°37′57″	98°37′57″	98°37′41″	98°33′50″	98°42′21″	98°36′38″	98°48′46″	98°38′37″	98°37′26″	98°37′26″	98°38′37″	98°36′38″
Altitude (m):	3080	3080	3960	3960	4170	n.d.	2970	3680	2550	3680	3520	3520	3680	3700
Distance from crater:	8 km NE	8 km NE	3·6 km N	3·6 km N	2 km NNW	14·2 km S	9·7 km NE	7·5 km N	24·6 km NW	7 km N	7·2 km N	7·2 km N	7 km N	7·8 km NNE
Y	16·9	18·0	15·9	15·5	15·3	17·2	5·5	9·0	15·2	18·4	24·9	15·8	10·1	n.d.
Zr	139·3	145·1	144·3	137·1	144·3	153·5	11·2	17·2	115·9	159·6	483·4	169·1	99·0	n.d.
Nb	5·08	5·17	5·01	4·56	5·61	5·72	1·22	3·89	4·18	6·18	8·03	4·91	2·84	n.d.
Mo	2·41	1·32	2·07	5·58	3·66	2·60	1·04	0·44	1·71	1·82	0·61	1·62	1·54	n.d.
Cs	3·52	2·91	1·95	2·67	2·53	2·44	0·11	0·08	0·96	1·99	1·45	2·38	1·03	n.d.
Ba	397·7	377·2	397·9	367·8	421·5	441·1	8·5	4·7	446·9	381·2	209·9	426·6	433·3	n.d.
La	15·37	15·23	15·60	14·87	15·39	15·73	4·30	5·46	13·56	17·67	21·44	15·20	7·13	n.d.
Ce	31·71	32·15	31·75	31·53	32·62	33·28	18·64	24·79	30·50	36·71	43·36	31·66	14·34	n.d.
Pr	3·46	3·57	3·25	3·18	3·46	3·51	1·38	2·43	3·28	3·71	4·38	3·25	1·57	n.d.
Nd (‡2·7%)	15·37	16·32	15·29	14·84	15·91	16·53	6·78	12·15	14·99	17·26	20·67	15·16	7·72	0·54‡
Sm	3·72	3·85	3·50	3·40	3·66	3·73	1·37	2·61	3·20	3·87	4·32	3·35	1·59	n.d.
Eu	1·02	1·11	1·19	0·95	1·04	1·17	0·31	0·51	1·05	1·16	1·09	1·03	0·45	n.d.
Gd	3·37	3·56	3·22	3·58	3·29	3·31	1·24	2·19	3·31	4·39	4·85	3·28	1·70	n.d.
Tb	0·45	0·49	0·60	0·47	0·63	0·70	0·23	0·34	0·55	0·68	0·78	0·56	0·28	n.d.
Dy	2·82	3·14	2·85	2·66	3·21	3·30	0·87	1·58	2·69	3·51	4·06	2·58	1·69	n.d.
Ho	0·58	0·60	0·51	0·50	0·62	0·62	0·20	0·28	0·47	0·56	0·79	0·45	0·36	n.d.
Er	1·68	1·93	1·47	1·53	1·71	1·94	0·55	1·00	1·42	1·85	2·51	1·51	0·95	n.d.
Tm	0·24	0·25	0·20	0·16	0·26	0·26	0·08	0·14	0·15	0·29	0·37	0·18	0·12	n.d.
Yb	1·52	1·70	1·63	1·39	1·61	1·55	0·52	0·99	1·38	1·96	2·65	1·27	1·16	n.d.
Lu	0·249	0·265	0·236	0·254	0·253	0·296	0·084	0·161	0·194	0·243	0·430	0·229	0·155	n.d.
Hf	4·14	4·09	3·68	3·86	4·15	4·14	0·22	1·25	2·98	4·28	11·60	4·38	2·57	n.d.
Ta	0·41	0·36	0·51	0·31	0·42	0·42	0·21	1·17	0·31	0·36	0·50	0·33	0·24	n.d.
Pb	12	9	16	27	13	13	<5	<5	5	8	<5	22	6	n.d.
Th	4·73	4·16	4·88	4·47	4·15	4·22	3·43	18·65	0·95	4·74	6·13	4·65	2·65	n.d.
U	1·87	1·65	1·70	1·66	1·55	1·55	0·17	1·39	0·42	1·87	2·30	1·72	1·91	n.d.
Ba/Nb	78·28	72·96	79·43	80·656	75·14	71·12								n.d.
Ce/Yb	20·86	18·91	19·48	22·68	20·26	21·47								n.d.
Fo av.	81·59													

Table 1: continued

Suite:		SCVF and Valley of Puebla scoria cones													
		Transitional							Alkaline			Primitive calc-alkaline			
Sample:		95385	9476	9428	9430	96333A	96359	96352	96357	96356A	96356B	96353	95103	96365	96354A
Location:		Tomacoco	Cerro Tres Cumbres	Cerro Yoteco	Tecomax-usco	Cerro Tlacuayol	Malpais	La Hoya	Cerro Citlaltepec	Cerro Santa Barbara	Cerro Santa Barbara	Cerro Mirador	Cerro Tecajete (Puebla Valley)	Cerro Pelagatos	Cerro Partido
Rock type:		Scoria	Scoria	Scoria	Lava	Lava	Lava	Scoria	Alk. basalt	Alk.dyke	Alk. basalt	Scoria	Scoria	Lava	Scoria
Mineralogy:		ol>po	opx>ol>ol>ox	pl>2px>ox>po	pl>2px	2px=pl>ol>ox>po	2px>pl>ol>ox	2px>pl	ol	ol	ol	ol	ol>cpx>pl	ol	ol
Latitude N:		19°07′15″	19°01′20″	18°56′22″	18°57′30″	19°04′53″	18°54′57″	19°00′36″	18°58′26″	18°58′57″	18°58′57″	18°58′50″	19°04′02″	19°06′54″	18°59′34″
Longitude W:		98°43′20″	98°48′58″	98°50′02″	98°48′52″	98°50′52″	98°53′05″	98°48′19″	98°56′20″	98°55′28″	98°55′28″	98°53′10″	98°24′03″	98°54′33″	98°53′41″
Altitude (m):		n.d.	2420	1830	2020	2500	1600	2300	1900	1900	1900	2000	2350	2680	1960
Distance from crater:		14·8 km NW	19·1 km W	23·2 km SW	20·6 km SW	23·2 km NW	28·1 km SW	18·6 km W	32·2 km W	31·4 km W	30·5 km W	26·4 km W	22·7 km NE	30 km NW	27·6 km W
wt %	Detection limit														
SiO_2		57·76	59·41	61·31	61·37	63·52	64·13	64·28	51·02	51·83	51·38	54·22	54·44	54·58	54·67
TiO_2		1·06	1·05	0·72	0·66	0·70	0·66	0·68	1·56	1·65	1·65	1·28	1·24	0·80	1·20
Al_2O_3		16·91	15·95	15·77	15·72	16·05	15·38	15·98	16·10	16·09	16·01	16·13	16·42	15·52	15·37
Fe_2O_3(tot)		6·94	6·53	5·25	4·81	4·94	4·75	5·03	9·42	9·16	9·42	8·14	7·97	7·90	8·25
MnO		0·10	0·10	0·08	0·08	0·08	0·07	0·07	0·14	0·13	0·14	0·12	0·12	0·13	0·12
MgO		3·61	4·01	4·57	3·94	3·38	3·50	3·85	8·59	8·11	7·94	7·85	7·44	9·23	8·85
CaO		6·55	5·14	5·07	4·63	4·71	4·61	4·55	8·21	7·82	8·09	7·08	7·27	7·80	7·37
Na_2O		4·21	4·04	4·01	4·22	4·24	3·95	4·28	3·28	3·84	3·86	3·84	3·87	3·26	3·48
K_2O		1·37	2·24	2·12	2·22	1·98	2·23	2·19	0·90	1·29	1·24	1·11	1·35	0·99	1·32
P_2O_5		0·27	0·34	0·21	0·17	0·17	0·16	0·18	0·036	0·45	0·46	0·28	0·29	0·17	0·28
LOI		0·02	0·18	0·95	1·02	0·87	0·23	<0·01	0·012	0·39	<0·01	<0·01	0·16	0·09	<0·01
Total		98·80	99·01	100·06	98·85	100·63	99·66	100·96	99·70	100·75	100·04	99·97	100·56	100·57	100·91
ppm															
Sc		15	15	13	12	12	11	12	24	22	22	20	22	24	21
Be		2	1	1	1	1	2	1	2	2	2	1	2	<1	1
V		129	105	100	90	88	82	89	164	144	167	140	156	153	150
Cr		52	119	220	169	90	98	149	325	192	268	334	336	468	411
Co		16·8	17·3	16·8	16·3	13·1	12·7	15	32·6	29·7	35·2	32·1	29·9	38·2	31·9
Ni*		24	76	115	98	72	85	92	207	193	211	229	134	248	209
Cu*		9	22	27	67	15	25	64	29	34	37	35	27	38	26
Zn*		80	89	66	18	69	62	27	80	80	83	76	78	83	80
Ga		n.d.	23	21	21	21	20	21	19	17	21	20	20	18	19
Rb	(†2)	31†	50·3	55·1	55·9	45·4	75·2	68·2	19·1	19·6	25·3	25·6	30·1	22·5	25·8
Sr	(†2)	557†	424·3	440·1	447·4	386·5	432·6	418·0	437·1	566·6	687·0	496·5	518·0	379·0	475·6

Suite:		SCVF and Valley of Puebla scoria cones													
		Transitional							Alkaline			Primitive calc-alkaline			
Sample:		95385	9476	9428	9430	96333A	96359	96352	96357	96356A	96356B	96353	95103	96365	96354A
Location:		Tomacoco	Cerro Tres Cumbres	Cerro Yoteco	Tecomax-usco	Cerro Tlacuayol	Malpais	La Hoya	Cerro Citlaltepec	Cerro Santa Barbara	Cerro Santa Barbara	Cerro Mirador	Cerro Tecajete (Puebla Valley)	Cerro Pelagatos	Cerro Partido
Rock type:		Scoria	Scoria	Scoria	Lava	Lava	Lava	Scoria	Alk. basalt	Alk.dyke	Alk. basalt	Scoria	Scoria	Lava	Scoria
Mineralogy:		ol>po	opx>ol> ol>ox	pl>2px> ox>po	pl>2px	2px=pl> ol>ox>po	2px>pl> ol>ox	2px>pl	ol	ol	ol	ol	ol> cpx>pl	ol	ol
Latitude N:		19°07′15″	19°01′20″	18°56′22″	18°57′30″	19°04′53″	18°54′57″	19°00′36″	18°58′26″	18°58′57″	18°58′57″	18°58′50″	19°04′02″	19°06′54″	18°59′34″
Longitude W:		98°43′20″	98°48′58″	98°50′02″	98°48′52″	98°50′52″	98°53′05″	98°48′19″	98°56′20″	98°55′28″	98°55′28″	98°53′10″	98°24′03″	98°54′33″	98°53′41″
Altitude (m):		n.d.	2420	1830	2020	2500	1600	2300	1900	1900	1900	2000	2350	2680	1960
Distance from crater:		14·8 km NW	19·1 km W	23·2 km SW	20·6 km SW	23·2 km NW	28·1 km SW	18·6 km W	32·2 km W	31·4 km W	30·5 km W	26·4 km W	22·7 km NE	30 km NW	27·6 km W
Y	(†1)	22†	25·1	16·3	15·8	15·5	17·0	17·0	24·8	24·4	28·7	21·5	24·5	18·1	21·5
Zr	(†5)	183†	268·9	160·7	145·5	145·8	175·3	174·3	195·9	174·5	211·8	161·3	155·4	111·2	148·4
Nb		n.d.	13·19	5·40	4·54	4·37	5·63	5·58	15·60	13·11	16·04	10·94	10·17	3·85	10·14
Mo		n.d.	2·56	3·43	2·34	2·03	2·07	2·49	1·37	1·04	1·66	1·31	3·21	1·38	2·19
Cs	(†0·5)	1·10	2·14	3·64	3·34	2·48	4·77	4·48	0·57	0·42	0·61	1·07	1·55	1·09	1·06
Ba	(†3)	363†	626·3	486·2	449·4	446·0	429·8	434·2	269·8	373·0	460·1	286·7	330·6	238·3	336·7
La		19·10	32·11	19·82	18·45	16·55	18·63	19·10	22·34	25·33	31·70	18·28	20·28	12·43	20·28
Ce		44·00	63·72	42·70	37·76	33·15	39·74	38·89	45·12	54·61	69·22	38·25	43·67	27·41	43·09
Pr		n.d.	6·12	4·29	3·92	3·26	3·79	4·09	4·78	6·12	7·14	3·99	4·46	3·27	4·77
Nd		22·00	28·06	20·75	18·33	14·92	18·67	18·25	21·39	29·04	33·55	19·04	20·78	14·94	21·65
Sm		4·94	6·67	5·11	4·77	3·56	3·92	3·93	4·35	6·35	8·08	4·50	5·69	3·64	5·29
Eu		1·54	1·89	1·35	1·20	1·12	1·02	1·03	1·74	1·87	2·32	1·39	1·54	1·08	1·41
Gd		n.d.	5·52	4·20	3·72	3·26	3·56	3·45	5·24	5·39	6·64	4·65	4·73	3·34	4·46
Tb		0·80	0·83	0·65	0·58	0·53	0·56	0·61	0·88	0·85	1·08	0·79	0·83	0·53	0·73
Dy		n.d.	4·40	2·95	2·47	3·05	3·02	2·95	4·58	4·45	5·11	4·41	4·40	3·27	3·91
Ho		n.d.	0·88	0·57	0·48	0·51	0·58	0·61	0·87	0·81	0·94	0·84	0·82	0·63	0·75
Er		n.d.	2·30	1·77	1·54	1·47	1·49	1·80	2·87	2·53	2·99	2·15	2·62	1·96	2·22
Tm		n.d.	0·35	0·20	0·21	0·22	0·21	0·21	0·37	0·28	0·40	0·24	0·32	0·25	0·28
Yb		2·28	2·20	1·67	1·14	1·64	1·48	1·84	2·46	2·18	2·65	2·18	2·09	1·78	2·02
Lu		0·30	0·327	0·210	0·223	0·200	0·214	0·252	0·399	0·322	0·403	0·331	0·342	0·276	0·278
Hf		4·60	6·08	4·77	4·06	3·73	4·59	4·84	4·35	3·92	4·66	3·83	3·60	3·27	3·57
Ta		0·70	0·81	0·41	0·36	0·34	0·45	0·43	1·00	0·81	0·95	0·75	0·62	0·24	0·58
Pb		12	15	11	7	8	16	16	6	<5	8	<5	<5	<5	9
Th	(†0·1)	2·9†	5·15	5·98	5·76	4·21	7·39	7·58	2·77	2·96	3·67	2·95	3·40	2·38	3·53
U	(†0·1)	1·3†	1·46	2·29	2·08	1·61	3·45	2·84	0·78	0·85	1·10	0·97	1·05	0·63	0·90
Ba/Nb			47·49	90·03	98·98	105·06	76·34	77·82	17·30	28·45	28·69	26·21	32·51	61·89	33·20
Ce/Yb		19·30	28·96	25·57	33·12	20·21	26·85	21·14	18·34	25·05	26·12	17·55	20·90	15·40	21·33
Fo av.											86·2		86·4	88·0	87·5

Table 1: continued

Suite:	SCVF scoria cones													
Sample:	96331A	96355	96348	96332	96347	96343	95110	96358	95107	96340	96335	96338	96336A	96339
Location:	Volcán Atlacorra	Cerro Xexquixtle	Loma Sa-cramento	Volcán Amoloc	Loma Sa-cramento	Cerro Cocotitlán	Quarry N Tenango	Quarry N Xochitlán	Volcán Aholo	Cerro Tepeixte	Cerro Xoyacán	N Cerro La Joya	Cerro La Joya	Cerro Tenayo
Rock type:	Scoria	Scoria	Scoria	Scoria	Scoria	Scoria	Scoria	Scoria	Scoria	Scoria	Lava	Lava	Scoria	Scoria
Mineralogy:	ol	ol	ol	ol	ol	ol>cpx>pl	ol>cpx>pl	ol>2px	ol	ol	2px>pl	pl>ol	ol	ol
Latitude N:	19°06′32″	18°59′03″	19°02′40″	19°06′34″	19°02′51″	19°14′22″	19°09′50″	18°53′56″	19°05′22″	19°10′45″	19°05′47″	19°11′18″	19°10′52″	19°11′07″
Longitude W:	98°53′27″	98°54′08″	98°53′17″	98°52′17″	98°53′33″	98°51′59″	98°51′27″	98°48′28″	98°51′10″	98°48′10″	98°48′25″	98°47′57″	98°47′46″	98°48′46″
Altitude (m):	2600	2000	3000	2600	3300	2235	2320	1800	2660	2475	2600	2430	2450	2520
Distance from crater:	28·4 km NW	27·8 km W	26·8 km W	26·5 km NW	27 km W	33·2 km NW	27·4 km NW	23 km SW	24·1 km NW	23·8 km NW	19·7 km NW	24·7 km NW	23·4 km NW	25·9 km NW
wt %														
SiO_2	54·72	55·03	55·71	55·75	55·77	56·19	56·45	56·59	57·44	57·64	57·68	57·71	57·73	58·53
TiO_2	1·02	1·20	1·09	1·47	1·11	1·31	1·14	1·00	0·96	1·20	1·25	1·18	1·18	1·29
Al_2O_3	16·66	15·70	16·71	16·21	17·00	16·59	15·30	14·78	16·15	15·71	15·97	15·79	15·82	15·85
Fe_2O_3(tot)	7·70	7·11	7·75	8·22	7·79	7·76	7·42	6·97	7·08	7·67	7·52	7·38	6·91	7·46
MnO	0·12	0·12	0·12	0·13	0·12	0·11	0·12	0·10	0·11	0·12	0·12	0·11	0·11	0·12
MgO	7·30	8·08	6·60	5·86	6·74	6·02	5·47	8·13	6·21	6·58	4·72	6·30	6·45	5·62
CaO	7·02	7·10	7·20	6·75	7·30	7·00	6·99	6·89	6·43	6·75	6·04	6·50	6·56	6·36
Na_2O	3·79	3·43	3·72	3·73	3·72	3·77	3·73	3·53	3·93	3·79	3·86	3·69	3·74	3·91
K_2O	1·07	1·16	1·32	1·65	1·23	1·66	1·61	1·19	1·33	1·47	1·77	1·51	1·50	1·77
P_2O_5	0·20	0·23	0·21	0·42	0·21	0·34	0·43	0·23	0·22	0·32	0·50	0·30	0·28	0·43
LOI	0·04	0·11	0·27	0·20	<0·01	0·20	<0·01	0·52	<0·01	<0·01	0·30	0·43	0·48	<0·01
Total	99·66	99·26	100·70	100·40	100·99	100·96	98·53	99·94	99·48	100·83	99·73	100·89	100·77	100·91
ppm														
Sc	22	22	21	21	21	20	18	18	18	19	17	19	19	18
Be	n.d.	1	1	2	1	2	2	1	1	2	2	1	1	2
V	161	151	145	143	144	130	124	118	132	130	130	130	129	134
Cr	397	399	205	203	241	170	205	363	297	281	142	257	264	181
Co	29·4	25·5	24·8	24·6	26·7	22·9	22·0	27·4	24·2	25·9	20·4	24·9	24·5	22·4
Ni*	174	179	137	81	136	97	110	232	161	130	69	124	131	132
Cu*	30	23	24	19	25	20	23	25	29	22	19	19	23	24
Zn*	72	77	70	87	71	75	91	71	77	79	90	76	80	87
Ga	21	19	18	22	19	21	20	19	22	20	24	21	21	22
Rb	20·3	29·7	26·5	34·8	27·8	31·1	39·2	25·4	29·3	32·7	41·1	32·4	33·2	35·5
Sr	373·3	446·3	389·5	384·0	421·8	450·6	434·0	471·6	420·7	516·3	457·9	504·0	528·8	618·3
Y	21·4	24·1	21·0	27·6	23·4	23·5	28·8	18·0	20·6	24·7	30·3	23·8	24·6	28·4

Suite:	SCVF scoria cones													
Sample:	96331A	96355	96348	96332	96347	96343	95110	96358	95107	96340	96335	96338	96336A	96339
Location:	Volcán Atlacorra	Cerro Xexquixtle	Loma Sacramento	Volcán Amoloc	Loma Sacramento	Cerro Cocotitlán	Quarry N Tenango	Quarry N Xochitlán	Volcán Aholo	Cerro Tepeixte	Cerro Xoyacán	N Cerro La Joya	Cerro La Joya	Cerro Tenayo
Rock type:	Scoria	Scoria	Scoria	Scoria	Scoria	Scoria	Scoria	Scoria	Scoria	Scoria	Lava	Lava	Scoria	Scoria
Mineralogy:	ol	ol	ol	ol	ol	ol>cpx>pl	ol>cpx>pl	ol>2px	ol	ol	2px>pl	pl>ol	ol	ol
Latitude N:	19°06′32″	18°59′03″	19°02′40″	19°06′34″	19°02′51″	19°14′22″	19°09′50″	18°53′56″	19°05′22″	19°10′45″	19°05′47″	19°11′18″	19°10′52″	19°11′07″
Longitude W:	98°53′27″	98°54′08″	98°53′17″	98°52′17″	98°53′33″	98°51′59″	98°51′27″	98°48′28″	98°51′10″	98°48′10″	98°48′25″	98°47′57″	98°47′46″	98°48′46″
Altitude (m):	2600	2000	3000	2600	3300	2235	2320	1800	2660	2475	2600	2430	2450	2520
Distance from crater:	28·4 km NW	27·8 km W	26·8 km W	26·5 km NW	27 km W	33·2 km NW	27·4 km NW	23 km SW	24·1 km NW	23·8 km NW	19·7 km NW	24·7 km NW	23·4 km NW	25·9 km NW
Zr	128·0	160·7	148·0	246·9	158·3	184·9	271·5	147·0	141·4	203·7	293·3	204·2	193·1	262·0
Nb	6·23	9·22	6·80	16·61	7·31	11·14	14·85	6·71	6·05	10·18	18·26	10·13	9·84	16·54
Mo	1·91	1·08	0·67	1·28	1·27	1·20	2·30	1·32	2·23	2·87	2·89	3·02	1·74	1·59
Cs	0·87	1·44	1·05	1·61	1·32	0·96	1·39	1·10	1·35	1·37	1·70	1·48	1·84	1·45
Ba	247·9	307·8	297·9	448·3	353·0	383·6	500·2	383·4	333·0	435·6	566·2	460·1	448·3	524·7
La	12·83	19·25	15·61	29·42	19·01	24·43	33·59	15·52	16·19	25·75	36·54	27·24	27·11	34·21
Ce	26·23	42·28	33·27	60·21	38·24	49·59	70·36	33·61	34·28	54·33	74·77	55·88	57·14	72·60
Pr	2·97	4·32	3·43	6·04	4·20	5·03	7·00	3·31	3·60	5·51	7·13	5·71	5·74	7·08
Nd	16·19	22·47	17·20	28·77	19·08	24·47	32·24	16·07	18·07	26·01	35·36	25·54	25·44	32·89
Sm	4·12	4·31	4·02	6·93	4·24	5·02	7·06	3·38	4·20	5·56	7·19	5·64	5·49	7·55
Eu	1·42	1·44	1·07	1·87	1·31	1·76	1·95	1·25	1·37	1·62	2·17	1·78	1·84	2·00
Gd	4·36	5·22	3·84	6·55	4·38	5·44	6·79	3·83	4·23	5·17	7·51	5·58	5·47	7·02
Tb	0·64	0·85	0·69	1·06	0·80	0·85	1·12	0·61	0·71	0·76	1·12	0·82	0·88	1·04
Dy	3·75	4·38	3·89	5·39	4·34	4·56	5·40	3·26	3·73	4·38	5·64	4·27	4·83	5·37
Ho	0·76	0·84	0·70	1·02	0·76	0·87	0·99	0·58	0·73	0·80	1·03	0·83	0·85	0·95
Er	2·16	2·26	2·14	2·91	2·43	2·45	3·03	1·75	1·83	2·28	2·89	2·38	2·58	2·78
Tm	0·31	0·32	0·27	0·42	0·34	0·30	0·43	0·27	0·30	0·36	0·44	0·36	0·33	0·32
Yb	2·07	2·04	1·90	2·71	2·22	2·17	2·31	1·49	2·24	2·11	2·58	2·33	2·17	2·63
Lu	0·305	0·322	0·283	0·399	0·343	0·359	0·421	0·233	0·281	0·340	0·412	0·339	0·318	0·379
Hf	3·28	4·17	3·80	5·58	3·72	4·23	5·98	3·47	3·73	4·91	6·39	5·07	4·74	5·73
Ta	0·36	0·58	0·42	0·91	0·42	0·70	0·89	0·42	0·39	0·60	1·01	0·60	0·59	0·96
Pb	6	<5	<5	<5	6	10	9	<5	8	10	13	10	<5	5
Th	2·14	3·58	2·99	4·08	3·22	3·98	4·59	2·92	3·17	4·27	5·11	4·58	4·33	5·23
U	0·66	0·98	0·81	1·33	0·98	0·95	1·43	0·88	1·03	1·27	1·39	1·27	1·24	1·39
Ba/Nb	39·79	33·39	43·80	26·99	48·29	34·53	33·68	57·14	55·04	42·79	31·01	45·42	45·56	31·73
Ce/Yb	13·64	20·73	17·51	22·22	17·23	22·85	30·46	22·56	15·30	25·75	28·98	23·98	26·33	27·60
Fo av.							83·8		85·6					

Table 1: continued

Suite:	SCVF and Valley of Puebla scoria cones												
Sample:	96342A	95367	95106	96350A	96344	96349	9598	96345	96366	96336B	96341A	96351	96346
Location:	near Tenayo	Cerro Zapotecas (Puebla Valley)	Volcán Cuauhtépetl	Cerro Escobeta	NW Tenango	Cerro La Mesa	Loma Te-penasco	Volcán Xoyasal	Cerro Zoceyuca	Cerro La Joya	Cerro Chiconquiat	La Atlaxeligia	Loma Talapaxco
Rock type:	Lava	Scoria	Scoria	Scoria	Lava	Scoria	Scoria	Scoria	Scoria	Scoria	Scoria	Lava	Lava
Mineralogy:	ol>opx	ol=2px	ol	ol=opx	ol>opx>pl	2px	ol>opx>po	2px>pl	ol=2px	2px>pl-hb	2px>pl	2px	opx>ol
Latitude N:	19°12′26″	19°04′40″	19°04′08″	19°01′42″	19°11′06″	19°01′43″	19°07′40″	19°03′33″	19°08′01″	19°10′52″	19°10′33″	19°02′50″	19°03′33″
Longitude W:	98°49′34″	98°20′02″	98°51′28″	98°52′04″	98°52′20″	98°52′30″	98°48′58″	98°53′33″	98°54′02″	98°47′46″	98°48′46″	98°52′00″	98°53′34″
Altitude (m):	2320	2300	2580	2600	2250	2600	2500	3200	2600	2450	2550	2420	3200
Distance from crater:	28·4 km NW	28·9 km NE	23·8 km NW	24·3 km W	31·1 km NW	25·4 km W	22·2 km NW	27 km W	30·8 km NW	23·4 km NW	24·6 km NW	24·6 km W	28·1 km W
wt %													
SiO_2	58·78	59·27	59·30	59·36	59·53	60·10	60·14	60·44	61·18	61·60	62·38	62·72	63·37
TiO_2	1·26	1·03	0·90	0·90	1·08	0·88	1·08	0·94	0·81	0·87	0·85	0·70	0·69
Al_2O_3	15·59	16·02	16·19	16·90	16·01	16·60	16·34	16·05	15·25	15·90	15·67	15·76	16·00
Fe_2O_3(tot)	7·32	6·47	6·33	6·44	6·68	6·41	6·35	5·90	5·57	5·87	5·69	5·29	5·02
MnO	0·11	0·10	0·10	0·10	0·10	0·10	0·10	0·09	0·09	0·10	0·10	0·08	0·08
MgO	5·52	5·14	5·36	5·00	4·95	4·66	4·61	4·77	5·83	4·71	4·62	4·44	3·80
CaO	6·34	5·76	5·64	6·24	6·09	5·95	5·34	5·75	5·31	5·45	5·83	4·83	4·53
Na_2O	3·93	3·89	3·98	3·64	3·90	3·72	4·19	3·87	4·03	3·92	3·92	4·06	4·20
K_2O	1·91	1·56	1·61	1·39	1·78	1·68	1·97	1·65	1·51	1·73	1·62	2·02	2·14
P_2O_5	0·45	0·25	0·22	0·15	0·31	0·17	0·27	0·19	0·21	0·22	0·19	0·19	0·20
LOI	<0·01	0·45	0·68	0·60	0·40	0·58	0·22	1·27	−0·11	0·12	<0·01	0·80	0·96
Total	100·85	99·95	100·32	100·71	100·83	100·85	100·61	100·90	99·77	100·47	100·74	100·89	100·99
ppm													
Sc	17	16	16	18	16	17	15	13	13	15	15	13	11
Be	2	2	2	2	1	1	2	1	1	2	2	1	1
V	122	121	104	117	120	129	110	102	99	112	97	91	87
Cr	194	192	166	181	193	160	166	166	261	183	180	195	143
Co	21·8	23·2	17·7	17·8	21·8	19·8	19·2	18·0	24·7	17·9	14·3	16·8	14·7
Ni*	149	116	139	60	97	51	117	123	186	109	100	136	106
Cu*	27	85	73	16	19	16	21	15	22	21	19	22	15
Zn*	85	22	20	77	77	71	77	70	68	75	71	72	71
Ga	22	20	17	20	21	21	23	22	19	21	20	22	22
Rb	35·6	38·8	30·3	29·8	40·6	38·8	43·4	39·2	43·0	40·6	41·6	44·5	46·5
Sr	721·8	481·5	382·4	390·2	464·5	381·3	407·1	550·9	583·3	471·4	476·7	461·3	496·0
Y	27·1	19·8	19·2	19·8	23·5	21·2	22·4	19·9	17·3	20·9	19·6	17·5	17·5
Zr	254·8	157·1	150·6	146·9	230·5	143·7	208·3	192·6	148·8	176·2	160·7	164·6	170·9
Nb	13·95	7·30	5·79	4·79	13·03	4·78	10·99	8·25	6·05	5·99	5·70	5·21	5·53

Suite:	SCVF and Valley of Puebla scoria cones												
Sample:	96342A	95367	95106	96350A	96344	96349	9598	96345	96366	96336B	96341A	96351	96346
Location:	near Tenayo	Cerro Zapotecas (Puebla Valley)	Volcán Cuauhtépetl	Cerro Escobeta	NW Tenango	Cerro La Mesa	Loma Te-penasco	Volcán Xoyasal	Cerro Zoceyuca	Cerro La Joya	Cerro Chiconquiat	La Atlaxeligia	Loma Talapaxco
Rock type:	Lava	Scoria	Scoria	Scoria	Lava	Scoria	Scoria	Scoria	Scoria	Scoria	Scoria	Lava	Lava
Mineralogy:	ol>opx	ol=2px	ol	ol=opx	ol>opx>pl	2px	ol>opx>po	2px>pl	ol=2px	2px>pl-hb	2px>pl	2px	opx>ol
Latitude N:	19°12′26″	19°04′40″	19°04′08″	19°01′42″	19°11′06″	19°01′43″	19°07′40″	19°03′33″	19°08′01″	19°10′52″	19°10′33″	19°02′50″	19°03′33″
Longitude W:	98°49′34″	98°20′02″	98°51′28″	98°52′04″	98°52′20″	98°52′30″	98°48′58″	98°53′33″	98°54′02″	98°47′46″	98°48′46″	98°52′00″	98°53′34″
Altitude (m):	2320	2300	2580	2600	2250	2600	2500	3200	2600	2450	2550	2420	3200
Distance from crater:	28·4 km NW	28·9 km NE	23·8 km NW	24·3 km W	31·1 km NW	25·4 km W	22·2 km NW	27 km W	30·8 km NW	23·4 km NW	24·6 km NW	24·6 km W	28·1 km W
Mo	2·05	1·70	1·44	1·81	2·77	0·94	2·79	1·97	1·70	2·77	1·89	1·12	2·17
Cs	1·24	1·88	1·47	1·52	1·41	2·05	1·68	1·56	2·23	1·77	1·83	2·45	2·43
Ba	613·4	414·3	333·9	397·1	515·3	381·3	509·0	509·5	396·6	491·5	511·8	527·2	566·4
La	38·02	18·67	14·43	18·96	27·75	19·71	26·48	25·02	18·68	23·21	22·04	21·78	23·65
Ce	79·32	39·46	30·70	37·38	56·92	35·27	54·55	51·27	39·24	47·23	44·91	44·03	47·68
Pr	8·20	4·40	3·14	4·02	5·65	3·78	5·27	4·98	4·27	4·69	4·54	4·10	4·82
Nd	36·37	20·54	16·20	18·44	26·06	18·76	25·27	24·10	19·45	22·36	19·41	20·18	21·92
Sm	7·83	4·73	3·76	4·21	5·76	3·75	5·57	5·58	4·36	4·77	4·43	3·94	4·45
Eu	2·22	1·41	1·17	1·27	1·51	1·23	1·63	1·54	1·31	1·38	1·31	1·27	1·48
Gd	7·36	4·36	3·79	4·08	4·98	4·10	5·19	5·24	3·81	4·26	4·45	4·03	4·19
Tb	1·06	0·61	0·54	0·72	0·75	0·67	0·74	0·68	0·54	0·67	0·67	0·63	0·62
Dy	5·20	3·51	3·16	3·74	4·49	3·49	4·13	3·76	3·05	3·40	3·43	3·13	3·18
Ho	1·03	0·70	0·67	0·70	0·82	0·70	0·80	0·63	0·59	0·67	0·67	0·66	0·62
Er	2·98	2·05	1·71	2·06	2·39	1·99	2·41	1·99	1·81	2·06	1·93	1·80	1·52
Tm	0·36	0·26	0·30	0·23	0·35	0·26	0·28	0·30	0·23	0·30	0·25	0·19	0·20
Yb	2·56	1·71	1·71	1·69	1·95	1·81	2·21	1·61	1·63	1·89	1·64	1·47	1·41
Lu	0·362	0·282	0·287	0·273	0·341	0·285	0·334	0·224	0·251	0·281	0·253	0·227	0·207
Hf	5·87	4·33	3·52	3·78	5·29	4·01	5·22	4·97	4·04	4·11	3·92	4·16	4·59
Ta	0·78	0·50	0·36	0·41	0·79	0·32	0·76	0·50	0·44	0·35	0·32	0·38	0·36
Pb	7	8	6	<5	6	11	13	8	9	12	<5	8	12
Th	5·68	3·56	3·19	4·09	4·93	3·91	5·16	4·85	3·90	4·83	4·72	5·34	5·61
U	1·62	1·17	0·85	1·38	1·32	1·32	1·44	1·30	1·33	1·31	1·47	1·83	1·87
Ba/Nb	43·97	56·76	57·66	82·91	39·55	79·77	46·31	61·75	65·55	82·06	89·80	101·18	102·43
Ce/Yb	30·98	23·08	17·95	22·12	29·19	19·49	24·68	31·84	24·07	24·99	27·38	29·95	33·82
Fo av.			85·2										

Major elements, Sc and Be determined by fusion ICP-ES; trace elements determined by fusion ICP-MS. pl, plagioclase; ol, olivine; px, pyroxene; ox, (FeTi)oxides; qz, quartz; hb, hornblende; bi, biotite; po, pyrrhotite; n.d., not determined; LOI, loss on ignition. Fo contents were detected by ion microprobe analysis.
*Total fusion ICP-MS.
†Fusion ICP-MS with different detection limits.
‡Isotope dilution mass spectrometry (at LUGIS; reproducibility for Nd and Sr concentrations).

The seven Popocatépetl pumices were sampled from radiocarbon-dated stratigraphic layers ranging between 1·100 and 23 ka BP (Fig. 3). Five of these samples were collected from the Paso de Cortés area on the north–NE flanks of the volcano and derived from Plinian eruptions. We have distinguished Plinian pumices according to their different colour hues [pink, yellow–brown (Lorenzo), ochre, Tutti Frutti, milky, grey, and white; Fig. 3]. A major phreato-plinian eruption occurred around 14 ka BP and produced a complex sequence of pyroclastic flow and fall deposits. Pumice fallout layers include the 'grey' and 'milky' pumices at the base of the sequence and culminated with the emplacement of the 'Tutti Frutti' Plinian fall deposit. This deposit, which was formerly called 'Pómez con andesita' by Mooser (1967), is one of the most distinctive units around the volcano and represents a unique stratigraphic marker in the Basin of Mexico and the SCVF. It consists of a heterolithological fall breccia that includes orange juvenile andesitic pumice and xenolithic clasts of granodiorite, pale green metamorphic siltstone, dark green skarn, whitish marble and other fragments from the local basement.

Lavas were sampled from the Nealtican flow (*c.* 2·150 ka BP; Siebe *et al.*, 1997) at the eastern flank of the volcano and from the *c.* 20 ka BP Tochimilco flow SE of the present summit (Fig. 2). Ash from the March 5 and 11, 1996, fallout deposits and ballistic fragments from the dome explosions on April 30, 1996, and on June 30, 1997, were sampled in the field shortly after deposition. Scoria clasts from the small January 22, 2001 pyroclastic-flow deposit were collected 2·5 km north of the cone (Fig. 2). These scoria clasts contain enclaves from earlier young domes including angular dense fragments as well as pumice fragments from the dome carapaces (Fig. 4b).

ANALYTICAL PROCEDURES

From all 82 samples thin sections were prepared for petrographic study. Reconnaissance electron microprobe analysis (EMPA) was conducted for all major minerals and glass, but here we focus on compositions of olivine (Fo) and matrix glass and glass inclusions for selected samples. EMPA was carried out at the Department of Geological Sciences at the University of Manitoba, Winnipeg, Canada, using a Cameca SX-50 electron microprobe equipped with three wavelength-dispersive X-ray (WDX) spectrometers and one energy-dispersive (EDX) spectrometer. Mineral and glass analyses were acquired using specific programs of standardization and secondary standards were used to monitor analysis quality. Wavelength-dispersive EMPA data for minerals and glass were obtained at 15 keV accelerating potential (20 keV for sulphides) with a 15 nA (20 nA for olivine) beam current. Sulphur and chlorine were determined in glass using 200 and 150 s count times, respectively. A beam diameter of 2–5 μm was used for the analyses of minerals, and a defocused electron beam of 10–20 μm was used for the analyses of melt inclusions and matrix glass to avoid loss of X-ray intensities for Na as a result of their migration from the electron beam excitation volume. Analyses of groundmass rich in microphenocrysts (less than ~50 μm length) were carried out using a defocused electron beam 20 μm in diameter and selecting random points in the thin sections to obtain average values of the chemistry. The precision of oxide analyses in olivine were ±0·4 wt % for SiO_2, ±0·2 wt % for MgO and FeO, and no more than ±0·02 wt % for CaO, MnO, and NiO. The precision of sulphur analyses of glass was ±25 ppm based on repeated analysis of standard GL36 with 1200 ppm sulphur, and the averages of analysed values were within ±2% of the recommended values. The precision of chlorine analysis was ±35 ppm based on repeated analysis of standard GL44 with a chlorine concentration of 1300 ppm, and the averages of analysed values were within ±4% of the recommended values. Relative analytical uncertainties (1σ) for major elements estimated by analyses of secondary standards were ±1–2% for Si, Al and Ca, ±2–5% for Fe, Mg and Na, ±5–8% for Ti and K for glasses.

For geochemical and isotope analyses between 5 kg (lava flows) and 150 g (xenoliths) of fresh sample material was crushed in a jawbreaker, ground in a disc mill, split into aliquots, and finally pulverized with a tungsten carbide mill set.

Major and trace element concentrations were determined by fusion inductively coupled plasma-emission spectroscopy (ICP-ES) and inductively coupled plasma-mass spectrometry (ICP-MS) at Activation Laboratories, Ancaster, Canada. Results and detection limits are listed in Table 1.

Twenty-one samples from Popocatépetl and two samples from SCVF scoria cones (Pelagatos and Zoceyuca) were selected for Sr–Nd–Pb isotope analysis, performed at the Laboratorio Universitario de Geoquímica Isotópica (LUGIS), Instituto de Geofisica, UNAM, Mexico City. Sample powders (100–150 mg) were first leached in Teflon bombs with 6N HCl (2 h at 90°C) to remove possible ambient Pb and then dissolved in HF, $HClO_4$, and HCl. Sr and rare earth elements (REE) were separated in quartz-glass columns with DOWEX cation exchange resin, calibrated by atomic absorption spectroscopy. Nd was separated with a different set of smaller columns, filled with Teflon powder coated with hydrogen di-ethylhexyl-phosphate (HDEHP). These columns were calibrated colorimetrically. Pb separation was performed with small Teflon tube columns using DOWEX anion exchange resin. Isotope compositions were measured with a Finnigan MAT 262 thermal ionization mass spectrometer, equipped with a variable multicollector system (eight Faraday cups) in static mode. Samples were loaded as chlorides on double rhenium filaments (Sr and Nd) or as a silicagel–H_3PO_4 mix on single rhenium filaments (Pb) and measured as metallic ions. Sixty isotopic ratios were determined for Sr and Nd, and 100 runs were performed for Pb isotopes. Results were corrected for mass fractionation by normalizing to $^{86}Sr/^{88}Sr = 0{\cdot}1194$ and $^{146}Nd/^{144}Nd = 0{\cdot}7219$. The fractionation factor for Pb isotopic ratios was determined by comparison with the mean value of the Pb NBS 981 standard [$^{206}Pb/^{204}Pb = 16{\cdot}8943 \pm 0{\cdot}05\%$ ($1\sigma_{rel}$); $^{207}Pb/^{204}Pb = 15{\cdot}4300 \pm 0{\cdot}08\%$; $^{208}Pb/^{204}Pb = 36{\cdot}5173 \pm 0{\cdot}11\%$; $n = 105$]. Total blanks during the run of these samples were 7·4 ng for Sr, 2·8 ng for Nd, and 450 pg for Pb.

PETROGRAPHY AND MINERALOGY

Phenocryst assemblages and compositions

Popocatépetl suite

Popocatépetl samples typically have >20 vol. % phenocrysts on a vesicle-free basis. Two distinctive mineral assemblages are represented in our samples: one dominated by plagioclase, orthopyroxene and clinopyroxene, with accessory titanomagnetite and ferrian ilmenite, and the other dominated by amphibole and pyroxene with lesser plagioclase and rare FeTi-oxides. Both assemblages have abundant to sparse apatite needles and FeCu-sulphides as inclusions in other minerals and matrix glass (Table 2). No zircon was observed in any of the samples. Earlier studies confirm that two-pyroxene andesites with abundant plagioclase phenocrysts (>20%) and accessory FeTi-oxides are the most common rock types (Boudal, 1985; Kolisnik, 1990). Crystal aggregates of pyroxene, plagioclase, and FeTi-oxides are common, indicating co-saturation of these phases. Amphibole is present as an important phenocryst in some of the andesites and dacites, most notably in the 23 ka BP and 14 ka BP Plinian sequences that included the white, grey, milky, and Tutti Frutti pumice layers. Amphibole commonly occurs in aggregates with pyroxene and more rarely with plagioclase. However, in the grey, milky, and Tutti Frutti pumices hornblende is euhedral whereas plagioclase is invariably sieve-textured. Pseudomorphs of amphibole replaced by aggregates of FeTi-oxides, pyroxene, and plagioclase ('gabbroic rims') are common in some lavas, implying that amphibole broke down during slower ascent of some magma batches (Jakes & White, 1972; Rutherford & Hill, 1993). Thin 'gabbroic rims' are also present on amphibole in some of the 1996 dome samples (Athanasopoulos, 1997; Fig. 5a).

Olivine grains, interpreted by past workers as xenocrysts related to magma mixing (Boudal, 1985; Kolisnik, 1990), are present in most Popocatépetl samples at low abundance. Olivine compositions from Popocatépetl and surrounding vents are summarized in Fig. 6. Popocatépetl pumice samples have the most Fe-rich olivine compositions, consistent with long residence time of chromite-bearing xenocrysts prior to eruption. Cores of olivine grains that lack orthopyroxene ± FeTi-oxide mantles (Fig. 5b) are typically $Fo_{86–89}$, whereas grains with mantles are invariably of lower Fo content. We argue below that original olivine compositions were typically $>Fo_{83}$, and compositions more Fe-rich than this are due primarily to re-equilibration. The presence of relict chromite inclusions in virtually all olivine grains (Fig. 5b) is consistent with this interpretation (Roeder, 1994). In some amphibole-bearing samples such as the Tutti Frutti pumice, it is common to find amphibole rims and/or earlier-formed orthopyroxene mantles on olivine. This texture suggests long residence time for olivine xenocrysts at chamber depths where amphibole was stable.

Surrounding scoria cones

Mineral assemblages and compositions of SCVF rocks have been described by a number of workers (e.g. Bloomfield, 1975; Nixon, 1989; Swinamer, 1989; Wallace & Carmichael, 1999; Siebe *et al.*, 2004*b*). Our samples were collected within 35 km of Popocatépetl's summit in the easternmost SCVF and Valley of Puebla (see Table 1 for distance from cone). These samples typically contain from 5 to 20 vol. % phenocrysts on a vesicle-free basis (Table 2) and were divided into two groups based on chemical and mineralogical variations. The least evolved samples dominated by olivine and virtually lacking plagioclase phenocrysts are most abundant and designated here as 'flanking vents' (FV), whereas those dominated by pyroxene and plagioclase are considered 'transitional' (T) to Popocatépetl samples based on mineral assemblage, texture, and proximity to the stratocone.

All FV samples have phenocryst assemblages dominated by olivine and pyroxene (Table 2) and virtually all samples with MgO >5·4 wt % contain only olivine phenocrysts (Fig. 5d). Olivine core compositions in FV samples range from Fo_{83} to Fo_{90} (Fig. 6). Compositions become less magnesian as a function of whole-rock MgO and cooling time of the sample (more slowly cooled lavas have more pronounced normal zoning at the rims). Most phenocrysts in flanking vents are unzoned, or normally zoned, as described previously for Pelado, Guespalapa and Chichinautzin monogenetic scoria cone samples by Swinamer (1989) and Siebe *et al.* (2004*b*). Virtually all of the samples dominated by olivine and orthopyroxene phenocrysts lack plagioclase phenocrysts or aggregates of plagioclase with olivine. Instead, they contain sparse to abundant microphenocrysts (<0·4 mm) of plagioclase that appear to have formed during final ascent, eruption, and cooling. A few samples have sparse plagioclase of larger size, but it never occurs in aggregates with olivine.

Table 2: Modal mineralogical data for selected samples

Sample	Suite	% Matrix	% Phenocrysts						Accessory phases			Comments
			Ol	Cpx	Opx	Plag	Ox	Hb	Chr	Ap	S	
95249	P	53·3	no	10·5	8·4	26·3	1·6	no	no	tr	tr	
95254	P	47·4	2·1	6·3	5·3	35·8	1·6	ps	no	tr	tr	Hb → Ox
95263	P	39·1	0·1	7·3	4·4	46·4	2·3	ps	no	tr	tr	Hb → Ox
95281	P	41·2	0·1	6·4	9·0	41·2	1·9	no	no	tr?	tr?	
95284	P	48·1	0·6	6·3	10·0	31·3	2·5	1·2	in(Ol)	tr	tr	Opx → Cpx; Ol → Opx
95296	P	62·7	no	1·2	2·6	32·6	0·7	no	in(Ol)	tr	tr	Opx → Cpx; Ol → Opx
95244	P	57·1	11·4	5·7	no	24·3	1·4	no	tr	tr?	no	Ol–Chr and Plag–Px assemblages
96D	P	63·7	1·4	0·9	5·1	25·6	no	no	in(Ol)	tr	no	Matrix mingling textures
9450p	P	78·9	2·3	1·5	2·1	14·9	0·4	no	in(Ol)	tr	tr	Ol → Opx; complex zoning
9490m,g, 9463tf	P	83	tr	2	2	1	tr	12	in(Ol)	tr	tr	Plag fritted, xenocrystic
9428	T	72·5	0·8	1·9	2·6	21·9	tr	no	in(Ol)	no	no	Opx → Cpx; Ol → Opx; fritted Plag
9430	T	61·1	no	4·0	2·0	31·8	1·0	no	no	no	tr	
9431*	T	55·4	1·2	4·8	3·6	33·7	1·2	no	no	no	tr	
96352	T	88	1	4	5	2	<1	no	in(Ol)	tr	tr	Ol → Opx; reverse zoning; disequilibrium textures
96359	T	83	1	4	6	6	<1	no	in(Ol)	tr	tr	Ol → Opx; reverse zoning; disequilibrium textures
9476	T	83·8	6·3	no	10·0	tr	tr	no	no	no	tr	
95106	FV VM	94	4	no	no	no	no	no	in(Ol)	no	tr	Ol → Px
96331A	FV VM	91	9	no	no	no	no	no	tr	no	tr	
95107	FV VM	85·9	12·1	no	no	no	no	no	tr	no	tr	
95110	FV VM	81·0	12·1	5·2	no	1·7	no	no	tr	no	tr	
96341A	FV VM	92·9	no	2·8	3·6	0·7	no	no	no	tr	tr	Complex zoning in Opx
96344	FV VM	95·5	3·0	no	1·0	0·5	no	no	in(Ol)	tr?	tr	Ol → Opx
96366	FV VM	84	8	2	6	no	tr	no	no	no	tr	Opx → Cpx
96338	FV VM	98·6	0·3	no	no	0·7	no	no	tr	no	vp	Ol → Px
96367	FV VP	80	10	3	7	no	tr	no	in(Ol)	no?	tr	Ol → Opx
96356A	FV VM(AB)	93	7	no	no	no	no	no	tr	no	tr	
95103	FV VP(pBA)	86·4	10·7	2·6	no	0·4	no	no	no	no	tr	
96354A	FV VM(pBA)	90·7	7·7	no	no	0·2	no	no	tr	no	tr	
96365	FV VM(pBA)	88	12	no	no	no	no	no	tr	no	tr	rare Plag fritted, xenocrystic

Point counts shown to nearest 0·1%; visual estimates shown to nearest 1%. All estimates on a vesicle-free basis; matrix crystals <0·4 mm; 96D is average of two samples of 1996 dome (Athanasopoulos, 1997). Ol, olivine; Cpx, clinopyroxene; Opx, orthopyroxene; Plag, plagioclase; Ox, FeTi-oxide; Hb, hornblende; Chr, chromite; Ap, apatite; S, sulphide; tr, trace amounts observed; no, not observed; ps, pseudomorphs; in( ), inclusion in mineral in parentheses; vp, vapor phase in cavities. Suites: P, Popocatépetl; T, transitional cones; FV, flanking vents; VM, Valley of Mexico (SCVF) cones; VP, Valley of Puebla cones; AB, alkali basalt; pBA, primitive basaltic andesite. →, reaction of one phase to another.
*Sample analysed only for petrography.

The general paucity of plagioclase phenocrysts in SCVF samples has been noted by previous workers, and distinguishes this suite from most other calc-alkaline rocks (e.g. Swinamer, 1989; Siebe *et al.*, 2004*b*). Accessory minerals in FV samples are chromite and FeCu-sulphides (inclusions in phenocrysts and as globules and blades in matrix glass; Larocque *et al.*, 1998). Chromite is present both as inclusions in olivine and in the groundmass, where it is commonly rimmed by titanomagnetite. Apatite needles are rare to absent, and zircon is not observed. Quartz xenocrysts are commonly present in trace abundance, especially in some more evolved samples.

Rocks described as 'transitional' (T) SCVF samples were collected mostly within 28 km of Popocatépetl (Fig. 2 and Table 1). They exhibit more complex mineralogical and compositional variations as well as

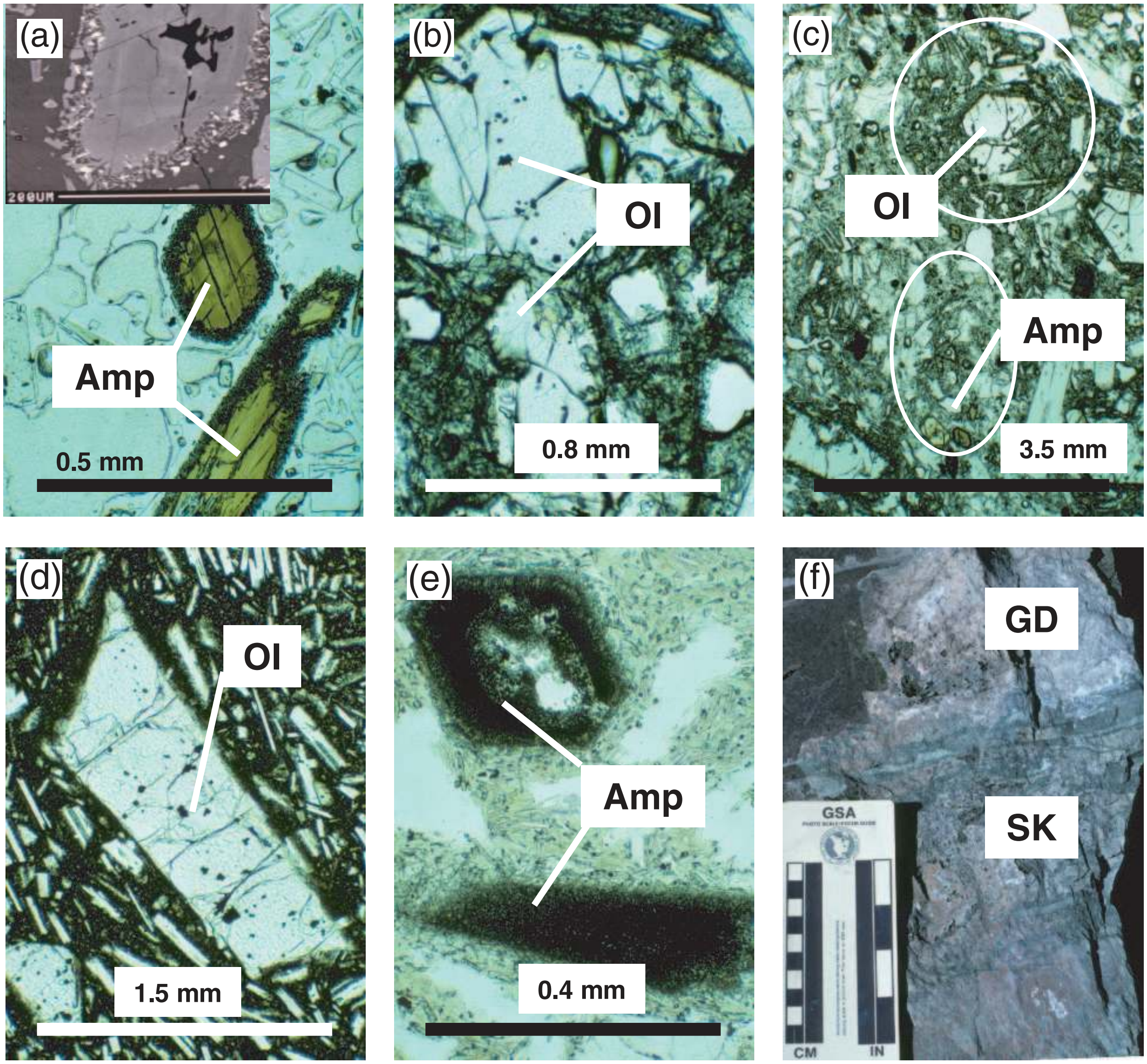

Fig. 5. Plane-polarized light photomicrographs of Popocatépetl and flanking-vent samples (a–e), and photograph of xenolith (f). (a) Vesicular 1996 dacite dome lava (96D) containing phenocrysts of amphibole (Amp) in a clear glass matrix. Amphibole grains have reaction rims (15–65 μm thick) that formed by the combination of mafic recharge and slow ascent (<14 days) (Athanasopoulos, 1997; Stimac *et al.*, 1997). Inset backscattered SEM image showing that the rim consists of pyroxene, opaque FeTi-oxides and plagioclase. (b) Skeletal olivine (Ol) crystals (Fo_{86-89}) with chromite inclusions from sample 96D. Olivine shows no sign of reaction with enclosing groundmass. (c) Millimetre- to centimetre-scale heterogeneities in the matrix and phenocryst assemblage of dome sample 96D indicating incomplete mixing of mafic, olivine-bearing magma and hornblende-bearing dacitic magma. Circled area with olivine consists of dark, microlite-rich zones surrounding olivine, whereas circled area containing amphibole and pyroxene consists of clear microlite-poor glass. (d) Olivine phenocryst in primitive basaltic andesite lava 96365 containing abundant chromite inclusions set in a matrix of glass and plagioclase microlites. (e) Pseudomorphs after amphibole in transitional dacite sample 96333. (f) Composite xenolith 9593 consisting of granodiorite (GD) and adjacent skarn (SK).

containing more abundant and larger plagioclase grains. Titanomagnetite microphenocrysts are also present in aggregates with pyroxene and plagioclase. Rare amphibole as well as more common pseudomorphs after amphibole are also observed (Fig. 5e). Olivine is absent or less abundant in the more evolved samples, or is mantled by fine-grained aggregates of pyroxene and plagioclase. Pyroxene and plagioclase phenocrysts in samples nearest Popocatépetl show evidence of resorption and multiple compositional reversals (Table 2) and plagioclase is typically present in aggregates with pyroxene phenocrysts. Apatite needles and FeCu-sulphide globules are present at trace concentrations in some samples.

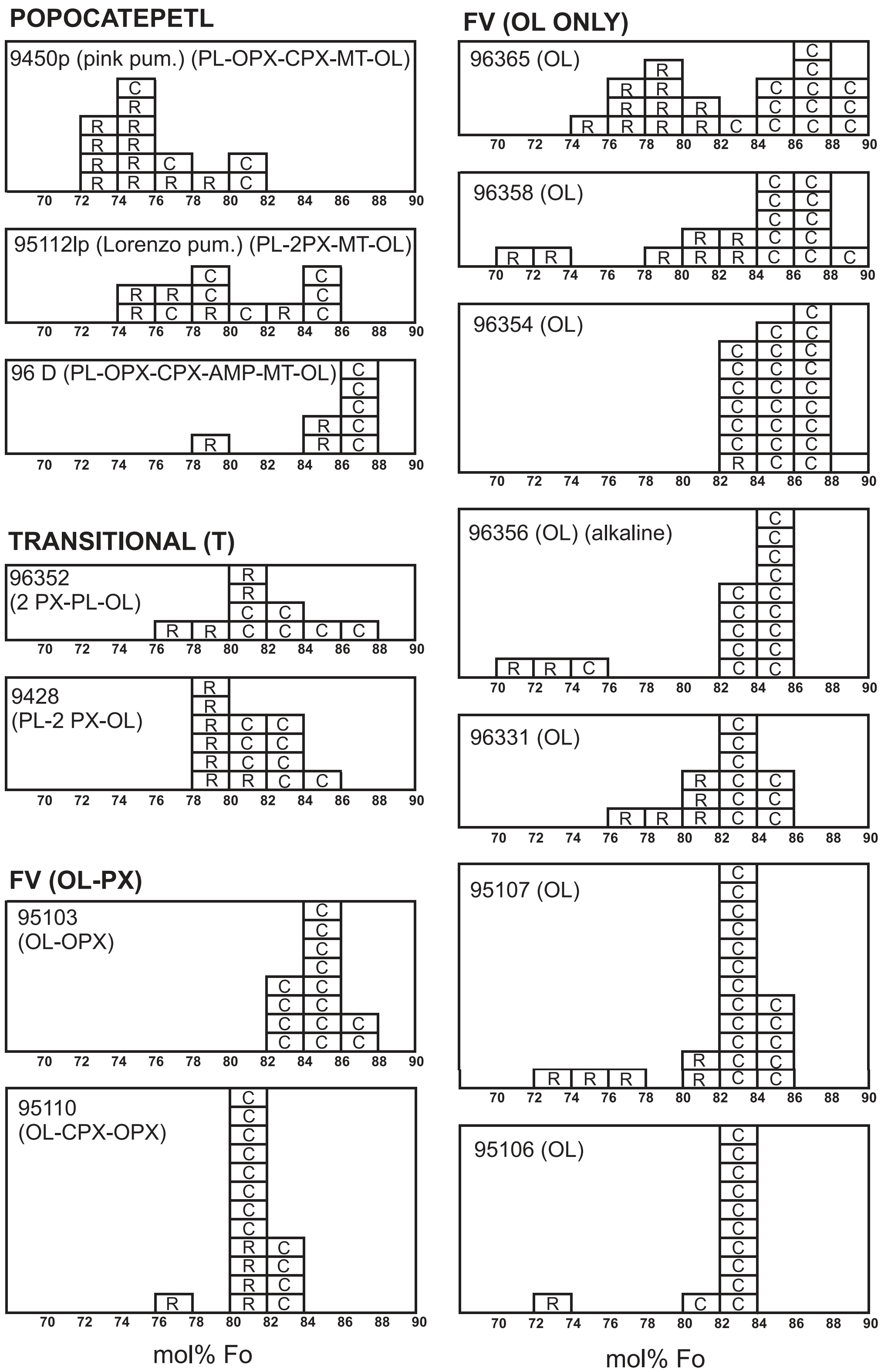

Fig. 6. Histograms of olivine composition in representative Popocatépetl, transitional cone (T), and flanking vent (FV) samples as a function of phenocryst assemblage. FV samples with olivine only have core compositions Fo_{83-89}, whereas T and Popocatépetl samples have both rim (R) and core (C) compositions ranging to more Fe-rich compositions. PL, plagioclase; OPX, orthopyroxene; CPX, clinopyroxene; MT, magnetite; OL, olivine; AMP, amphibole.

Table 3: Compositions of glass inclusions and matrix in 1996 dome sample (96D) and FV basaltic andesite sample 96365

Sample	*n*	Description	SiO_2	TiO_2	Al_2O_3	FeO	MnO	MgO	CaO	Na_2O	K_2O	P_2O_5	Total	Cl (ppm)	S (ppm)
96D	7	Gl in Px	73·92	0·42	13·07	2·08	0·04	0·32	1·30	3·15	3·47	0·07	97·84	677	101
96D	9	light matrix	73·00	0·48	13·35	1·70	0·03	0·25	1·47	4·32	3·41	0·10	98·11	500	<30
96D	7	dark matrix	67·09	0·56	15·32	2·79	0·05	1·13	3·32	4·66	2·56	0·23	97·71	410	<30
96D	5	Gl in Ol	62·09	0·45	19·87	2·10	0·03	1·67	3·75	5·91	2·59	0·26	98·72	1200	833
96D A1-6	1	Gl in Ol	54·65	0·76	20·15	3·87	0·05	4·76	5·74	5·44	1·29	0·27	96·98	1600	2483
96365	13	Gl in Ol	58·86	1·10	19·48	3·05	0·06	1·43	7·16	5·08	1·47	0·25	97·94	1308	1100
96365 L1	1	Gl in Ol	58·57	0·77	21·60	2·35	0·06	1·21	6·61	5·99	1·40	0·27	98·83	1800	2603

Composition in wt % unless specified; Gl; glass inclusion; Px, pyroxene; Ol, olivine.

In summary, the main differences between samples from Popocatépetl and FV are the greater percentage of phenocrysts, the greater abundance of plagioclase, and the presence of hornblende and FeTi-oxides as early crystallizing phases in the former, even at the same silica content. FV samples are relatively phenocryst poor with assemblages dominated by olivine and pyroxene. A few monogenetic cone samples collected mostly within 28 km of Popocatépetl display mineral assemblages and textures more akin to those observed in stratocone lavas and pumices, and are therefore classified as transitional (T).

Matrix glass and inclusions in phenocrysts

Glass or melt inclusions (MI) are present in many phenocrysts, but were examined only in reconnaissance fashion in a few samples from the 1996 dacite dome (96D) and most primitive FV high-Mg basaltic andesite (96365). In the case of the dacite dome, matrix glass compositions were also determined. Although some of the MI analysed had clearly been affected by post-entrapment crystallization (see Cervantes & Wallace, 2003), dramatically different compositional patterns are still distinguishable when inclusions in different minerals and matrix glass are compared. Melt inclusions in olivine and pyroxene from the 1996 dacite dome have distinct compositions and volatile contents. MI in pyroxene are rhyolitic in composition (*c.* 74 wt % SiO_2) with low S (*c.* 100 ppm) and moderate Cl (*c.* 680 ppm), whereas MI in olivine are andesitic (55–62 wt % SiO_2) with high S (830–2500 ppm) and Cl (1200–1600 ppm) concentrations (Table 3). Bulk compositions of clear, microlite-poor glass and darker, microlite-rich glass in the 1996 dome sample were also determined for comparison with MI. Major element compositions of MI in pyroxene overlap with those of microlite-poor clear matrix glass (70–74 wt % SiO_2) but are generally more evolved than the darker, microlite-rich matrix material (65–68 wt % SiO_2). These relationships are consistent with other textural and compositional data indicating that pyroxene grew from an evolved dacite magma, whereas olivine was derived from a mafic magma (Fig. 5c). MI in olivine from Pelagatos FV (sample 96365) with a similar composition (core Fo_{84-90}) to that in the 1996 dome (Fig. 6) was also analysed. This sample is among the most primitive Mg-rich calc-alkaline basaltic andesite lavas analysed and is thought to be representative of the dominant parental magma for Popocatépetl and surrounding more mafic centers. Uncorrected analyses of MI in olivine from the Pelagatos sample are andesitic (SiO_2 *c.* 59 wt %; K_2O 1·5 wt %) with 1100–2600 ppm S and 1300–1800 ppm Cl; inclusions with the highest S content also have the highest Cl concentrations. A few inclusions having very high Cl (1900–2100 ppm) but low S (400–500 ppm) may have suffered from more severe post-entrapment crystallization and/or formation of immiscible sulphide globules. Although such globules were not observed directly in the matrix or phenocrysts of our thin sections, this might be due to their occurrence beyond the plane of the section. Our data for MI in olivine from both the 1996 dome and the Pelagatos volcano are similar to those from a more comprehensive study of melt inclusions in olivine (Fo_{85-90}) from SCVF high-Mg basalts by Cervantes & Wallace (2003). They determined that MI trapped at upper- to mid-crustal pressures (1–6 kbar) contain 1·3–5·2 wt % H_2O and >1000 to 6000 ppm S.

Xenoliths

Crustal xenoliths are common in the Nealtican lava flow (e.g. in samples 9485 and 95281), and are particularly frequent and large in the 14 ka BP Tutti Frutti pumice layer. The Tutti Frutti fallout unit contains clasts up to 1 m in maximum diameter near the vent (Siebe *et al.*, 1996). In order of decreasing abundance the most common xenoliths are: (1) calc-silicate skarn; (2) a variety of plutonic rocks (fine-grained pyroxene–hornblende granodiorite, coarse-grained pyroxene diorite to gabbro, and

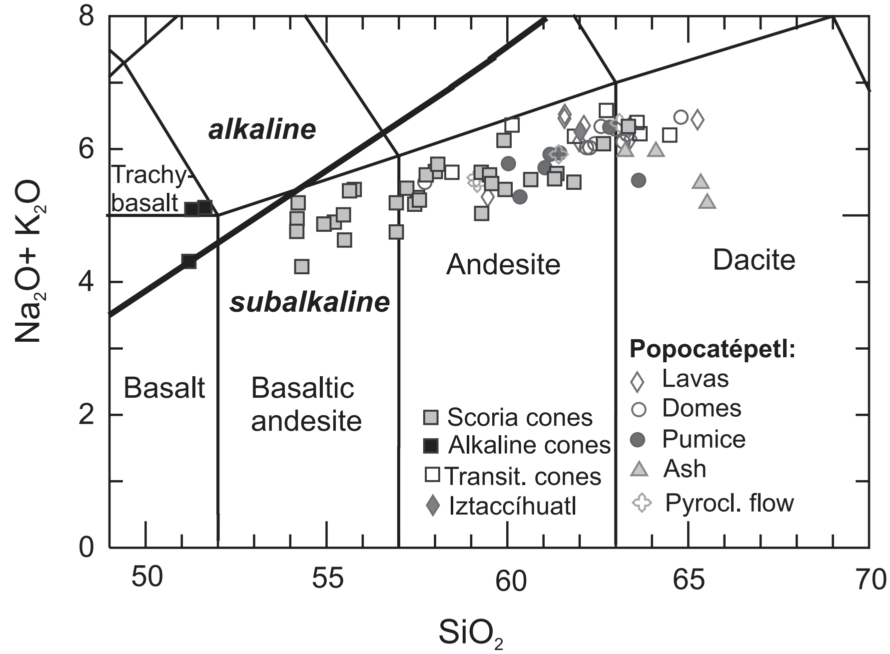

Fig. 7. Total alkalis ($Na_2O + K_2O$; wt %) vs silica (SiO_2; wt %) diagram after Le Bas *et al.* (1986) for all analysed volcanic rocks. Data are from Table 1 and normalized on an anhydrous basis. The subdivision into alkaline and subalkaline series (MacDonald & Katsura, 1964) is also shown.

fine-grained hornblende–biotite granodiorite); (3) meta-siltstone; (4) andesitic volcanic rocks. Moreover, the three most common xenolith types form composite xenoliths, typically with rounded skarn clasts enclosed in granodiorite (Fig. 5f). Less common xenoliths in the 14 ka BP tephra sequence are foliated biotite tonalite, marble, and strongly reacted, cordierite–sillimanite and hercynite-bearing pelitic clasts. Similar xenoliths have also been described from Iztaccíhuatl (Nixon, 1989). Calc-silicate skarn xenoliths have been taken as evidence that a sedimentary sequence including limestone underlies the volcano (Robin, 1984; Boudal, 1985; Kolisnik, 1990). Skarn xenoliths are massive to weakly layered or spotted, porous and friable, with abundant cavities lined by vapour-phase minerals. The mineral assemblage is most commonly dominated by epidote, actinolite, diopside, sphene, magnetite, and sulphate minerals, but garnet, wollastonite, and idocrase are also present in some samples. Meta-siltstones consist of fine-grained detrital quartz enclosed in a recrystallized matrix consisting of pyroxene and feldspar.

Plutonic xenoliths are angular to subrounded, equigranular to weakly porphyritic, fine-grained (<5 mm), and weakly miarolitic (<1 vol. % quartz and biotite in cavities). They contain no interstitial glass indicative of partial melting or incomplete solidification. Contact zones consist of layers of pyroxenite and plagioclase microlites enclosed in large masses of late-stage quartz or granophyric intergrowths of quartz and feldspar, commonly in association with biotite or amphibole. Apatite needles and zircon are common late-stage accessory minerals. Pyroxene diorite xenoliths contain olivine with chromite inclusions mantled or completely replaced by orthopyroxene and FeTi-oxides. Even though these xenoliths represent completely solidified material that had already precipitated late-stage quartz, some large olivine grains remain intact, presumably because of armouring by orthopyroxene overgrowths.

Composite xenoliths consisting of hornblende granodiorite enclosing or in contact with skarn and metasiltstone (Fig. 5f) are interpreted as either (1) the solidified carapace of the Tutti Frutti magma reservoir and its immediate wall-rocks, or (2) an earlier, completely crystallized Popocatépetl magma body sampled by later eruptions. The intact, holocrystalline textures are consistent with very rapid incorporation and transport of these samples from reservoir depths to the surface.

GEOCHEMISTRY

Major element compositions

Whole-rock silica contents in 32 volcanic rock samples from Popocatépetl (including sample 9594 from Iztaccíhuatl) range between 57·7 and 65·5 wt % (normalized values, Fig. 7). The lowest value corresponds to an andesitic dome fragment ejected during the June 30, 1997 event (sample 97D1), whereas the highest value is from the March 5, 1996 bulk ash-fall sample (sample 9601K) collected at Tlamacaz. SiO_2 contents in 42 SCVF and Valley of Puebla scoria cone samples range between 51·2 and 64·5 wt %. The lowest value corresponds to an alkaline basalt from Citlaltepec scoria cone (sample 95357) and the highest value is for a transitional sample (sample 96359) from the Malpaís lava flow. Total alkali ($Na_2O + K_2O$) contents range between 4·2 and 6·6 wt %, with lower values more typical for the scoria cones (Fig. 7). The majority of the samples (lava flows, pumices, domes, and juvenile clasts from pyroclastic-flow deposits) from Popocatépetl have andesitic compositions. Samples from three lava flows, three dome fragments, two pumice clasts (including a sample from the January 22, 2001 pyroclastic-flow deposit), and all four bulk ash-fall samples from the current eruption are dacitic (SiO_2 >63 wt %). Although Popocatépetl and surrounding scoria cone samples partially overlap in SiO_2 and other element concentrations, FV samples are generally more mafic. The majority of the monogenetic scoria cones and associated lavas (22 samples) are andesitic, 13 samples have basaltic andesite compositions, four samples have dacitic compositions, two are trachybasalts and only one sample is strictly basaltic. The transitional vent samples are more enriched in silica, sodium and potassium, and some of them have even higher contents of these elements than typical stratocone samples (Fig. 7). Of the 42 FV and T samples, only Cerro Santa Barbara (samples 96356 A and B) and Cerro Citlaltepec (sample 96357) have alkaline compositions lying above the MacDonald & Katsura line in Fig. 7. Alkaline basalts are restricted to the far-western edge of the study area (Fig. 2) and are volumetrically the least significant magmas in this region.

All of the analysed rocks are hy-normative and none are ne-normative. Trends of Popocatépetl samples are compared with the surrounding monogenetic cones (FV and T samples) in Harker diagrams in Fig. 8. In the SiO_2 vs MgO diagram (Fig. 8a), the various suites of the study area are clearly distinguishable. The three alkaline FV samples have lower SiO_2 concentrations at equivalent MgO concentrations compared with SCVF and Valley of Puebla calc-alkaline basaltic andesite samples. The abundant basaltic andesites form a continuous trend with more evolved FV and T samples, which overlap with the less evolved samples from Popocatépetl volcano. MgO decreases sharply with increasing SiO_2 in the FV suite, consistent with fractionation of olivine and pyroxene. Similar decreases in TiO_2 (Fig. 8b) and P_2O_5 (Fig. 8c) with increasing SiO_2 are discernible; however, in comparison with MgO, TiO_2 and P_2O_5 in Popocatépetl and transitional SCVF cones do not decrease continuously with increasing SiO_2. The more scattered TiO_2 and P_2O_5 distributions in the upper left converge in the lower right parts of the diagrams and their trends become flatter. The overall decline in TiO_2 and P_2O_5 with increased SiO_2 to about 60% is interpreted to be the result of Ti-magnetite and apatite fractionation in these magmas. Popocatépetl samples generally have higher Al_2O_3/CaO ratios than FV samples. The ratios are highest in the ash fallout samples (Fig. 8d). The increase of the Al_2O_3/CaO ratio with increasing SiO_2 indicates that clinopyroxene fractionation is important. In all Harker diagrams (including those that are not shown in Fig. 8), transitional vents generally plot in a similar manner to Popocatépetl samples.

Combined major and trace element diagrams

In a Ba vs MgO diagram (Fig. 8e) two trends are visible: FV samples generally display a negative correlation, whereas Popocatépetl samples show a positive correlation (see arrow in Fig. 8e), with the highest Ba concentrations (*c.* 550 ppm) at MgO contents between 4 and 5 wt %. The increase in Ba with decreasing MgO is consistent with a lack of plagioclase fractionation in the FV suite. Conversely, the relative Ba depletion and decreasing Ba with decreasing MgO in Popocatépetl samples are probably the result of variable plagioclase fractionation. Chromium concentrations ranging from 11 to 499 ppm show a strong positive correlation when plotted against MgO (Fig. 8f). The very rapid decrease in Cr from 9 to 4 wt % MgO in FV samples can be ascribed to fractionation of olivine with Cr-spinel inclusions.

Trace element compositions

The most primitive [whole-rock Mg-number >68, where Mg-number = $100Mg/(Mg + Fe^{2+})$; MgO >8 wt %; Ni >150 ppm] FV calc-alkaline basaltic andesites and alkaline basalts display large and systematic differences in trace element compositions. REE distributions of selected FV samples and least evolved Popocatépetl rocks are plotted in Fig. 9 and are characterized by enriched light REE (LREE) concentrations with respect to the heavy REE (HREE; La/Lu_{CN} 4·6–8·8) and the absence of significant Eu anomalies (Eu/Eu* 0·81–0·99).

Alkaline basalts have the highest total REE concentrations (140–170 ppm) and are also enriched in most other trace elements relative to the most primitive calc-alkaline basaltic andesites from Cerro Pelagatos, Cerro Partido, and Cerro Tecajete (ΣREE 75–113 ppm). These basaltic andesites also have lower REE abundances than the most primitive basalts from the nearby mildly alkaline Chichinautzin volcano of the central SCVF [ΣREE 186–196 ppm; data from Siebe *et al.* (2004*b*)]. In comparison, least evolved Popocatépetl samples (andesitic lava, pumice, and scoria samples) show the lowest REE concentrations (71–85 ppm) in Fig. 9. These four rock groups from Chichinautzin volcano and other closely spaced monogenetic cones surrounding Popocatépetl volcano display element patterns that cannot be related to one another only by fractional crystallization processes or differential partial melting of a common homogeneous mantle source (Siebe *et al.*, 2004*b*). Instead, they point towards a

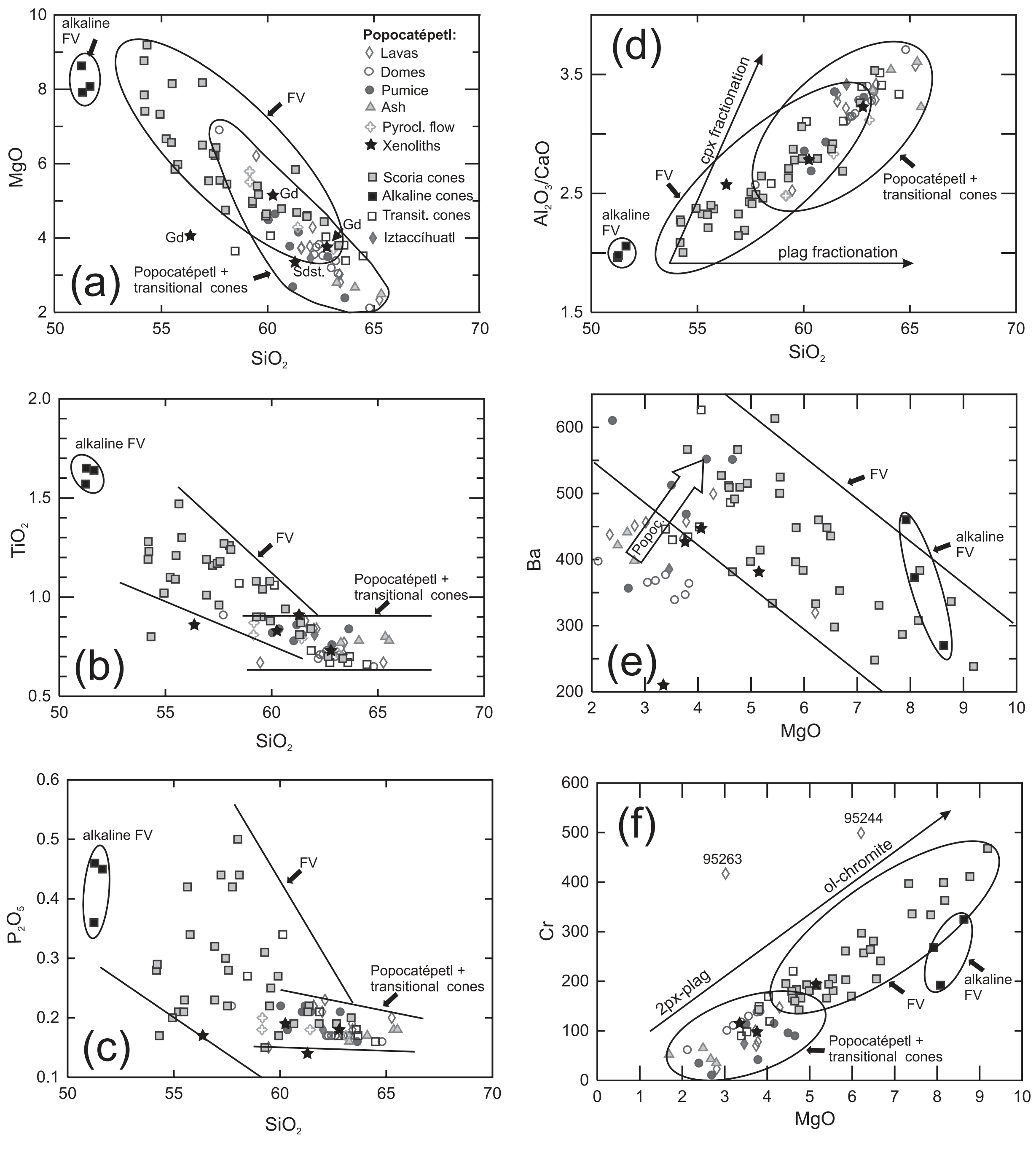

Fig. 8. Harker diagrams showing selected major (wt %, normalized on an anhydrous basis) and trace elements (in ppm) plotted against silica (a–d) or MgO (e and f). Xenoliths shown are granodiorites (samples 96341B, 9490B, and 95142C) and metasandstone sample 95142A. Analytical data are from Table 1. FV, flanking vents; Gd, granodiorite; Sdst., sandstone.

heterogeneous mantle source. The relatively flat HREE tails of these least evolved Popocatépetl and FV samples suggest a garnet-free source and therefore relatively shallow depths of magma genesis (<100 km) from partial melting of a variably depleted spinel peridotite mantle.

The characteristic differences between the suites are particularly well displayed in primitive mantle normalized trace element variation diagrams (Fig. 10). Examination of the trace element patterns of progressively more magnesian samples from the FV suite (ranging from 5 to 8 wt % MgO) shows that they have smoothly decreasing incompatible element trends and smoothly increasing compatible element trends (Fig. 10a) relative to the primitive basaltic andesites and alkaline cones.

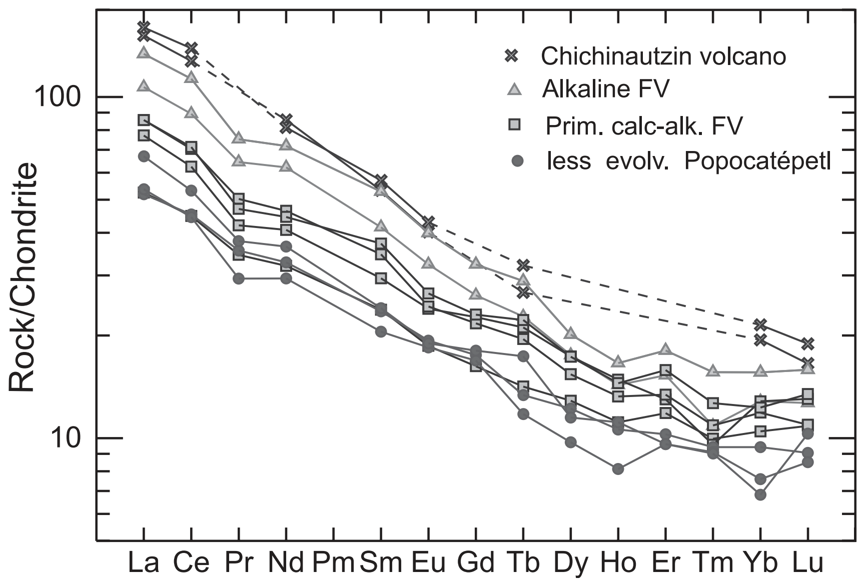

Fig. 9. Chondrite-normalized (Sun & McDonough, 1989) REE compositions from four suites: least evolved Popocatépetl (samples 0101s, 9479o, and 95244), primitive calc-alkaline flanking vents (FV) (samples 96353, 95103, and 96365), alkaline FV (samples 96357 and 96356A; all data from Table 1), and two samples from Chichinautzin volcano [data from Siebe *et al.* (2004*b*)].

These patterns are consistent with crystal fractionation of a phenocryst assemblage dominated by olivine, chromite, clinopyroxene, and minor orthopyroxene. In FV and T samples (with <4 wt % MgO), a progressive enrichment in large ion lithophile elements (LILE) and LREE, and a decline in compatible elements and HREE is noticeable with respect to increasing/decreasing SiO_2 contents (Fig. 10b). The decreasing trend in HREE and Y implies either fractionation of a phase that concentrates HREE such as hornblende, or the assimilation of HREE-poor material such as observed in sandstone xenoliths, or both.

Comparison of Popocatépetl samples with the FV and T suites shows that Popocatépetl samples are very similar to the T samples (Fig. 10b), but attain slightly higher incompatible element concentrations, and are more depleted in elements that are incorporated into the fractionating assemblage observed at Popocatépetl: plagioclase, clinopyroxene, orthopyroxene, FeTi-oxides, and apatite. All FV and especially Popocatépetl samples are enriched in Pb relative to other trace elements. Pb is among the most incompatible trace elements and its high abundance in Popocatépetl and FV samples might reflect sediment-derived fluxes that originated from the subducted slab and to a lesser extent from upper-crustal assimilation.

Sr, Nd, and Pb isotopes

Sr–Nd–Pb isotope ratios were determined in 23 selected samples, mainly from Popocatépetl. We analysed seven pumices, five xenoliths (four were collected from the Tutti Frutti pumice layer), four samples from the January 22, 2001, pyroclastic-flow deposits, three ballistic dome clasts from the April 30, 1996, and June 30, 1997 events, and two lava flows (Nealtican and Cañada Xallipilcáyatl). In addition, we analysed two mafic samples from the surrounding SCVF cones, including the most primitive calc-alkaline sample 96365 from Cerro Pelagatos and sample 96366 from Cerro Zoceyuca, near Juchitepec (Fig. 2).

Sr and Nd isotope compositions are listed together with the standard deviations of the runs in Table 4. Popocatépetl samples display a considerable range of $^{87}Sr/^{86}Sr$ (from 0·70397 to 0·70463) and ε_{Nd} (+6·2 to +3·0) whereas the two FV samples have $^{87}Sr/^{86}Sr$ and ε_{Nd} of 0·70365 and 0·70414 and +6·4 and +4·7, respectively. Sr and Nd isotope signatures are plotted in a $^{87}Sr/^{86}Sr$ vs ε_{Nd} diagram (Fig. 11) in which previously published data from the Popocatépetl (Boudal, 1985; Siebe *et al.*, 1999) and Nevado de Toluca stratovolcanoes (Martínez-Serrano *et al.*, 2004), as well as from late Pleistocene–Holocene Pelado, Guespalapa, Chichinautzin, Cajete and Xitle monogenetic volcanoes from the central part of the SCFV (Siebe *et al.*, 2004*b*), are also shown for comparison. The most depleted isotope compositions among the Popocatépetl rocks are represented by scoria samples of the January 22, 2001 pyroclastic-flow deposits and andesitic ballistic dome fragments of the April 30, 1996 event. Other dacitic samples from the January 22, 2001 pyroclastic-flow deposit and the April 30, 1996 and June 30, 1997 dome explosions are more enriched (higher $^{87}Sr/^{86}Sr$, lower ε_{Nd}), together with the slightly less siliceous pumices from the Tutti Frutti and major

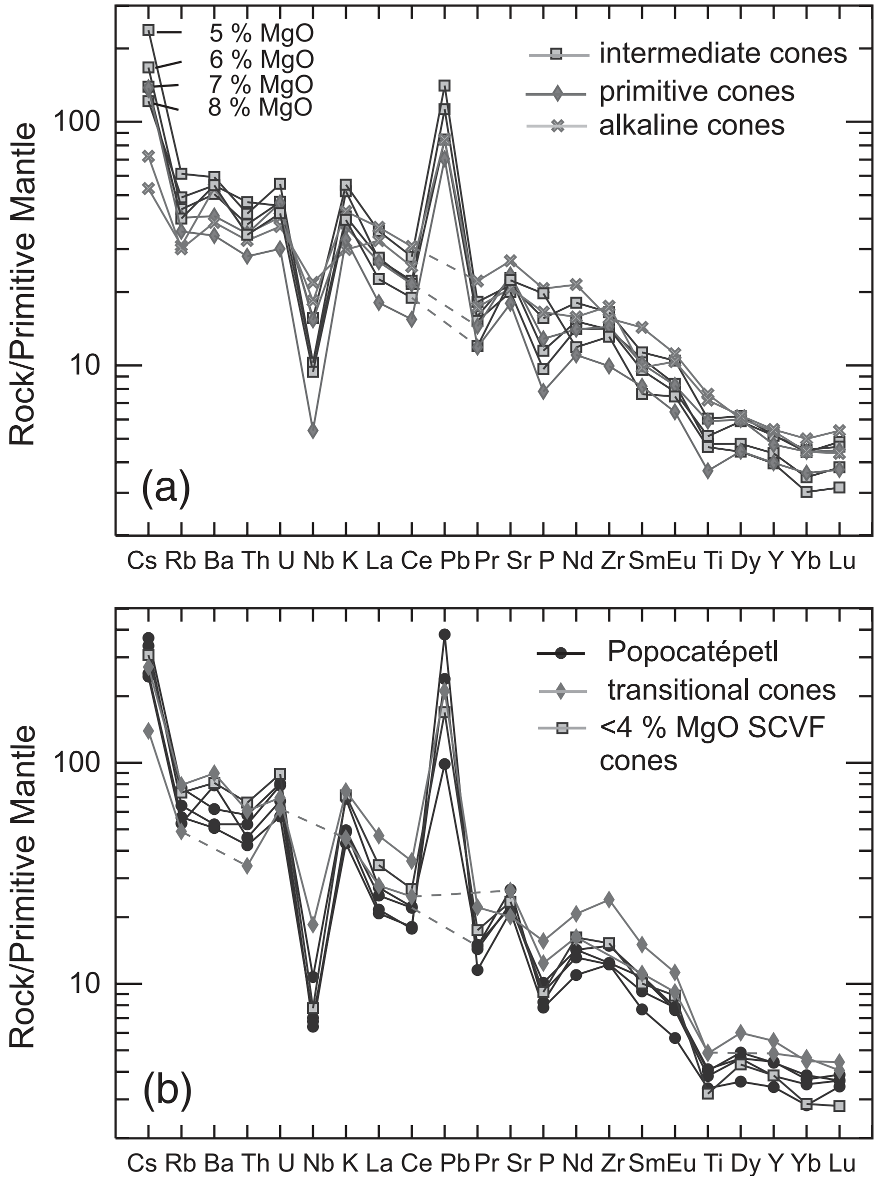

Fig. 10. Trace element distribution diagrams normalized to primitive mantle values from Sun & McDonough (1989). (a) SCVF monogenetic cones showing intermediate rocks with MgO from 5 to 8 wt % (samples 95367, 96343, 96347 and 96358), primitive rocks with MgO >8 wt % (samples 95365 and 96354A), and alkaline basalts (samples 96356A and B). (b) Popocatépetl rocks (lava flow 95296, pumice samples 9479o and 9463tf, bulk ash 9601K) in comparison with transitional cones (samples 96352 and 9428) and a mean value for <4 wt % MgO SCVF cones.

Holocene Plinian fallout layers. Lava flows and the remaining more silicic pumices represent the most isotopically enriched members of the Popocatépetl suite.

Xenoliths from the Tutti Frutti Plinian layer can be divided in two groups: (1) granodiorite sample 95142C displays a nearly identical $^{87}Sr/^{86}Sr$ ratio and ε_{Nd} to the coeval Tutti Frutti pumice (sample 9463, Table 4); (2) a meta-sandstone xenolith (9490C) consists of detrital minerals such as quartz and rare zircon, in a recrystallized matrix of feldspar, pyroxene, and sphene; and a skarn fragment (9463A) from a contact-metamorphic zone (presumably adjacent to the granodiorite) consisting mainly of Ca-pyroxene, plagioclase, sphene, apatite, and FeTi-oxides, suggesting strong contributions of magmatic–hydrothermal components during recrystallization. The metasedimentary xenoliths show more radiogenic $^{87}Sr/^{86}Sr$ ratios (around 0·707), but heterogeneous ε_{Nd} values. The siltstone and the marble xenolith have more or less typical crustal ε_{Nd} values of $-0·5$ and $-8·0$, respectively, whereas the skarn xenolith has an ε_{Nd} of $+3·8$, comparable with the pumices, but in an abnormal position in the upper right quadrant of Fig. 11b,

Table 4: Sr–Nd–Pb isotope ratios of selected samples

Sample	Rock type	$^{87}Sr/^{86}Sr$	$\pm 1\sigma_{abs}$	$^{143}Nd/^{144}Nd$	$\pm 1\sigma_{abs}$	ε_{Nd}	$^{206}Pb/^{204}Pb$	$\pm 1\sigma_{rel}$	$^{207}Pb/^{204}Pb$	$\pm 1\sigma_{rel}$	$^{208}Pb/^{204}Pb$	$\pm 1\sigma_{rel}$
Popocatépetl												
95281	Lava	0·704514	35	0·512834	19	3·8	18·6735	0·020	15·5797	0·021	38·4160	0·021
95284	Lava	0·704633	30	0·512806	16	3·3	18·7026	0·022	16·6032	0·022	38·5041	0·023
9479o	Pumice	0·704162	41	0·512902	36	5·15	18·6356	0·018	15·5778	0·017	38·3731	0·019
9310w	Pumice	0·704598	50	0·512791	48	3·0	18·6697	0·027	15·5772	0·034	38·4147	0·044
9490 g	Pumice	0·704434	32	0·512830	37	3·7	18·6545	0·031	15·5893	0·041	38·4301	0·055
9463tf	Pumice	0·704180	34	0·512881	42	4·7	18·6472	0·016	15·5912	0·018	38·4225	0·019
9490 m	Pumice	0·704218	43	0·512877	32	4·7	18·6255	0·034	15·5640	0·035	38·3325	0·035
95112lp	Pumice	0·704271	38	0·512875	34	4·6	18·6603	0·023	15·5935	0·026	38·4444	0·030
9450p	Pumice	0·704504	33	0·512837	17	3·9	18·6749	0·033	15·5968	0·037	38·4642	0·038
Pyroclastic flow												
0101s	Scoria	0·704064	36	0·512929	18	5·7	18·6316	0·054	15·5776	0·055	38·3779	0·058
0102s	Scoria	0·704002	30	0·512919	20	5·5	18·7811	0·056	15·6699	0·087	38·7884	0·105
0103d	Dome fragm.	0·704157	43	0·512884	20	4·8	18·6390	0·014	15·5855	0·014	38·3977	0·014
0104p	Pumice	0·704390	36	0·512848	14	4·1	18·6497	0·024	15·5897	0·027	38·4206	0·031
Domes												
96D4-A1	Dome fragm.	0·704248	31	0·512865	26	4·4	18·6183	0·048	15·5655	0·049	38·3232	0·054
97D1	Dome fragm.	0·703973	35	0·512958	17	6·2	18·6734	0·025	15·5987	0·026	38·4349	0·029
97D2	Dome fragm.	0·704137	34	0·512898	25	5·1	18·6392	0·022	15·5863	0·026	38·3976	0·033
Xenoliths												
9463A	Skarn	0·706877	41	0·512832	40	3·8	n.d.		n.d.		n.d.	
9490C	Sandstone	0·707446	29	0·512611	63	−0·5	n.d.		n.d.		n.d.	
0401m	Marble	0·707093	38	0·512230	85	−8·0	n.d.		n.d.		n.d.	
96341B	Granodiorite	0·704215	28	0·512813	32	3·4	n.d.		n.d.		n.d.	
95142C	Granodiorite	0·704265	55	0·512876	26	4·6	n.d.		n.d.		n.d.	
SCVF cones												
96365	Lava	0·703651	37	0·512969	12	6·45	18·6443	0·034	15·5841	0·044	38·4009	0·056
96366	Scoria	0·704145	36	0·512877	29	4·7	18·6936	0·026	15·5948	0·031	38·4828	0·041

$1\sigma_{abs}$ errors refer to the last two digits. During the analyses of these samples the NBS 987 Sr standard and the Nd La Jolla standard were measured as follows: $^{87}Sr/^{86}Sr = 0{\cdot}710237 \pm 21$ ($1\sigma_{abs}$, $n = 310$); $^{143}Nd/^{144}Nd = 0{\cdot}511875 \pm 21$ ($n = 148$). Data were not further corrected. n.d., not determined.

which is discussed further below. The grandiorite xenolith from Cerro Chiconquiat FV (sample 96341A) plots close to the granodiorite xenolith from the Tutti Frutti fallout layer.

Two flanking SCVF scoria cones are also shown in Fig. 11. Basaltic–andesitic Cerro Pelagatos scoria cone (sample 96365) displays the most depleted Sr and Nd isotope ratios of all samples investigated ($^{87}Sr/^{86}Sr = 0{\cdot}70365$; $\varepsilon_{Nd} = +6{\cdot}5$), whereas the andesitic Zoceyuca cone (sample 96366) lies within the typical Popocatépetl range.

For comparison, Sr and Nd data for rocks from Nevado de Toluca and five monogenetic volcanoes located in the central part of the SCVF (Siebe *et al.*, 2004*b*) are also plotted in Fig. 11. These samples generally have less radiogenic Sr isotope ratios than Popocatépetl samples. On the other hand, ε_{Nd} values for the SCFV cones are very similar to those for Popocatépetl, whereas Nevado de Toluca shows a trend towards slightly more radiogenic ε_{Nd} values and intermediate $^{87}Sr/^{86}Sr$ ratios.

Pb isotope ratios are compiled in Table 4 and presented in Fig. 12 in a $^{206}Pb/^{204}Pb$ vs $^{207}Pb/^{206}Pb$ diagram. Values are relatively homogeneous, ranging between 18·61 and 18·70 for $^{206}Pb/^{204}Pb$, and between 15·56 and 15·60 for $^{207}Pb/^{206}Pb$. Popocatépetl lavas (samples 95281 and 95284) and one of the SCFV samples (96365) are slightly more enriched in radiogenic Pb. Contrary to its depleted Sr–Nd isotope ratios, one of the

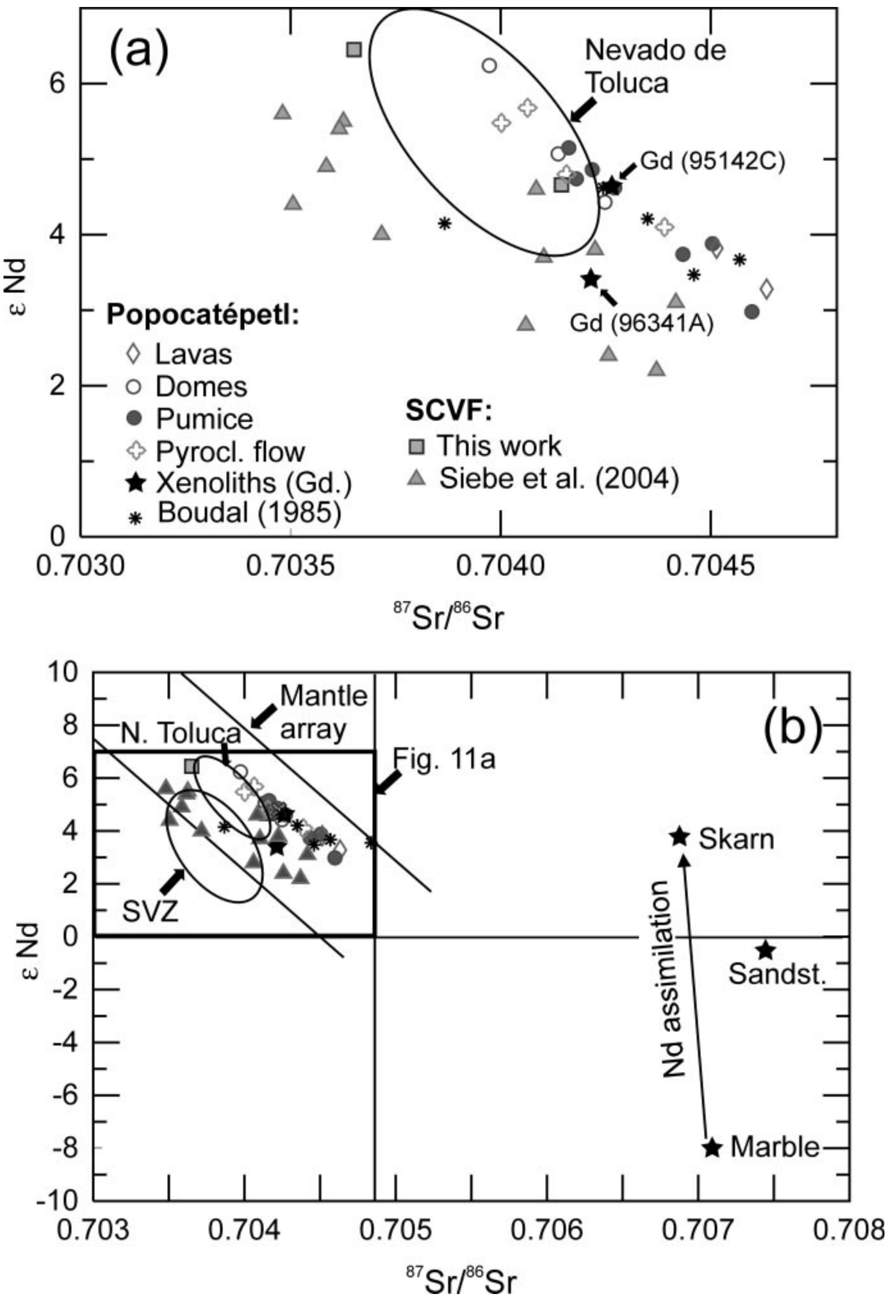

Fig. 11. $^{87}Sr/^{86}Sr$ vs ε_{Nd} diagrams for 18 Popocatépetl samples, including two granodiorite (Gd) xenoliths and two monogenetic SCVF cones (data from Table 4). (a) Detailed plot showing the isotopic variation of different Popocatépetl units in comparison with other monogenetic SCVF cones [data from Siebe *et al*. (2004*b*)] and Nevado de Toluca stratovolcano [data from Martínez-Serrano *et al*. (2004)]. Popocatépetl isotopic data from Boudal (1985) are also plotted. (b) Expanded diagram showing in addition Sr–Nd isotope ratios from metasedimentary Popocatépetl xenoliths (skarn, metasandstone, and marble) together with data from the Southern Volcanic Zone (SVZ) of the Andes [data from Hickey *et al*. (1986)]. Nd assimilation of skarn xenolith 9463A is discussed in the text.

scoria samples from the January 22, 2001 pyroclastic-flow deposit (sample 0102 s) displays anomalously enriched Pb isotopic ratios ($^{206}Pb/^{204}Pb$ 18·78; $^{207}Pb/^{206}Pb$ 15·67; Fig. 12b). Because this is the only sample with such characteristics, it is difficult to determine whether these enriched values are truly representative or related to small-scale heterogeneities in the dome lava. A field for East Pacific Rise (EPR) mid-ocean ridge basalts (MORB) from Zindler & Hart (1986) and a field for Cocos Plate marine sediments recovered by the Deep Sea Drilling Project (DSDP) at sites 467 and 488 (Verma, 2000) are also shown in

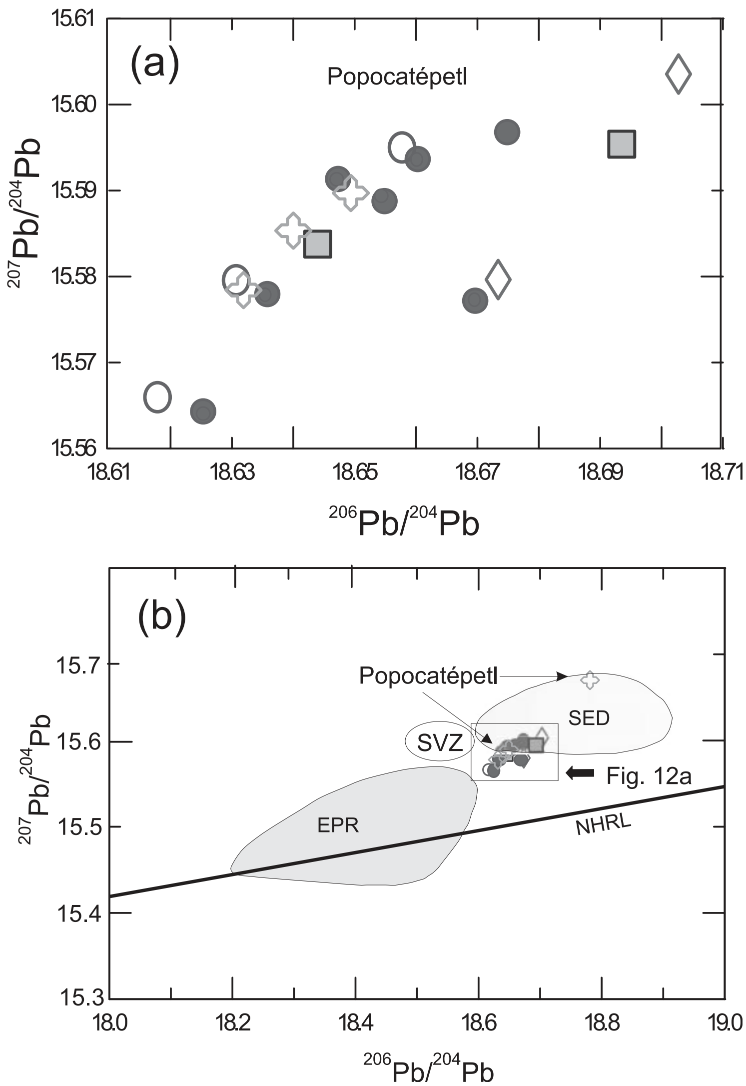

Fig. 12. $^{206}Pb/^{204}Pb$ vs $^{207}Pb/^{204}Pb$ ratios for Popocatépetl and two SCVF samples (data from Table 4, symbols as in Fig. 11). (a) Small-scale variation diagram. (b) Expanded plot, showing Popocatépetl data in comparison with MORB from the East Pacific Rise [EPR; data from Zindler & Hart (1986)], marine sediments (SED) from the Cocos Plate (Verma, 2000) and the Southern Volcanic Zone, Chile [SVZ; data from Harmon *et al.* (1984) and Hickey *et al.* (1986)]. Northern Hemisphere Reference Line (NHRL) is from Zindler & Hart (1986).

Fig. 12b. Popocatépetl samples are in an intermediate position between the MORB and DSDP marine sediment fields. Finally, a comparison of Sr, Nd, and Pb isotope ratios of Popocatépetl products with their radiometric ages (<23 ka BP) does not allow the recognition of any particular trend.

MAGMA GENESIS AND TECTONIC CONTEXT

Popocatépetl is located at the front of the central TMVB, 350 km to the NE of the Middle America Trench, where the Cocos Plate is being subducted beneath the North American Plate (Fig. 1). The subduction zone is the dominant tectonic feature in southern Mexico and its spatial link with the TMVB clearly indicates a genetic relationship (e.g. Siebe *et al.*, 2004*b*, and references therein). Although the Wadati–Benioff zone is not well defined where it is closest to Popocatépetl, interpretation of seismic data (Suárez *et al.*, 1990; Pardo & Suárez, 1995) indicates that the Cocos Plate dips along the Guerrero coast at a shallow angle (10–12°) to a depth of *c.* 50 km (Fig. 1). Between 110 and 275 km from the trench, the subducted slab follows a sub-horizontal trajectory. Beyond this distance it cannot be traced because of the lack of seismic events. The slab probably steepens north of the flat portion, reaching a depth of *c.* 100 km beneath the central TMVB (Suárez *et al.*, 1990). This depth would be consistent with the average depth of 110 km, corresponding to pressures of *c.* 35 kbar, typical of most volcanic

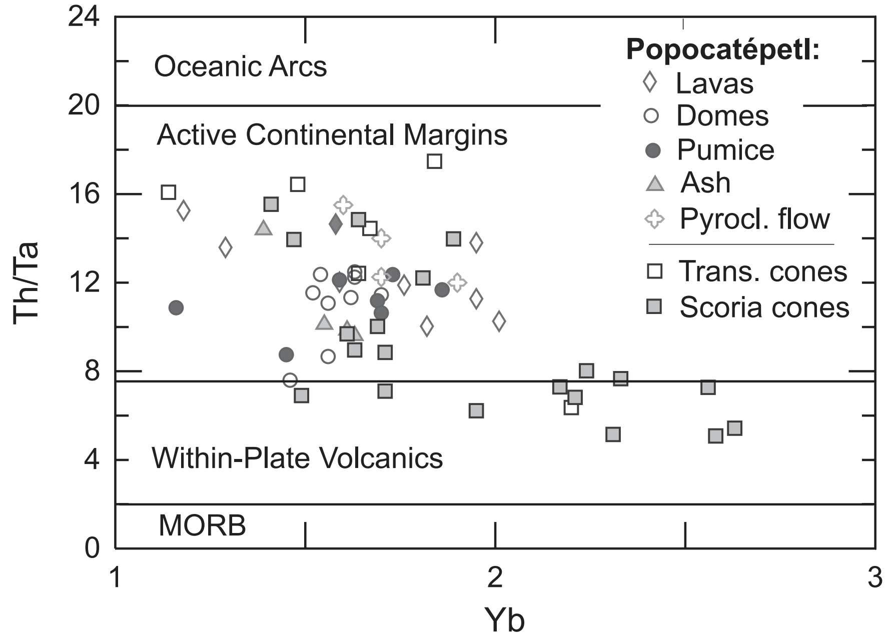

Fig. 13. Yb vs Th/Ta discrimination diagram for felsic and intermediate volcanic rocks (Gorton & Schandl, 2000). The plot shows andesitic–dacitic Popocatépetl and flanking vent samples.

fronts in subduction zones (e.g. Gill, 1981; Plank & Langmuir, 1988). Estimates for the crustal thickness in central Mexico based on seismic and gravimetric data range between 42 and 50 km (e.g. Fix, 1975; Valdés-González *et al.*, 1986). In addition, tectonic and geophysical evidence indicates that the central part of the TMVB is related to a roughly north–south-oriented extensional stress field with prominent east–west normal faults and shallow crustal seismicity (e.g. Siebe *et al.*, 2004*b*, and references therein). With this tectonic framework in mind, the following discussion will address different aspects of magma genesis underneath Popocatépetl and its flanking vents. This discussion will include possible material contributions to the mantle wedge from the dehydration of the subducting slab, composition and generation of primary magmas in the mantle wedge, crystal fractionation during magma ascent, mingling and mixing processes in a shallow magma chamber, and crustal contamination prior to eruption. From these processes the earliest (dehydration of the oceanic crust and primary magma generation in the mantle wedge) are the most difficult to discern, whereas evidence for fractional crystallization, magma mixing, and crustal assimilation are more obviously displayed by the available mineralogical, textural, chemical, and isotopic evidence.

Role of the subducting slab

Direct proof of the subducting slab being involved in magma generation processes of continental arcs is generally difficult to achieve, in particular in relatively evolved magmatic products such as those from Popocatépetl. For that reason we have also investigated the more primitive magmatic products of the SCFV and Valley of Puebla scoria cones.

Plank & Langmuir (1998) noted that the sediment section being subducted along the Middle America Trench includes *c.* 200 m of carbonates overlain by *c.* 200 m of siliceous ooze. A chemical contribution from these marine sediments in our samples can be deduced from elevated Ba/Nb ratios (between 17 and 232, mean value 68, $n = 63$; Table 1) because Ba is usually concentrated in oceanic sediments containing hydrothermal minerals and clays. Furthermore, incompatible trace elements are elevated in most of Popocatépetl samples and *c.* 50% of the FV samples and plot in the Active Continental Margin field of the Yb vs Th/Ta diagram (Gorton & Schandl, 2000; Fig. 13). Both Popocatépetl and FV samples show pronounced positive Pb spikes (<5–27 ppm, Table 1) in primitive mantle (Sun & McDonough, 1989) normalized trace element diagrams (Fig. 10). Their parental mantle-derived magmas must have obtained a considerable Pb contribution from subducted oceanic sediments. Plank & Langmuir (1998) reported 105–107 ppm Pb in sediments at DSDP Site 487, whereas, for comparison, Zindler & Hart (1986) reported 0·056 ppm Pb for typical MORB source mantle.

Sr–Nd–Pb isotope ratios (Figs 11 and 12) in Popocatépetl and FV samples are comparable with ratios in volcanic rocks from the Southern Volcanic Zone (SVZ) in

Chile ($^{87}Sr/^{86}Sr$ 0·7038–0·70455; ε_{Nd} +1·0 to +4·9; $^{206}Pb/^{204}Pb$ 18·55–18·64; $^{207}Pb/^{204}Pb$ 15·58–15·61) where substantial proof for material additions from subducted hydrous fluids into the mantle wedge was provided, by, for instance, Hickey *et al.* (1986).

Generation and composition of primary melts

The upper mantle is generally considered to be heterogeneous at a 100–1000 km scale (Zindler & Hart, 1986; Condie, 2001). Wallace & Carmichael (1999) and Siebe *et al.* (2004*b*) have shown that at least two different mantle sources must exist beneath the central SCVF at an even smaller scale (<10 km). Although primitive magmas of alkaline affinity are relatively rare in the immediate area of Popocatépetl, data presented here indicate that this conclusion also applies to monogenetic volcanoes within a 35 km radius of Popocatépetl's crater.

Various models attempting to explain upper-mantle heterogeneity below the TMVB have been proposed. Luhr (1997) and Wallace & Carmichael (1999) argued that slab-induced convection in the mantle wedge beneath the TMVB causes advection of back-arc asthenospheric mantle into the region of magma generation. Ferrari (2004) proposed a more complicated model in which lateral propagation of slab-detachment processes induces deeper mantle material to flow into the wedge region through slab windows and hence contribute to the generation of small batches of OIB-type magmas. In this context, it should be kept in mind that the subduction zone in front of Pacific Mexico constitutes one of the oldest subduction zones worldwide. For more than 100 Myr, subduction-related magmatism has led to the formation of batholiths during the Cretaceous (e.g. Gastil *et al.*, 1978; Schaaf *et al.*, 1995) and extensive ignimbrite emplacement (Sierra Madre Occidental Province) during the Tertiary (e.g. McDowell & Clabaugh, 1979). Various periods of plate reorganization, leading to changes in slab geometry and truncation of the fore-arc, have affected the evolution of the magmatic arc and contributed different proportions of material components to the mantle wedge. Mantle heterogeneities produced by variable amounts of chemically different subducted materials should therefore not be surprising and are compatible with the above-cited models in explaining the present mantle situation underneath the TMVB.

The relatively depleted Sr and Nd isotope compositions of the andesitic pumice from the June 30, 1997 explosions indicate a strong mantle affinity. The high Ni and low Ca values of olivine phenocrysts (Fig. 14) and the high Fo content of unreacted olivine in some Popocatépetl samples (e.g. dome samples 96D; Fig. 6) also argue for a relatively primitive deep source input to the more evolved upper-crustal Popocatépetl storage chamber. Although not entirely pristine mantle melts, several SCVF samples of mildly alkaline basalt and high-Mg basaltic andesite compositions qualify as primitive magmas (Table 1) when applying the criteria proposed by Wallace & Carmichael (1999): whole-rock Mg-number >68, MgO >8 wt %, and Ni >150 ppm. These primitive samples display a wide range in chemical composition whereas calc-alkaline basaltic andesites are more homogeneous. Primitive samples from our study area have high MgO and SiO_2 and low Al_2O_3 and CaO compared with most primitive calc-alkaline magmas reported from other magmatic arcs, as was previously noted for central Mexican lavas by Blatter & Carmichael (1998) and Wallace & Carmichael (1999). These samples are dominated by olivine + chromite and olivine–chromite–pyroxene mineral assemblages. In this respect they are similar to high-Mg andesites (sanukitoids) from SW Japan (Tatsumi & Ishizaka, 1982; Swinamer, 1989). The alkalic source component in the SCVF samples (96356 and 96357, Table 1), however, cannot be regarded as a volumetrically dominant parental magma source although this source becomes somewhat more common farther west in the SCFV (Wallace & Carmichael, 1999; Siebe *et al.*, 2004*b*).

Fractional crystallization sequence

Both Popocatépetl and its flanking vents produced moderate-K, calc-alkaline magmas, with the two suites differing mainly in phenocryst assemblages and the extent of differentiation. The monogenetic cones flanking Popocatépetl are dominantly basaltic to andesitic, primarily formed by crystal fractionation of olivine (Fo_{80-90}) + chromite, clinopyroxene–orthopyroxene ± olivine, and pyroxene ± plagioclase ± hornblende assemblages, with assimilation of minor crustal debris (e.g. xenocrysts of quartz). The presence of chromite inclusions in olivine is typical of relatively primitive magmas that have not yet undergone significant fractionation of clinopyroxene (e.g. Roeder, 1994). The andesitic to dacitic rocks of Popocatépetl are dominated by plagioclase–pyroxene–FeTi-oxide ± hornblende sequences with variable amounts of olivine (Fo_{70-90}) + chromite xenocrysts. The occurrence of chromite-bearing olivine in two-pyroxene andesite is a good indication that it was derived from mixing or mingling involving more mafic magma rather than through crystal fractionation (Anderson, 1976; Sakuyama *et al.*, 1981; Nixon, 1988*a*, 1988*b*). Table 2 and Fig. 5d show the higher amounts of olivine in the flanking vents in comparison with the stratovolcano samples, dominated by orthopyroxene–clinopyroxene–plagioclase assemblages.

The concentration of water in the region of melting has been identified as critical both to the silica content of the melt (Kushiro, 1990; Baker *et al.*, 1994; Cervantes & Wallace, 2003) and to whether plagioclase is an early

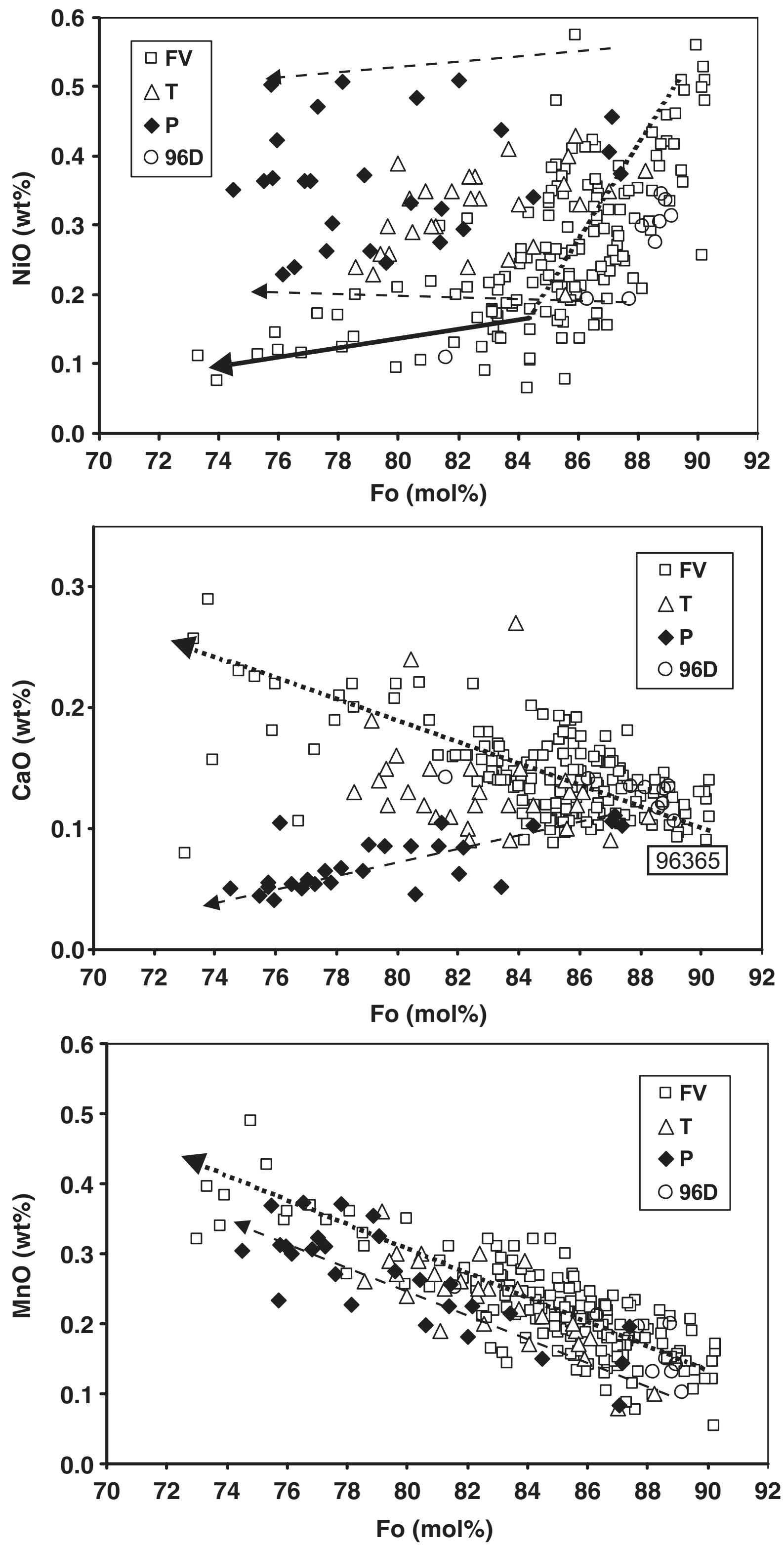

Fig. 14. Concentration of NiO, CaO, and MnO in olivine as a function of forsterite content. Legend symbols: FV, flanking vent; T, transitional; P, Popocatépetl pumices; 96D, 1996 dacite dome. Olivine in the most primitive FV sample (96365) is shown for reference. Bold dotted lines show the trends in crystal cores in FV samples; bold continuous lines show compositions of crystal rims in more slowly cooled lava samples; fine dashed lines show trend for Popocatépetl samples.

crystallizing phase (Sisson & Grove, 1993*a*, 1993*b*). In addition, the initial concentrations of Al and Ca place a further constraint on plagioclase saturation (see also Blatter & Carmichael, 1998, 2001). As inferred from experiments on high-alumina basalt (HAB) under both anhydrous and hydrous conditions, plagioclase crystallization is probably suppressed in favour of a spinel phase in water-saturated melts at high pressure (Sisson & Grove, 1993*a*, 1993*b*). The ubiquitous presence of chromite crystallizing with olivine in magmas that reached the surface indicates that fractionation of these phases was incomplete at depth. The almost complete lack of early-formed plagioclase phenocrysts also explains the occurrence of MgO-rich SCVF basaltic andesites that are relatively rich in CaO and Al_2O_3. Phenocryst assemblages observed in primitive FV lavas (e.g. augite + hypersthene and olivine + augite) are consistent with experimental results reported by Blatter & Carmichael (2001), who obtained these assemblages from high-Mg andesite powders under H_2O-saturated conditions at shallow pressures of up to 3 kbar and high temperatures (~1050°C). Their data support the crystal fractionation history considered here. Additionally, we share their opinion that high-Al_2O_3 basalt is not an appropriate magma for the central part of the TMVB, where the mantle in most cases must be far too depleted to produce magma of that composition.

Popocatépetl and FV suites appear to share parental MgO-rich basaltic magmas, but compositions and textures of Popocatépetl samples reflect longer crustal residence in shallower magma chambers, resulting in higher crystallinity and more evolved mineral compositions and assemblages. These features reflect greater opportunity for recycling of earlier emplaced plutons, assimilation of country rock, and degassing in relatively evolved magma chambers (Stimac *et al.*, 1997). The volatile contents and oxidation state of Popocatépetl rocks appear also to be similar to their parental high-Mg basaltic andesites. Coexisting magnetite and ilmenite from the 1996 dacite dome yield temperatures and fO_2 estimates of 915–950°C and +1·2 to +1·5 FMQ (where FMQ is the fayalite–magnetite–quartz buffer). This is consistent with the lack of anhydrite phenocrysts in the magma despite prolific SO_2 emissions. Anhydrite was present in early phreatic eruptions, being derived from wall-rock or crater deposits (e.g. Obenholzner *et al.*, 2003). According to Wallace & Carmichael (1999), most flanking vents of the SCVF have oxygen fugacities ranging from nickel–nickel oxide buffer (NNO) − 1 to NNO + 1 at temperatures of *c.* 1200°C. As described above, high S concentrations in MI found in olivine xenocrysts in the 1996 dome lava are within the range of S contents observed in MI from olivine in sample 96365 and other SCVF lavas studied in more detail by Cervantes & Wallace (2003).

Mixing and mingling in an upper-crustal magma chamber

A number of previous studies have emphasized the importance of magma mixing at Popocatépetl and Iztaccíhuatl volcanoes (Boudal, 1985; Nixon & Pearce, 1987; Nixon, 1988*a*, 1988*b*; Kolisnik, 1990). Among these, the detailed textural and compositional studies of Nixon & Pearce (1987), Kolisnik (1990) and Pearce & Kolisnik (1990) provided compelling evidence for the importance of recharge and pre-eruptive mixing of mafic and silicic magmas in the genesis of calc-alkaline andesite. These workers showed that zoning of plagioclase is complex and varied in style, even at the scale of a single thin section. One of the most common zoning patterns is displayed by calcic zones overlying resorption surfaces, which record a 10–30 mol % increase in An content. This pattern of reverse zoning is commonly repeated several times in a single crystal. Similar reverse zoning events in orthopyroxene are also common. Although not ruling out other mechanisms of disequilibrium, these patterns, taken along with the presence of olivine xenocrysts and chemical trends consistent with binary mixing, point to mafic recharge, mixing and convective circulation as the cause for complex, repeated growth and dissolution patterns in plagioclase.

The presence of olivine xenocrysts provides clear evidence for the nature of the mafic end-member replenishing these neighbouring systems (Nixon, 1988*a*, 1988*b*). Based on textural, mineralogical, and chemical evidence from Iztaccíhuatl andesite and dacite lavas and associated mafic vents, Nixon (1988*a*) distinguished two types of mixed lavas. His Type I lavas contain abundant olivine (Fo_{88-90}) with skeletal overgrowths, whereas his Type II lavas contain minor olivine (Fo_{88-73}) with well-developed orthopyroxene mantles. Type II lavas also have more complex zoning and reaction textures. He interpreted Type I lavas as the product of binary, single-stage mixing, whereas Type II lavas have undergone more complex mixing and fractionation histories involving multiple recharge events. Very similar olivine compositions and textures were observed at Popocatépetl in this study and by Kolisnik (1990). Olivine in Popocatépetl samples ranges from Fo_{70} to Fo_{90} (Fig. 6) and invariably contains chromite inclusions. Orthopyroxene mantles are present on all grains in some samples (e.g. pink pumice), but absent in others (e.g. 1996 dome clasts). As observed at Iztaccíhuatl, olivine grains mantled by orthopyroxene are more Fe-rich than skeletal olivine grains lacking mantles. The fact that skeletal crystals lacking orthopyroxene mantles are invariably more Mg-rich than crystals with mantles suggests that more extensive re-equilibration of olivine to more Fe-rich compositions occurred during longer residence in silicic chambers. This is consistent with diffusion-rate experiments by Gerlach & Grove

(1982), which indicated that olivine re-equilibrates with melt in days to weeks. Those workers annealed zoning in olivine in 3–14 days.

Trace element concentrations in olivine grains are summarized in Fig. 14. It can be seen that most olivine analyses from Popocatépetl and FV samples have higher NiO and lower CaO concentrations than would be expected for their Fo values. We argue that the presence of chromite inclusions in both types of olivines, along with relationships between Fo content and NiO, CaO, and MnO concentrations, indicate that grains $<Fo_{83}$ have re-equilibrated to lower Fo contents as they were exposed to lower temperatures and more Fe- and Si-rich (and Ni-poor) residual melt compositions. Because Ca and, to some extent, Ni diffuse at a slower rate than Fe and Mn (e.g. Petry *et al.*, 1998; Stahl *et al.*, 1998), these elements tend to more faithfully reflect their original concentrations, and imply that the olivine grains in Popocatépetl pumices and transitional cones were originally more magnesian. Thus the range of olivine compositions observed in Popocatépetl samples is more reflective of the degree of re-equilibration of this mineral as a function of declining temperature than of the original composition of the recharging magmas. In summary, we argue that olivine grains found in Popocatépetl samples originally were Fo_{83-90}, consistent with the occurrence of abundant chromite inclusions (Roeder, 1994). Similar olivine compositions were reported in experiments by Blatter & Carmichael (2001) under low pressure (3 kbar), high temperature (up to 1100°C), oxygen fugacities between −8·20 and −10·40 (log fO_2), and water-saturated conditions (6·5–2·5 wt % H_2O).

Plagioclase analyses from Popocatépetl range from An_{21} to An_{71}, whereas orthopyroxene is generally $<En_{80}$ (Boudal, 1985; Kolisnik, 1990). The lack of plagioclase and orthopyroxene compositions that might be ascribed to a primitive mafic end-member replenishing the system is explained if that end-member contained only Mg-rich olivine phenocrysts, as do virtually all the more primitive FV samples described in this study.

Popocatépetl samples exhibit a variety of features indicating mingling or incomplete blending in some samples, and more thorough mixing in others. Kolisnik (1990) noted the general lack of quenched mafic inclusions and other signs of magma mingling in Popocatépetl andesites. She stressed that most samples represent homogeneous, well-blended hybrids. However, evidence for incomplete homogenization can be found in most samples from the current cycle of eruption. As noted above, the current eruptions are dominantly dacitic in composition, but contain admixed mafic scoria and crystal debris including olivine. Thus mingling is probably most evident when contrasts in the end-member magma compositions are largest (Bacon, 1986; Sparks & Marshall, 1986). The most recent eruptive episode, as characterized by samples of dome material ejected during the April 30, 1996 and June 30, 1997 events, indicates involvement of two different magmas (Stimac *et al.*, 1997). Dacites and basaltic andesites (e.g. 1997 dome samples 97D1 and 97D2, Table 1) did not mix to form a homogeneous hybrid. As mentioned previously, 1996 dome samples contain abundant skeletal olivine xenocrysts (core compositions of Fo_{88-89}) that lack orthopyroxene reaction rims (Fig. 5c). These olivine grains are typically present in darker groundmass patches that have more mafic bulk composition than areas of groundmass distal to olivine grains. These relationships are consistent with incomplete mixing of an olivine-bearing basaltic andesite end-member.

The fact that olivine in the 1996 dome samples lacks orthopyroxene mantles is significant because Tsuchiyama (1986) showed that such mantles can form on olivine (Fo_{91}) immersed in andesitic liquid in only a few hours. He concluded that the most common origin of this texture in volcanic rocks is mixing of olivine-bearing basaltic magma with a more silicic magma. The lack of orthopyroxene mantles on olivine in the 1996 dome samples suggest that little time elapsed between the entrainment of the olivine-bearing mafic magma within the dacitic magma and final dome extrusion.

Hornblende crystals have rims of orthopyroxene and FeTi-oxides indicating reaction during ascent, whereas olivine crystals remain largely unreacted (Fig. 5c; Athanasopoulos, 1997). Using the methods of Rutherford & Hill (1993) based on the thickness of 'gabbroic mantles' on amphibole, Athanasopoulos (1997) estimated transit time from a magma storage chamber at about 8 km depth to the surface at 10–14 days. We infer that olivine should have undergone significant reaction like hornblende if they had resided in the same deep magma body and ascended together. Instead, olivine is present as euhedral and skeletal grains without rims. Hornblende clearly grew in the dacitic magma and the reaction rims had apparently already formed when the basaltic andesite magma was added to the upper-crustal magma chamber, promoting eruption and excess degassing as for the April 30, 1996 event. Some olivine grains show more evidence of reaction in the 1997 eruptions, suggesting that multiple recharge events had occurred by that time. Rapid ascent might be expedited by such mingling, as it would trigger volatile oversaturation and bubble growth in an olivine-bearing mafic magma similar to the water-saturated basaltic andesites thought to be typical of the Zitácuaro–Valle de Bravo region (Blatter & Carmichael, 1998, 2001) and the SCVF (Cervantes & Wallace, 2003). The explosion on April 30, 1996 occurred several days after dome emplacement and seismic quiescence, indicating that dome explosions were the result of cooling accompanied by internal pressure build-up in the dome.

Crustal contamination

In comparison with mixing and fractional crystallization, crustal assimilation seems to have been a less important factor in Popocatépetl magma genesis, although there is some chemical and textural evidence for its occurrence in both Popocatépetl and FV samples.

Granodiorite xenoliths (samples 95142C and 96341B) have similar chemical and Sr and Nd isotope ratios (Tables 1 and 4) to Popocatépetl pumice samples and can be regarded as remnants of shallow magma chamber margins or an earlier emplaced pluton. The metasedimentary xenoliths, meta-arkosic sandstone (9490C), skarn (9463A), and marble (0401 m), however, are interpreted by us as fragments of shallow basement adjoining the chamber. The unusual position of the skarn xenolith in the upper right quadrant of the $^{87}Sr/^{86}Sr$ vs ε_{Nd} diagram (Fig. 11b) is probably the result of metasomatic fluid infiltration (including Nd assimilation) of the limestones by the magma. Limestone should be receptive to this type of contamination during recrystallization because of its low original REE concentration.

The more radiogenic Sr but nearly identical Nd isotope ratios in the Popocatépetl samples in comparison with the Pelado, Guespalapa, Chichinautzin, Cajete, and Xitle volcanoes from the central SCVF and Nevado de Toluca stratovolcano (Fig. 11) can be interpreted as the result of greater interaction and assimilation of shallow basement rocks, principally carbonates of the Cretaceous Cuautla and Morelos formations (Siebe *et al.*, 2004*b*; Fig. 2). Elevated amounts of CO_2 in Popocatépetl gas plumes (Goff *et al.*, 2001) have also been explained by the ingestion of limestone into the rising magma. This process would certainly lead to elevated total Sr concentrations and radiogenic Sr-isotope contamination of the magmas as proposed by Siebe *et al.* (2004*b*). Crustal lithologies suggest a high level of magma reservoir emplacement (*c.* 7–8 km), and the lack of reaction rims on amphibole in Tutti Frutti pumices is consistent with very rapid ascent from depths of 7–10 km (Rutherford & Hill, 1993; Athanasopoulos, 1997). Such a depth of the magma reservoir is confirmed by seismological studies carried out during the current eruption cycle (Espíndola *et al.*, 2004; Valdés-González *et al.*, in preparation).

CONCLUSIONS

The recent activity of Popocatépetl volcano can be understood in the context of its past eruptions and those of the surrounding monogenetic volcanoes of the Basin of Mexico and Valley of Puebla. The knowledge of the magmatic processes that were operative during the evolution of 'modern' Popocatépetl is crucial for the development of a model that will aid in prediction of its future behaviour.

Popocatépetl and surrounding monogenetic cones are located 350 km from the Middle America Trench at the front of the TMVB in an area of >40 km thick continental crust and produced mainly moderate-K calc-alkaline magmas. Generation of these magmas in a subduction regime with chemical contributions from the subducted slab is confirmed by incompatible trace element distributions (e.g. Pb, Ba, and Th) as well as Pb isotopic evidence. Popocatépetl and surrounding scoria cones display mineral assemblages and textures reflecting similar but distinct petrogenetic histories. Popocatépetl produced andesitic to dacitic rocks formed by crystal fractionation of variable amounts of olivine (Fo_{70-90}) ± chromite, clinopyroxene, orthopyroxene, plagioclase, FeTi-oxides ± apatite ± hornblende. Monogenetic vents generally produced basalts to andesites dominated by olivine (cores Fo_{83-89}) + chromite, clinopyroxene, orthopyroxene ± plagioclase ± apatite assemblages. Popocatépetl and most of the scoria cones share common parental high-MgO basaltic magmas that differ noticeably in their ascent histories and residence times in the upper crust. These differences are responsible for divergent chemical and mineralogical trends in the most evolved members of each group. Some andesitic to dacitic magmas from the near flanks of Popocatépetl (within 28 km of the central vent) are transitional in character between the products of Popocatépetl and more distal vents. This finding allows us to constrain the horizontal dimensions of the magma reservoir of one of the largest TMVB stratovolcanoes at *c.* 30 km.

Different REE patterns for least evolved Popocatépetl, FV and other closely spaced SCVF volcanoes cannot be explained by differential partial melting of a uniform mantle source. This observation confirms earlier findings (Siebe *et al.*, 2004*b*) of a small-scale (<1 km) heterogeneous depleted/undepleted mantle beneath the central TMVB. Although most of the magmas originated from a depleted sub-arc mantle, a few scoria cones (e.g. Cerro Santa Bárbara and Cerro Citlaltepec) display an alkaline affinity pointing towards an asthenospheric mantle source.

Popocatépetl samples exhibit a variety of features indicating magma mingling in most dacites and more thorough magma mixing in most andesites. Mingling processes between dacite and olivine-bearing mafic magmas are well displayed in the compositions and textures of the 1996 and 1997 dome samples. Juvenile fragments are the mingling product of two mineralogically and chemically distinct magmas. The dominant type is a light grey hornblende dacite with a vesicular rhyolitic matrix. The dacite contains dark grey, microlite-charged bands containing unreacted, chromite-bearing olivines (cores Fo_{88-89}) identical to those found in adjacent scoria cones. Hornblendes found in the dacite with plagioclase and pyroxene have reaction rims that formed during ascent (estimated at <14 days), whereas the commingled olivine-bearing mafic magma appears to have ascended independently at a more rapid pace. The dome eruptions confirm that dacitic magma currently resides beneath Popocatépetl and is episodically recharged by more mafic magma, fostering rapid final ascent, eruption, and excess sulphur degassing.

Magma mixing is documented by mafic contributions to andesitic and dacitic products of Popocatépetl. The presence of Mg-rich olivine is associated with other textural and compositional evidence for mixing that includes plagioclase with fritted cores and calcic overgrowths, and reversely zoned pyroxene. It appears that the dominant recharge magma to both Popocatépetl and flanking vents is a primitive, olivine-bearing basaltic andesite with relatively high volatile content, as previously proposed by Cervantes & Wallace (2003) for other volcanoes in central Mexico.

A large variety of xenoliths found in the 14 ka BP Tutti Frutti pumice deposits attests to the composition of the shallow crustal basement underneath Popocatépetl volcano. Major and trace element compositions and Sr and Nd isotope ratios indicate that granodiorite xenoliths are comagmatic plutonic rocks from the margin of the magma chamber or earlier emplaced plutons, whereas skarn and marble xenoliths were produced by contact-metamorphism and partially assimilated into Popocatépetl's magma chamber. These results emphasize that both crustal and subcrustal processes contribute to geochemical and isotopic variations in Popocatépetl and surrounding monogenetic scoria cones.

ACKNOWLEDGEMENTS

We would like to acknowledge Adrienne Larocque, Pat Athanasopoulos and Ron Chapman (University of Manitoba) for their assistance with various aspects of this study including electron microprobe analysis. Many thanks go to Gabriela Solís, Teodoro Hernández and Juan Morales (LUGIS-UNAM) for assistance with the isotopic analyses. Giovanni Sosa prepared the samples for Pb isotope analyses. Renato Castro, Ignacio Hernández, Gabriel Valdez and Gerardo Zenteno helped with the drawing of the figures. The manuscript was improved considerably through reviews by Dawnika Blatter, Jim Luhr and Kevin Righter, and Dennis Geist's editorial handling. Many thanks go to Alejandro López (Parque Nacional Izta-Popo) and to Marcos Galicia (Protección Civil) for their co-operation during the project. This work was supported by Consejo Nacional de Ciencia y Tecnología (CONACyT grant 32330-T to P.S. and grant U 40346-F to C.S.), the National Science and Engineering Research Council of Canada (grant to J.S.) and the Universidad Nacional Autónoma de México (grant DGAPA-IN 109202 to P.S. and IN 103302 to C.S.).

REFERENCES

Anderson, A. T. (1976). Magma mixing: petrological process and volcanological tool. *Journal of Volcanology and Geothermal Research* **1**, 3–33.

Athanasopoulos, P. (1997). The origin and ascent history of the 1996 dacitic dome, Volcan Popocatépetl, Mexico. B.Sc. thesis, University of Manitoba, Winnipeg, 105 pp.

Bacon, C. R. (1986). Magmatic inclusions in silicic and intermediate volcanic rocks. *Journal of Geophysical Research* **91**, 6091–6112.

Baker, M. B., Grove, T. L. & Price, R. (1994). Primitive basalts and andesites from the Mt. Shasta region, N. California: products of varying melt fraction and water content. *Contributions to Mineralogy and Petrology* **118**, 111–129.

Blatter, D. L. & Carmichael, I. S. E. (1998). Hornblende peridotite xenoliths from central Mexico reveal the highly oxidized nature of subarc upper mantle. *Geology* **26**, 1035–1038.

Blatter, D. L. & Carmichael, I. S. E. (2001). Hydrous phase equilibria of a Mexican high-silica andesite: a candidate for a mantle origin. *Geochimica et Cosmochimica Acta* **21**, 4043–4065.

Blatter, D. L., Carmichael, I. S. E., Deino, A. L. & Renne, P. R. (2001). Neogene volcanism at the front of the central Mexican volcanic belt: basaltic andesites to dacites, with contemporaneous shoshonites and high TiO_2 lava. *Geological Society of America Bulletin* **113**, 1324–1342.

Bloomfield, K. (1975). A late-Quaternary monogenetic volcano field in central Mexico. *Geologische Rundschau* **64**, 476–497.

Boudal, C. (1985). Petrologie d'un gran volcan andesitique mexicain: le Popo—le rôle de mélanges de magmas dans les dynamismes de l'activité. D.Sc. thesis, Université de Clermont-Ferrand II, Centre de Recherches Volcanologiques, 140 pp.

Boudal, C. & Robin, C. (1988). Relations entre dynamismes éruptifs et réalimentations magmatiques d'origine profonde au Popocatépetl. *Canadian Journal of Earth Sciences* **25**, 955–971.

Bowen, N. L. (1928). *The Evolution of Igneous Rocks*. Princeton, NJ: Princeton University Press, 332 pp.

Carmichael, I. S. E., Lange, R. A. & Luhr, J. F. (1996). Quaternary minettes and associated volcanic rocks of Mascota, western Mexico: a consequence of plate extension above a subduction modified mantle wedge. *Contributions to Mineralogy and Petrology* **124**, 302–333.

Cervantes, P. & Wallace, P. (2003). Role of H_2O in subduction-zone magmatism: new insights from melt inclusions in high-Mg basalts from central Mexico. *Geology* **31**, 235–238.

Condie, K. C. (2001). *Mantle Plumes and their Record in Earth History*. Cambridge: Cambridge University Press, 306 pp.

Eichelberger, J. C. (1980). Vesiculation of mafic magma during replenishment of silicic magma reservoirs. *Nature* **288**, 446–450.

Espíndola, J. M., Godinez, M. L. & Espíndola, V. H. (2004). Models of ground deformation and eruption magnitude from a deep source at Popocatépetl volcano, central Mexico. *Natural Hazards* **31**, 191–207.

Ferrari, L. (2004). Slab detachment control on mafic volcanic pulse and mantle heterogeneity in central Mexico. *Geology* **32**, 77–80.

Fix, J. E. (1975). The crust and upper mantle in central Mexico. *Geophysical Journal of the Royal Astronomical Society* **43**, 453–499.

Friedländer, I. (1921). La erupción del Popocatépetl. *Societé Scientifique Antonio Alzate, Memoires* **40**, 219–227.

Gastil, R. G., Krummenacher, D. & Jensky, W. A., II (1978). Reconnaissance geology of west–central Nayarit, Mexico. *Geological Society of America, Map and Chart Series* **MC-24**, 1–8.

Gerlach, T. & Grove, T. (1982). Petrology of Medicine Lake Highland volcanics: characterization of end members of magma-mixing: *Contributions to Mineralogy and Petrology* **80**, 147–159.

Gill, J. B. (1981). *Orogenic Andesites and Plate Tectonics*. Berlin: Springer, 390 pp.

Goff, F., Janik, C., Delgado, H., Werner, C., Counce, D., Stimac, J. A., Siebe, C., Love, S. P., Williams, S. N., Fischer, T. & Johnson, L. (1998). Geochemical surveillance of magmatic volatiles at Popocatépetl volcano, Mexico. *Geological Society of America Bulletin* **110**, 695–710.

Goff, F., Love, S. P., Warren, R., Counce, D., Obenholzner, J., Siebe, C. & Schmidt, S. C. (2001). Passive infrared remote sensing evidence for large, intermittent CO_2 emissions at Popocatépetl volcano, Mexico. *Chemical Geology* **177**, 133–156.

Gorton, M. P. & Schandl, E. S. (2000). From continents to island arcs: a geochemical index of tectonic setting for arc-related and within-plate felsic to intermediate volcanic rocks. *Canadian Mineralogist* **38**, 1065–1073.

Grove, T. L. & Donnelly-Nolan, J. M. (1986). The evolution of young silicic lavas at Medicine Lake Volcano, California: implications for the origin of compositional gaps in calc-alkaline series lavas. *Contributions to Mineralogy and Petrology* **92**, 281–302.

Global Volcanism Network (1998). Volcanic events: Popocatépetl volcano, cyclical dome extrusions that by late 1997 filled one third of the crater capacity. *Global Volcanism Network Bulletin* **23**(2), 2–4.

Harmon, R. S., Barreiro, B. A., Moorbath, S., Hoefs, J., Francis, P. W., Thorpe, R. S., Déruelle, B., McHugh, J. & Viglino, J. A. (1984). Regional O-, Sr-, and Pb-isotope relationship in late Cenozoic calc-alkaline lavas of the Andean Cordillera. *Journal of the Geological Society, London* **141**, 803–822.

Hickey, R. L., Frey, F., Gerlach, D. C. & López-Escobar, L. (1986). Multiple sources for basaltic arc rocks from the Southern Volcanic Zone of the Andes (34°–41°S): trace element and isotopic evidence for contributions from subducted oceanic crust, mantle, and continental crust. *Journal of Geophysical Research* **91**(B6), 5963–5983.

Jakes, P. & White, A. J. H. (1972). Hornblendes from calc-alkaline volcanic rocks of island arcs and continental margins. *American Mineralogist* **57**, 887–902.

Kolisnik, A. M. E. (1990). Phenocryst zoning, and heterogeneity in andesite and dacite of Volcan Popocatépetl, Mexico, M.Sc. thesis, Queen's University, Kingston, Ont., 247 pp.

Kushiro, I. (1990). Partial melting of mantle wedge and evolution of island arc crust. *Journal of Geophysical Research* **95**, 15929–15939.

Larocque, A. C. L., Stimac, J. A. & Siebe, C. (1998). Metal-residence sites in lavas and tuffs from Volcan Popocatépetl, Mexico: implications for metal mobility in the environment. *Environmental Geology* **33**, 197–208.

Le Bas, M. J., Le Maitre, R. W., Streckeisen, A. & Zanettin, B. (1986). A chemical classification of volcanic rocks based on the total alkali–silica diagram. *Journal of Petrology* **27**, 745–750.

Love, S. P., Goff, F., Counce, D., Siebe, C. & Delgado, H. (1998). Quantitative passive infrared spectroscopy of the eruption plume at Popocatépetl volcano, Mexico. *Nature* **396**, 563–567.

Luhr, J. F. (1997). Extensional tectonics and the diverse primitive volcanic rocks in the western Mexican Volcanic Belt. *Canadian Mineralogist* **35**, 473–500.

Luhr, J. F., Allan, J. F., Carmichael, I. S. E., Nelson, S. A. & Hasenaka, T. (1989). Primitive calc-alkaline and alkaline rock types from the western Mexican Volcanic Belt. *Journal of Geophysical Research* **94**, 4515–4530.

MacDonald, G. A. & Katsura, T. (1964). Chemical composition of Hawaiian lavas. *Journal of Petrology* **5**, 83–133.

Macías, J. L. & Siebe, C. (2005). Popocatépetl's crater filled to the brim: significance for hazard evaluation. *Journal of Volcanology and Geothermal Research* (in press).

Martínez-Serrano, R. G., Schaaf, P., Solís-Pichardo, G., Hernández-Bernal, M. S., Hernández-Treviño, T., Morales-Contreras, J. J. & Macías, J. L. (2004). Sr, Nd and Pb isotope and geochemical data from the Quaternary volcanism of Nevado de Toluca and Tenango Volcanic Field, Mexico: a source of recent adakitic magmatism? *Journal of Volcanology and Geothermal Research* **138**, 77–110.

McDowell, F. & Clabaugh, S. E. (1979). Ignimbrites of the Sierra Madre Occidental and their relation to the tectonic history of western Mexico. *Geological Society of America, Special Papers* **180**, 113–124.

Mooser, F. (1967). Tefracronología de la Cuenca de México para los últimos 30,000 años. *Instituto Nacional de Antropología e Historia, Boletín* **30**, 12–15.

Negendank, J. F. W. (1972). Volcanics of the Valley of Mexico; Part 1, Petrography of the volcanics. *Neues Jahrbuch für Mineralogie, Abhandlungen* **116**, 308–320.

Nixon, G. T. (1988*a*). Petrology of the younger andesites and dacites of Iztaccíhuatl volcano, Mexico: I. Disequilibrium phenocryst assemblages as indicators of magma chamber processes. *Journal of Petrology* **29**, 213–264.

Nixon, G. T. (1988*b*). Petrology of the younger andesites and dacites of Iztaccíhuatl volcano, Mexico: II. Chemical stratigraphy, magma mixing, and the composition of basaltic magma influx. *Journal of Petrology* **29**, 265–303.

Nixon, G. T. (1989). *The Geology of Iztaccíhuatl Volcano and Adjacent Areas of the Sierra Nevada and Valley of Mexico. Geological Society of America, Special Papers* **219**, 58 pp.

Nixon, G. T. & Pearce, T. H. (1987). Laser-interferometry study of oscillatory zoning in plagioclase: the record of magma mixing and phenocryst recycling in calc-alkaline magma chambers, Iztaccíhuatl volcano, Mexico. *American Mineralogist* **72**, 1144–1162.

Obenholzner, J. H., Schroettner, H., Golob, P. & Delgado, H. (2003). Particles from the plume of Popocatépetl volcano, Mexico—the FESEM/EDS approach. In: Oppenheimer, C., Pyle, D. M. & Barclay, J. (eds) *Volcanic Degassing. Geological Society, London, Special Publications* **213**, 123–148.

Panfil, M. S., Gardner, T. W. & Hirth, K. G. (1999). Late Holocene stratigraphy of the Tetimpa archaeological sites, northeast flank of Popocatépetl volcano, central Mexico. *Geological Society of America Bulletin* **111**, 204–218.

Pardo, M. & Suárez, G. (1995). Shape of the subducted Rivera and Cocos plates in southern Mexico: seismic and tectonic implications. *Journal of Geophysical Research* **100**, 12357–12373.

Pearce, T. H. & Kolisnik, A. M. (1990). Observations of plagioclase zoning using interference imaging. *Earth-Science Reviews* **29**, 9–26.

Petry, C., Chakraborty, S. & Palme, H. (1998). Ni diffusion in olivine. *EOS Transactions, American Geophysical Union* **79**(Supplement), 370.

Plank, T. & Langmuir, C. H. (1988). An evaluation of the global variation in the major element chemistry of arc basalts. *Earth and Planetary Science Letters* **90**, 349–370.

Plank, T. & Langmuir, C. H. (1998). The chemical composition of subducting sediment and its consequences for the crust and mantle. *Chemical Geology* **145**, 325–394.

Robin, C. (1984). Le Volcan Popocatépetl (Mexique): structure, evolution pétrologique et risques. *Bulletin Volcanology* **47**, 1–23.

Robin, C. & Boudal, C. (1987). A gigantic Bezymianny-type event at the beginning of modern Volcan Popocatépetl. *Journal of Volcanology and Geothermal Research* **31**, 115–130.

Roeder, P. L. (1994). Chromite: from the fiery rain of chondrules to the Kilauea Iki lava lake. *Canadian Mineralogist* **32**, 729–746.

Rutherford, M. J. & Hill, P. M. (1993). Magma ascent rates from amphibole breakdown: an experimental study applied to the 1980–1986 Mount St. Helens eruptions. *Journal of Geophysical Research* **98**, 19667–19685.

Sakuyama, M. (1981). Evidence of magma mixing: petrological study of Shirouma-Oike calc-alkaline andesite volcano, Japan. *Journal of Petrology* **22**, 553–583.

Schaaf, P., Morán-Zenteno, D., Hernández-Bernal, M. S., Solís-Pichardo, G., Tolson, G. & Köhler, H. (1995). Paleogene continental margin truncation in southwestern Mexico: geochronological evidence. *Tectonics* **14**, 1338–1350.

Shapiro, N. M., Singh, S. K., Iglesias-Mendoza, A., Cruz-Atienza, V. M. & Pacheco, J. F. (2000). Evidence of low Q below Popocatépetl volcano, and its implication to seismic hazards in Mexico City. *Geophysical Research Letters* **27**, 2753–2756.

Siebe, C. & Macías, J. L. (2004). Volcanic hazards in the Mexico City metropolitan area from eruptions at Popocatépetl, Nevado de Toluca, and Jocotitlán stratovolcanoes and monogenetic scoria cones in the Sierra Chichinautzin Volcanic Field. *Field Guide, Penrose Conference, Neogene–Quaternary Continental Margin Volcanism, January 2004, State of Puebla, México.* Boulder, CO: Geological Society of America, 77 pp., doi: 101130/0-8137-0005(2004)0005<0000:VHITMC>2.0CO;2.

Siebe, C., Abrams, M. & Macías, J. L. (1995). Derrumbes gigantes, depósitos de avalancha de escombros y edad del actual cono del Volcán Popocatépetl. In: *Comité Científico Asesor Universidad Nacional Autónoma de México–Centro Nacional de Prevención de Desastres: Volcán Popocatépetl, estudios realizados durante la crisis de 1994–199*5. *Edición Especial, Secretaría de Gobernación*, 195–220.

Siebe, C., Abrams, M., Macías, J. L. & Obenholzner, J. (1996). Repeated volcanic disasters in pre-Hispanic time at Popocatéptl, Central Mexico: past key to the future? *Geology* **24**, 399–402.

Siebe, C., Macías, J. L., Abrams, M., Rodríguez, S. & Castro, R. (1997). Catastrophic eruptions at Popocatépetl and Quaternary explosive volcanism in the Serdán–Oriental Basin, East–Central Mexico. In: *International Association of Volcanology and Chemistry of the Earth's Interior, General Assembly, Puerto Vallarta, Mexico. Field Trip Guidebook* **4**, 88 pp.

Siebe, C., Schaaf, P. & Urrutia-Fucugauchi, J. (1999). Mammoth bones embedded in a late Pleistocene lahar from Popocatépetl volcano, near Tocuila, Central Mexico. *Geological Society of America Bulletin* **111**, 1550–1562.

Siebe, C., Rodríguez-Lara, V., Schaaf, P. & Abrams, M. (2004*a*). Radiocarbon ages of Holocene Pelado, Guespalapa, Chichinautzin scoria cones, south of Mexico City: implications for archaeology and future hazards. *Bulletin of Volcanology* **66**, 203–225.

Siebe, C., Rodríguez-Lara, V., Schaaf, P. & Abrams, M. (2004*b*). Geochemistry, Sr–Nd isotope composition, and tectonic setting of Holocene Pelado, Guespalapa and Chichinautzin scoria cones, south of Mexico City. *Journal of Volcanology and Geothermal Research* **130**, 197–226.

Sisson, T. W. & Grove, T. L. (1993*a*). Experimental investigations of the role of H_2O in calc-alkaline diffentiation and subduction zone magmatism. *Contributions to Mineralogy and Petrology* **113**, 143–166.

Sisson, T. W. & Grove, T. L. (1993*b*). Temperatures and H_2O contents of low-MgO high-alumina basalts. *Contributions to Mineralogy and Petrology* **113**, 167–184.

Sparks, R. S. J. & Marshall, L. A. (1986). Thermal and mechanical constraints on mixing between mafic and silicic magmas. *Journal of Volcanology and Geothermal Research* **29**, 99–124.

Stahl, S., Hain, A., Chakraborty, S., Laqua, W. & Palme, H. (1998). Tracer diffusion of ^{42}Ca in olivine as a function of pO_2 between 800°C and 1500°C. *EOS Transactions, American Geophysical Union* **79** (Supplement), 370.

Stimac, J., Siebe, C., Schaaf, P. & Obenholzner, J. (1997). Magmatic processes at Popocatépetl, Mexico. In: *International Association of Volcanology and Chemistry of the Earth's Interior, General Assembly, Puerto Vallarta, Mexico, Abstracts*, p. 76.

Straub, S. M. & Martin-Del Pozzo, A. L. (2001). The significance of phenocryst diversity in tephra from recent eruptions at Popocatépetl volcano (central Mexico). *Contributions to Mineralogy and Petrology* **140**, 487–510.

Suárez, G., Monfret, T., Wittlinger, G. & David, C. (1990). Geometry of subduction and depth of the seismogenic zone in the Guerrero gap. *Nature* **345**, 336–338.

Sun, S. S. & McDonough, W. F. (1989). Chemical and isotopic systematics of oceanic basalts: implications for mantle composition and processes. In: Saunders, A. D. & Norry, M. J. (eds) *Magmatism in the Ocean Basins. Geological Society, London, Special Publications* **42**, 313–345.

Swinamer, R. T. (1989). The geomorphology, petrography, geochemistry, and petrogenesis of the volcanic rocks in the Sierra del Chichinautzin, Mexico. M.Sc. thesis, Queens University, Kingston, Ont. 212 pp.

Tatsumi, Y. & Ishizaka, K. (1982). Origin of high-magnesian andesites in the Setouchi volcanic belt, southwest Japan, II. Melting phase relations at high pressures. *Earth and Planetary Science Letters* **60**, 304–317.

Tsuchiyama, A. (1986). Experimental study of olivine–melt reaction and its petrological implications. *Journal of Volcanology and Geothermal Research* **29**, 245–264.

Valdés-González, C. M., Mooney, W. D., Singh, S. K., Meyer, R. P., Lomnitz, C., Luetgert, J. H., Helsley, C. E., Lewis, B. T. R. & Mena, M. (1986). Crustal structure of Oaxaca, Mexico, from seismic refraction measurements. *Seismological Society of America, Bulletin* **76**, 547–563.

Verma, S. P. (2000). Geochemistry of the subducting Cocos plate and the origin of subduction-unrelated mafic volcanism at the volcanic front of the central Mexican Volcanic Belt. In: Delagado-Granados, H., Aguirre-Díaz, G. & Stock, J. M. (eds) *Cenozoic Tectonics and Volcanism of Mexico. Geological Society of America, Special Papers* **334**, 195–222.

Waitz, P. (1921). Popocatépetl again in activity. *American Journal of Sciences, 5th Series* **1**, 81–85.

Wallace, P. J. & Carmichael, I. S. E. (1999). Quaternary volcanism near the Valley of Mexico: implications for subduction zone magmatism and the effects of crustal thickness variations on primitive magma compositions: *Contributions to Mineralogy and Petrology* **135**, 291–314.

Werner, C., Janik, C. J., Goff, F., Counce, D., Johnson, L., Siebe, C., Delgado, H., Williams, S. N. & Fischer, T. P. (1997). Geochemistry of summit fumarole vapors and flanking thermal/mineral waters at Popocatépetl Volcano, Mexico. Los Alamos National Laboratory Report LA-13289-MS, UC 903, 1–33.

Zindler, A. & Hart, S. R. (1986). Chemical geodynamics. *Annual Review of Earth and Planetary Sciences* **14**, 493–571.